TURUN YLIOPISTON JULKAISUJA
ANNALES UNIVERSITATIS TURKUENSIS

SARJA - SER. D OSA - TOM. 1051

MEDICA - ODONTOLOGICA

IMAGING OF TUMOUR MICROENVIRONMENT FOR THE PLANNING OF ONCOLOGICAL THERAPIES USING POSITRON EMISSION TOMOGRAPHY

by

Gaber Komar

TURUN YLIOPISTO
UNIVERSITY OF TURKU
Turku 2012

From Department of Oncology and Radiotherapy and Turku PET Centre, University of Turku, Turku Finland

Supervised by

Professor Heikki Minn, MD, PhD
Turku PET Centre and Department of Oncology and Radiotherapy
University of Turku
Turku, Finland

and

Adjunct Professor Marko Seppänen, MD, PhD
Turku PET Centre and Department of Clinical physiology and Nuclear medicine
University of Turku
Turku, Finland

Reviewed by

Adjunct Professor Eva Brun, MD, PhD
Department of Oncology,
Lund University Hospital, Lund, Sweden

and

Adjunct Professor Morten Busk, MD, PhD
Department of Experimental Clinical Oncology,
Aarhus University Hospital, Aarhus, Denmark

Dissertation opponent

Jens Sörensen, MD, PhD
Department of Radiology, Oncology and Radiation Science, Section of Nuclear Medicine and PET,
Uppsala University Hospital and
Department of Medical Sciences, Clinical Physiology
University of Uppsala, Uppsala, Sweden

ISBN 978-951-29-5270-0 (PRINT)
ISBN 978-951-29-5271-7 (PDF)
ISSN 0355-94 83
Painosalama Oy, Turku, Finland 2012

To Henna

ABSTRACT

Gaber Komar

IMAGING OF TUMOUR MICROENVIRONMENT FOR THE PLANNING OF ONCOLOGICAL THERAPIES USING POSITRON EMISSION TOMOGRAPHY

Department of Oncology and Radiotherapy and Turku PET Centre, University of Turku

Annales Universitatis Turkuensis

Tumour cells differ from normal tissue cells in several important ways. These differences, like for example changed energy metabolism, result in altered microenvironment of malignant tumours. Non-invasive imaging of tumour microenvironment has been at the centre of intense research recently due to the important role that this changed environement plays in the development of malignant tumours and due to the role it plays in the treatment of these tumours. In this respect, perhaps the most important characteristics of the tumour microenvironment from this point of view are the lack of oxygen or hypoxia and changes in blood flow (BF).

The purpose of this thesis was to investigate the processes of energy metabolism, BF and oxygenation in head and neck cancer and pancreatic tumours and to explore the possibilities of improving the methods for their quantification using positron emission tomography (PET). To this end [^{18}F]EF5, a new PET tracer for detection of tumour hypoxia was investigated. Favourable uptake properties of the tracer were observed. In addition, it was established that the uptake of this tracer does not correlate with the uptake of existing tracers for the imaging of energy metabolism and BF, so the information about the presence of tissue hypoxia cannot therefore be obtained using tracers such as [^{18}F]FDG or [^{15}O]H_2O. These results were complemented by the results of the follow-up study in which it was shown that the uptake of [^{18}F]EF5 in head and neck tumours prior to treatment is also associated with the overall survival of the patients, indicating that tumour hypoxia is a negative prognostic factor and might be associated with therapeutic resistance.

The influences of energy metabolism and BF on the survival of patients with pancreatic cancer were investigated in the second study. The results indicate that the best predictor of survival of patients with pancreatic cancer is the relationship between energy metabolism and BF. These results suggest that the cells with high metabolic activity in a hypoperfused tissue have the most aggressive phenotype.

Pancreatic tumours were further studied in a prognostic study comparing the diagnostic properties of [^{18}F]FDG PET/CT, MRI, and CT in evaluating patients with suspected pancreatic malignancy. In this study, [^{18}F]FDG PET/CT was shown to be more sensitive than conventional imaging in the diagnosis of both primary pancreatic adenocarcinoma and associated distant metastases. In contrast, the sensitivity of [^{18}F]FDG PET/CT was poor in detecting local lymph node metastasis, which would have been important for the assessment of resectability.

In addition, a simple method for non-invasive measurement of BF using PET was developed and validated. The method was shown to be of benefit particularly in tissues like the cerebellum and resting skeletal muscle, but may also be useful in tissues with higher and more heterogeneous blood flow like tumours.

The results of all the projects indicate that PET-imaging of the tumour microenvironment is feasible and could add clinical value to treatment planning of malignant tumours.

Keywords: malignant tumours, tumour microenvironment, hypoxia, blood flow, PET, ^{18}F]EF5, [^{18}F]FDG, head and neck cancer, pancreatic tumours, radiation therapy.

TIIVISTELMÄ

Gaber Komar

KASVAINTEN MIKROYMPÄRISTÖN KUVANTAMINEN POSITRONIEMISSIOTOMOGRAFIALLA HOITOJEN SUUNNITTELUA VARTEN

Onkologia ja Sädehoito sekä Valtakunnallinen PET-keskus, Turun yliopisto
Annales Universitatis Turkuensis

Kasvaimen mikroympäristön kajoamaton kuvantaminen on kerännyt viime aikoina paljon tieteellistä huomiota. Tämä johtuu mikroympäristön tärkeästä roolista pahanlaatuisten kasvainten etenemisessä ja hoidon suunnittelussa. Hoidon kannalta kenties tärkeimmät mikroympäristön ominaisuudet ovat hapen puute, verenvirtaus sekä solujen aineenvaihdunnan aktiivisuus. Nämä vaikuttavat sekä säde- että solunsalpaajahoidon tehoon.

Väitöskirjatyössä tutkittiin solujen sokeriaineenvaihduntaa, verenvirtausta sekä hapettumista pään ja kaulan alueen syövässä ja haiman kasvaimissa positroniemissiotomografialla (PET). Tarkoitus oli kehittää ja parantaa kvantitatiivisia menetelmiä mikroympäristön ominaisuuksien mittaamiseen. Ensinnäkin työssä kehitettiin uutta huonosti hapettuvat eli hypoksiset syöpäsolut osoittavaa positronisäteilevää merkkiainetta [^{18}F]EF5:tä, jota tutkittiin ensimmäistä kertaa ihmisessä. Uuden hypoksiamerkkiaineen kerääntymisdynamiikka pään ja kaulan alueen syövässä selvitettiin ja luotiin yksinkertainen kliiniseen käyttöön soveltuva PET-kuvausprotokolla. Tutkimukset osoittivat myös, että [^{18}F]EF5-merkkiaineen kerääntyminen kasvaimessa ei korreloi verenvirtaukseen tai solujen sokeriaineenvaihduntaan, joten hapetuksen kuvantaminen vaatii oman merkkiaineen. Näitä alustavia tuloksia täydennettiin seurantatutkimuksella, jossa todettiin [^{18}F]EF5-merkkiaineen vahvan kertymisen ennustavan lyhentynyttä eloonjäämistä ja paikallista uusiutumaa.

Toisessa osaprojektissa selvitettiin [^{18}F]-merkatulla fluorideoksiglukoosilla (FDG) mitatun solujen energia-aineenvaihdunnan ja kasvaimen verenvirtauksen vaikutusta haimasyöpäpotilaiden eloonjäämiseen. Tulokset osoittivat, että korkea energia-aineenvaihdunnan ja verenvirtauksen suhde on ennusteellisesti tärkeämpi kuin kumpikaan syöpäsolujen mikroympäristöä kuvaava omaisuus yksinään. Tämä viittaa siihen, että ne syöpäsolut joilla on matalasta verenvirtauksesta huolimatta korkea sokeriaineenvaihdunnan aktiivisuus ovat sopeutuneet parhaiten huonosti hapettuneeseen ympäristöön. Tällaiset syöpäsolut ovat siten geneettiseltä ilmiasultaan eli fenotyypiltään erityisen aggressiivisia.

Väitöskirjan kolmantena osatyönä vertailtiin tietokonetomografian (TT), magneettikuvauksen (MK) ja [^{18}F]FDG PET/TT:n kykyä havaita ja määrittää haimassa todetun muutoksen luonne ja levinneisyys potilailla, joiden muutoksen taustalla epäiltiin olevan pahanlaatuinen kasvain. [^{18}F]FDG PET/TT osoittautui tietokonetomografiaa ja magneettikuvausta herkemmäksi sekä paikallisen muutoksen luonteen että kaukoetäpesäkkeiden havaitsemisessa. Toisaalta PET/TT oli perinteisiä kuvantamismenetelmiä (TT, MK) huonompi tunnistamaan taudin leviämistä paikallisiin imusolmukkeisiin.

Lisäksi omana osaprojektina kehitettiin yksinkertainen kajoamaton menetelmä verenvirtauksen mittaamista varten potilailla, joilla oli todettu pään ja kaulan alueen syöpä. Menetelmä osoittautui luotettavaksi pikkuaivojen ja kaulan lihasten verenvirtauksen määrittämisessä, mutta tietyissä sovelluksissa sitä voidaan käyttää myös pään ja kaulan alueen kasvaimissa. Kaikkien osatöiden tulokset osoittavat, että kasvainten mikroympäristön PET-kuvantamista eri merkkiaineilla voi käyttää syövän yksilöllisessä hoidon suunnittelussa, sillä perinteiset kuvantamismenetelmät eivät kykene antamaan yhtä täsmällistä tietoa ennusteesta tai kudosten toiminnasta.

Avainsanat: Pahanlaatuiset kasvaimet, kasvaimen mikroympäristö, hypoksia, verenvirtaus, PET, [^{18}F]EF5, [^{18}F]FDG, pään ja kaulan alueen syöpä, haiman syöpä, sädehoito

TABLE OF CONTENTS

ABBREVIATIONS

[^{18}F]EF5	[^{18}F] 2-(2-nitro-1-H-imidazol-1-yl)-N-(2,2,3,3,3-pentafluoropropyl)-acetamide
[^{18}F]FETNIM	4-[^{18}F]fluoro-2,3-dihydroxil-1-(2'-nitroimidazole-1'-yl)-acetamide
[^{18}F]FMISO	1H-1-(3—[18]fluoro-2-hydroxypropyl)-2-nitroimidazole
[^{18}F]FDG	[^{18}F]-fluoro-6-deoxy-glucose
[^{15}O]H_2O	[^{15}O]-water
BF	Blood flow
BGV	Biological gross volume
BTV	Biological target volume
BMI	Body mass index
BSA	Body surface index
CECT	Contrast-enhanced computed tomography
CT	Computed tomography
CTA	Computed tomography angiography
EGFR	Epidermal growth factor receptor
FUR	Fractional uptake ratio
GlcP	Plasma glucose value
GLUT	Glucose transporter protein
HIF	Hypoxia-induced factor
HS	Hypoxic sub-volume
IF	Input function
IMRT	Intensity-modulated radiotherapy
LC	Lump constant
MAV	Metabolically active volume
MDCT	Multi-detector row computed tomography
MRI	Magnetic resonance imaging
MTGA	Multiple-time graphical analysis
NET	Neuroendocrine tumour
NPV	Negative predictive value
PET	Positron emission tomography
PHA	Percent hypoxic area
p.i.	Post injection
PPV	Positive predictive value
ROI	Region of interest
RT	Radiation therapy
RCT	Radiochemotherapy

SCC	Squamous cell carcinoma
SD	Standard deviation
TAC	Time activity curve
$T_{1/2}$	Physical half-life
T/M	Tumour-to-muscle ratio
VD	Volume of distribution
VEGF	Vascular endothelial growth factor

LIST OF ORIGINAL PUBLICATIONS

This dissertation is based on the following original publications, which are referred to in the text by the corresponding Roman numerals, I – V.

I. **Komar G**, Seppänen M, Eskola O, Lindholm P, Grönroos TJ, Forsback S, Sipilä H, Evans SM, Solin O, Minn H. 18F-EF5: A New PET Tracer for Imaging Hypoxia in Head and Neck Cancer. J Nucl Med. 2008 Dec; 49(12):1944-51.

II. **Komar G**, Kauhanen S, Liukko K, Seppänen M, Kajander S, Ovaska J, Minn H, Nuutila P. Decreased blood flow with increased metabolic activity: A sign of aggressive tumour phenotype in pancreatic malignancies. Clin Cancer Res. 2009 Sept; 15(17): 5511-17.

III. Kauhanen SP, **Komar G**, Seppänen MP, Dean KI, Minn HR, Kajander SA, Rinta-Kiikka I, Alanen K, Borra RJ, Puolakkainen PA, Nuutila P, Ovaska JT. A Prospective Diagnostic Accuracy Study of ^{18}F-Fluorodeoxyglucose Positron Emission Tomography/Computed Tomography, Multidetector Row Computed Tomography, and Magnetic Resonance Imaging in Primary Diagnosis and Staging of Pancreatic Cancer. Ann Surg. 2009 Dec; 250(6):957-63.

IV. **Komar G**, Oikonen V, Sipilä H, Seppänen M, Minn H. Noninvasive Parametric Blood Flow Imaging of Head and Neck Tumours Using [^{15}O]H_2O and PET/CT. Nucl Med Comm. Nucl Med Commun. 2012 Nov; 33(11):1169-78.

V. **Komar G**, Seppälä J, Lehtiö K, Seppänen M, Eskola O, Lindholm P, Grenman R, Sipilä H, Solin O, Minn H. Prognostic values of tumour blood flow, [^{18}F]EF5 and [^{18}F]FDG PET/CT imaging in patients with head and neck cancer treated with radiochemotherapy. Manuscript

1 INTRODUCTION

Malignant tumours have a very complex tissue microenvironment which, among other things, determines how they respond to therapeutic attempts to eradicate them. This microenvironment can differ greatly between tumours; nevertheless there are some common characteristics typical for malignant tissues.

The most important alterations in cell physiology are sometimes also referred to as the hallmarks of cancer. These are self-sufficiency in growth signals, insensitivity to growth-inhibitory signals, evasion of programmed cell death or apoptosis, limitless replicative potential, sustained angiogenesis, and tissue invasion and metastasis, along with two new characteristics recently added to this list: altered energy metabolism and the tendency to evade the body's immune system (Hanahan & Weinberg, 2011). However, while all hallmark-characteristics are almost always present in malignant tissue, the consequences of these hallmarks may vary in their intensity and extensity in specific cancers. The specificity of anti-cancer therapies is usually based on one of these differences between normal and malignant tissues, and the success of the treatment therefore depends on the presence and prevalence of this specific characteristic/difference in the treated tumour.

In recent years, it has become widely acknowledged that the presence of the treatment-defining characteristics is not only associated with a tumour type, but also varies greatly within tumours of a certain type. Non-specific use of highly specific therapies has therefore rarely been shown to result in therapeutic success that justifies the great increase in costs associated with these new therapies. This is, for example, demonstrated by the established association between KRas mutation and the response to EGFR-inhibiting drugs such as panintumab and cetuximab in colon cancer. While tumours with the wild type KRas gene will respond to such treatment, those with a mutation on this gene will not (Lievre *et al.*, 2006). For these reasons, efforts have been focused on pre-treatment characterization of malignant tumours, and selection of therapies based on this characterization and testing patients for the presence of this mutation have become a routine part of treatment planning in colorectal cancer. In some trials, this has resulted in higher success rates. Many specific therapies have already been developed, and in many of these cases the next challenge lies in the development of diagnostic methods that would be able to reliably and preferably noninvasively characterize the presence and the extent of such tumour-specific characteristics in vivo, thereby enabling optimal use of such treatments.

2 REVIEW OF THE LITERATURE

2.1 TUMOUR MICROENVIRONMENT

The physiology of malignant tissues and in particular that of malignant solid tumours is significantly different from the physiology of normal tissue. It is determined by the six hallmarks of cancer which are, according to Hanahan and Weinberg, self-sufficiency in growth signals, insensitivity to growth-inhibitory (antigrowth) signals, evasion of programmed cell death (apoptosis), limitless replicative potential, sustained angiogenesis, and tissue invasion and metastasis (Hanahan & Weinberg, 2000). In addition to these six characteristics, two more have recently been suggested as fundamental traits of cancer biology warranting their inclusion as hallmarks. These are altered energy metabolism and the ability to evade the body's immune system (Hanahan & Weinberg, 2011).

While these complex processes may not be as tightly regulated as they are in normal cells and tissues, they are in a way guided by the basic enabling circumstances of genetic instability and tumour-promoting inflammation, as well as the selective pressure on the mutating cell populations. Due to the lack of strict regulation, these processes may appear chaotic. In particular, angiogenesis, the process of forming new blood vessels in malignant solid tumours, results in large numbers of functionally poor blood vessels that fail to provide the growing tissue with the needed oxygen and nutrients.

2.1.1 Tumour metabolism

In aerobic conditions, most human cells convert glucose to energy with the help of oxygen in a process called oxidative phosphorylation in mitochondria. The end products of this process are water and carbon dioxide. This is a complex, but highly effective way of energy utilization. In anaerobic conditions, however, glucose is converted to lactic acid. This is a much less effective extraction of energy than oxidative phosphorylation, which is therefore used in normal cells whenever oxygen is present.

Tumour metabolism is defined by the relative simplicity of malignant cells (as evidenced by low level of histologic direntiation) and by the insufficient supply of oxygen due to the dysfunctional vasculature. This results in the glycolytic pathway being the dominant form of energy metabolism in tumours. In the 1920s, Otto Warburg and co-workers discovered that despite the presence of oxygen cells in solid tumours excrete large amounts of lactic acid (Warburg *et al.*, 1927). Since then it has become clear that tumour metabolism is characterized by much higher glycolysis rates than those in normal tissues, resulting in production of lactic acid. Metabolism of glucose is anaerobic also in the presence of oxygen, which Warburg attributed to cells' inability to metabolise glucose aerobically, due to dysfunctional mitochondria (Warburg, 1956b,

a). Later it has been shown that this is not the true reason in most solid cancers. Nevertheless, the anaerobic extraction of energy in the presence of oxygen, typical for solid (malignant) tumours has since become known as the Warburg effect.

The molecular mechanisms leading to increased glycolysis in tumours are not entirely known. The first and in many ways crucial step is the transport of glucose into cells by membrane transporter proteins called glucose transporters or GLUTs. The number of proteins comprising the GLUT family is growing and currently at least 13 different glucose transporter proteins have been identified. Based on their genetic sequence similarities these are divided into three classes: Class I (GLUT 1-4), Class II (GLUT 5, 7, 9 and 11), and Class III (GLUT 6, 8, 10, 12 and H+/myoinositol transporter or HMIT) (Joost & Thorens, 2001). Since normally glucose can only be synthesised in hepathocytes, glucose has to be actively transported into the cells that use it. GLUT up-regulation is therefore necessary in the case of increased glycolysis. Typical for cancerous tissue is the up-regulation of GLUT-1 and GLUT-3 transporters. GLUT-1 is widely expressed in different types of cells and is responsible for the basic uptake of glucose, while GLUT-3 is typical for neurons.

Substantial evidence links high glycolysis rates in cancer cells to an over-expression of certain types of hexokinases (Gosalvez & Weinhouse, 1976; Weinhouse, 1976; Christofk *et al.*, 2008) which might be responsible and indeed required for the high glycolytic rates, as well as the proliferation rates observed in cancer cells.

An important side effect of anaerobic metabolism of cancer cells is also the high production of lactic acid and the resulting acidosis which also seems to play an important role in tumour development and treatment resistance (Dhup *et al.*, 2012).

However, regardless of the molecular mechanisms behind the development of the anaerobic phenotype, it seems that this type of cell is very well adapted to the fast changing environment of malignant tumours. Relatively simple anaerobic metabolism is also an advantage when malignant cells are spreading throughout the body, creating distant metastases. The very unreliable and mostly inadequate supply of nutrients and most importantly oxygen in cancer might therefore be seen as selective pressure favouring the simple and robust anaerobic metabolism and providing these cells with an evolutionary advantage (Graeber *et al.*, 1996).

On the other hand, the high glycolytic rate also has practical implications for use in cancer diagnostics since Fluorine 18 labeled glucose (FDG) PET has been shown to be one of the most sensitive tools for differentiating malignant from normal tissues and is used widely in cancer diagnostics (Fletcher *et al.*, 2008).

2.1.2 Angiogenesis and vasculature

As cells proliferate, development of new blood vessels providing the emerging tissue with nutrients and oxygen is a necessary process that enables the growth of the tissue. In normal tissue, this process is tightly regulated and results in a complex network of functional arteries, capillaries and veins. Proliferating cells are initially oxygenated by simple diffusion. When the tissue grows beyond the limit of oxygen diffusion, new vessels are required. Low level of oxygen or hypoxia is a central impulse triggering vessel growth. This is achieved through hypoxia-inducible factors or HIFs of which HIF-1α may be the most important. Normally, vessels expand by sprouting and protruding into unvascularized tissue. This is followed by the process of maturing during which vessels acquire the ability to supply tissues with oxygen and other nutrients in a controlled manner. Growth and maturation are very complex and depend on the coordinated signalling between vascular cells and tissue cells.

These processes are often derailed in pathological conditions and some of the diseases characterized by abnormal or excessive angiogenesis are cancer, psoriasis, autoimmune disorders, endometriosis, primary pulmonary hypertension, and arthritis.

Particularly in malignant neoplasms, with their high proliferative activity and abundance of growth factors, angiogenesis plays an important role. Tumours cannot grow beyond the size of a few millimetres, if tissue growth is not accompanied by growth of blood vessels (Folkman, 1995; Bergers & Benjamin, 2003). At this point a threshold is reached which is sometimes also referred to as angiogenic switch (Gimbrone & Gullino, 1976). Further growth can only occur with initiation of angiogenesis. Those populations of cancer cells that manage to overcome this obstacle produce large amounts of angiogenic growth factors and release them into their environment in response to hypoxia. This release is poorly controlled and the ensuing vessel growth is therefore disorganized and erratic (Figure 1).

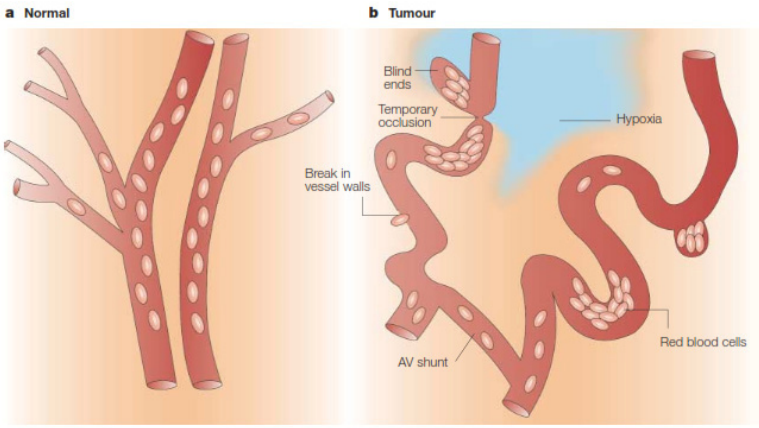

Figure 1 – Chaotic and dysfunctional vasculature of malignant tumours (Brown et al, 2004.)

As early as 1907 Goldman observed that malignant growth is accompanied by growth of blood vessels (Goldman, 1907), however quite some time passed before this was seen as having a potentially therapeutic role (Folkman, 1971). Great efforts have since been invested into identifying the pieces in this network and targeting them to achieve therapeutic effects.

It is nowadays widely accepted that angiogenesis is orchestrated by a variety of angiogenic activators and inhibitors (Bergers & Benjamin, 2003). When these are in balance the resulting vasculature is sufficient and functional. However, in the case of malignant tissue, angiogenesis activators like vascular endothelial growth factor (VEGF), fibroblast growth factors (FGFs), platelet-derived growth factor (PDGF), and epidermal growth factor (EGF) are being over-expressed and prevail over inhibitors like thrombospondin-1, angiostatin, endostatin, canstatin, and tumstatin. For this reason, the vessel growth is not only excessive but also results in blood vessels that are structurally irregular, dilated and tortuous or have dead ends. Also the distinction between venules, arterioles and capillaries is lost and the networks they form are leaky and haemorrhagic. The endothelial cell layer of these vessels is dysfunctional and leaky with cells displaying poor connectivity and multiple protrusions (Jain, 2005). Defective basement membrane is also characteristic of tumour vasculature (Carmeliet & Jain, 2000; Tsuzuki *et al.*, 2000). All these changes in vascular architecture impair tissue perfusion and oxygenation which, in turn, additionally upregulate the already overexpressed angiogenetic factors. A vicious circle is formed that further exacerbates tumour hypoxia. It has been suggested that tumour cells try to escape this circle by increasing invasiveness and metastatic activities (Ebos *et al.*, 2009; Loges *et al.*, 2009). This would explain the clinically observed increased invasiveness and malignancy of hypoxic tumours.

2.1.3 Tumour perfusion

As a result of the dysfunctional vasculature described above the blood flow in malignant tumours is far from efficient. The flow is slower and sometimes even changes direction. Due to the irregular shape of vessels, blood cells are sometimes not able to pass and blood flow consists only of plasma with cells stacking into palisades (Molls *et al.*, 1998). Vascularisation and the ensuing tissue perfusion of tumours are also very heterogeneous with parts of high vessel density and parts of very low density. On the other hand, the flow may be interrupted by the sporadic vasospasms. Changes in vascular permeability also cause changes in interstitial pressure, which in conjunction with the disrupted vascular architecture, causes occasional vascular collapse. Due to overproduction of growth factors and the lack of coordination between them, tumour blood flow cannot be adjusted to the current metabolic demands of the tissue as is the case in normal tissues. All these changes result in intermittent periods of insufficient oxygen supply (Brown & Wilson, 2004).

In malignant tumours, not all blood components delivered to the tissue necessarily reach the cells. This is best described with the terms blood flow and tissue perfusion. While blood flow refers to the delivery of a volume of blood in a unit of time, the term perfusion is sometimes used to describe the physiologically efficient flow of blood through the tissue, i.e. blood flow per volume of tissue. In practice, however, the two terms often overlap. For reasons described earlier, these two parameters may differ significantly in malignant tumours.

This is of particular importance when evaluating methods for measuring these parameters in vivo. Due to their specific characteristics, some methods are not able to distinguish between the two while others are.

The values of blood flow vary greatly between studies. The differences are not only a consequence of the already mentioned high level of heterogeneity of tumour vasculature, but also due to the use of different methods for quantification of blood flow. While average blood flow in normal tissues varies depending on the tissue type from as low as 3 ml/100g /min in adipose tissue (Viljanen *et al.*, 2009) to around 250 ml/100g/min in stressed myocardium (Koivuviita *et al.*, 2009), the blood flow of malignant tumours seems to be independent of the tissue of origin. Typical for tumour blood flow is, on one hand, great heterogeneity and large standard deviation while, on the other hand, this deviation is independent of tissue type of origin. In its great variety, tumour blood flow usually has an average value between 30 – 50 ml/g/min. This is the case in head and neck cancer (Lehtio *et al.*, 2004), as well as, for example, in brain (Leenders, 1994; Mineura *et al.*, 1999; Bruehlmeier *et al.*, 2004) and pancreatic cancer (Komar *et al.*, 2009).

Perfusion has also been studied in tumours of the breast (Wilson *et al.*, 1992; Mankoff *et al.*, 2002; Zasadny *et al.*, 2003; Dunnwald *et al.*, 2008), kidney (Kudomi *et al.*, 2009), prostate (Muramoto *et al.*, 2002; Kurdziel *et al.*, 2003), liver (Yamaguchi *et al.*, 2000; Burke *et al.*, 2001), and lung (Logan *et al.*, 2002; Groves *et al.*, 2009).

2.2 TUMOUR HYPOXIA

The importance of oxygen in tumour biology and its role in radiation treatment resistance were first observed by Gray and co-workers in the 1950s (Gray *et al.*, 1953; Thomlinson & Gray, 1955; Gray, 1961). They demonstrated that patterns of necrosis in malignant lung tumours after irradiation are distributed in accordance with vessel architecture where necrotic cells are surrounding the vessels. This offered the first evidence in support of their hypothesis that oxygen is required for radiation therapy to be effective.

2.2.1 Availability of oxygen in normal and tumour tissue

Oxygen is needed for normal and effective utilization of energy in most tissues of the human body. As mentioned above, normal partial pressure (normoxia) of oxygen in well-perfused tissues is around 15-65 mm Hg. This level can be much lower in tissues like bone marrow or thymus (Vanderkooi *et al.*, 1991). Despite being low, these levels can still be considered normal, since the tissues function normally.

Hypoxia, on the other hand, is typical for many pathological conditions like wound healing or ischemic cardiac disease. It is also a typical feature of high altitude environments and altitude sickness associated with it. Since oxygen is delivered to the tissues via the red blood cells it is vital that the vasculature in this tissue is sufficient and functional.

Due to abnormalities in vascular architecture and the following irregular blood perfusion, the perfusion levels are much lower in solid malignant tumours, and hypoxia is a typical characteristic of most solid malignant tumours. Tumour hypoxia is usually defined as pO_2 below 10 mm Hg, and clinically significant hypoxia is most commonly defined as pO_2 below 2.5 mm Hg (Vaupel & Mayer, 2007). Level of oxygen in the tissue is of course continuous parameter and at different levels it affects different processes in the cell. While the effect of radiotherapy is becoming noticeable at levels below 15 mmHg, the molecular mechanisms become disturbed at pO_2 levels below 10 mmHg, and genetic instability only becomes evident at levels below 5 mmHg or even lower than 1 mmHg (Hockel & Vaupel, 2001).

Due to this reason, due to the technical limitations in measuring tissue pO_2, and due to the dynamic nature of hypoxia, it is very difficult *in vivo* to determine any precise, clinically relevant pO_2 level/cut-off value.

The presence of hypoxia has been demonstrated, for example, in head and neck, cervical, breast, colon, and brain tumours (Molls *et al.*, 1998). Hypoxia gained the attention of the wider scientific community in the late 1990s when it was recognised that, in addition to being an obstacle in radiation treatment, it is also an important factor in the progression of both the genotype and phenotype of malignant tumours (Osinsky *et al.*, 2009).

Tumour hypoxia can be roughly divided into chronic and acute with several different subtypes (Bayer *et al.*, 2011). Chronic hypoxia is a consequence of the irregular vascularisation described above, which results in large distances between blood vessels and cells. Since oxygen can only diffuse for approximately 150 μm (Horsman, 1998) from vessels into tissue, cells beyond this distance are in a permanently hypoxic environment and usually do not survive (Figure 2).

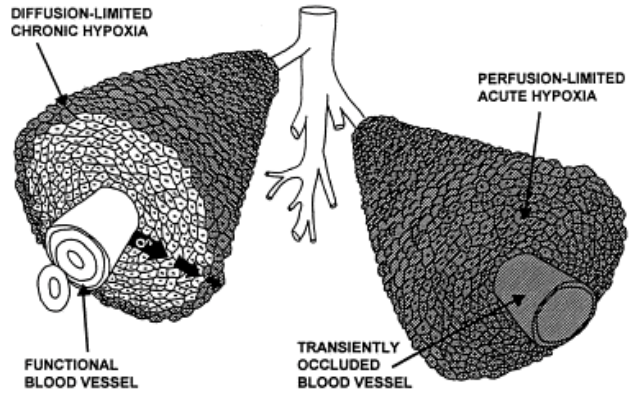

Figure 2 – Diffusion-limited hypoxia of malignant tumours (Horsman, 1998)

For this reason, chronic hypoxia is often referred to as diffusion-limited hypoxia. On the other hand, acute hypoxia is a result of tumour vessels' functional instability which might cause vessels to suddenly contract in a vasospasm, become transiently occluded for blood cells (while still allowing the flow of plasma), or become permanently occluded by thrombosis. For this reason acute hypoxia is also referred to as perfusion-limited hypoxia, which is believed in most cases to be of a transient or even cyclic nature.

While hypoxia in itself has a negative effect on cell proliferation and survival it is also a strong selecting factor, favouring the survival of cells that are more likely to survive therapeutic attempts to eradicate them. Since hypoxia is a consequence of poor vascularisation and blood flow, hypoxic tumours are harder to reach with chemotherapeutics via the blood stream. In addition to this, most current chemotherapeutic agents affect only dividing cells and are therefore less efficient against rather non-dividing hypoxic cells. As mentioned above, the presence of oxygen also plays a crucial role in radiation therapy.

2.2.2 Metabolic adaptation to hypoxic environment and its consequences

As mentioned above, low levels of oxygen are not an insurmountable obstacle for tumour cells and do not even necessarily prevent cells from proliferating (Ljungkvist *et al.*, 2002). Tumour cells form a population under strong selective pressure, and due to the relatively high proliferation rate, this may result in the survival of resistant cell clones. This type of change has been observed in vitro (Smalley *et al.*, 2005) and also may explain the more aggressive phenotype of hypoxic tumours (Rofstad & Danielsen, 1999; Evans & Koch, 2003).

On the molecular level, hypoxia induces complex coordinated mechanisms often referred to as hypoxic response. The central role in this mechanism is played by hypoxia inducible factors (HIF) and, in particular, by HIF-1α, but there are also other

systems responsive to oxygen levels such as nuclear factor κB (NF- κB), p53, activating transcription factors (ATFs) and, in particular, AMP-activated protein kinase (Graeber *et al.*, 1994; Blais *et al.*, 2004; Cummins *et al.*, 2007; Ahn *et al.*, 2012).

These mechanisms eventually lead to the prognostically negative phenotype of hypoxic tumours. HIF-1α is directly or indirectly responsible for changes in oxygen transport and delivery, changes in glucose metabolism, changes in cell cycle and proliferation, transcriptional regulation, and even cell migration. These changes enable cells to survive in conditions of low oxygen availability or, alternatively, trigger controlled cell death if hypoxia is too severe.

2.2.3 Molecular markers for the detection of tumour hypoxia

Currently among the most relevant molecular markers for hypoxia are HIF-1α and carbonic anhydrase IX (CA IX). These are at the moment at the centre of intense efforts to identify potential molecular markers suitable for diagnostic and prognostic use. However, there are also many other markers being investigated (Toustrup *et al.*, 2012).

Alongside HIF-1α, the HIF family of transcriptional factors also includes HIF-2α and HIF-3α. While HIF-1α and HIF-2α have been relatively extensively studied, the role of HIF-3α is relatively poorly understood. While there is some overlap between the functionality of HIF-1α and HIF-2α, they also seem to have specific roles. However, as noted by Mayer et al. (Mayer *et al.*, 2008), it must be kept in mind that despite the strong correlation of these markers to hypoxia in vitro, this is not transferable to the clinical assessment of oxygenation status in patients in a clinical setting.

2.2.3.1 HIF-1α

HIF-1 is formed by two subunits α and β. While both units are constitutively expressed, only the β subunit can be detected in cells in a normoxic environment. Under these conditions, the α subunit is hydroxylated by prolyl-hydrohylases (PHD) in an oxygen-dependent manner and later degraded by proteasome (Jiang *et al.*, 1996a). In hypoxic conditions, on the other hand, hydroxylation and the subsequent degradation are reduced. The intact HIF-1α enters the nucleus where it combines with the β subunit to form the final HIF-1 complex. This complex acts as a transcription factor by binding to hypoxia-responsive elements of the DNA, resulting in expression of a plethora of hypoxia-related genes producing the hypoxic response. The levels of HIF-1α increase exponentially as pO_2 levels decline (Jiang *et al.*, 1996b), and it could therefore serve as a molecular marker for hypoxia detectable in tissue samples or even in blood or plasma samples. This has indeed been investigated in several studies.

HIF-1α is over-expressed in a wide range of malignant tumours raging from head and neck cancer through breast cancer and pancreatic cancer to melanoma and ovarian cancer (Semenza, 2010). It correlates with poor prognosis in breast cancer

(Giatromanolaki *et al.*, 2001) and particularly in head and neck cancer (Aebersold *et al.*, 2001; Hui *et al.*, 2002; Koukourakis *et al.*, 2002).

Regardless of the results, the method for determining tissue HIF levels requires a biopsy sample (unless detectable in blood samples) to be obtained, and the method is therefore poorly suited to routine clinical use in tumours not close to the surface of the body. Even though biopsy samples are often obtained for diagnostic purposes, the sample might not be representative due to heterogenous and irregular distribution of hypoxia inside the tumour. This is additionaly complicated by the complex relationship between the oxygenation of the subcutaneous metastatic lymph nodes and the primary tumour, despite some studies reporting a significant effect on treatment and treatment outcome based on lymph node status (Toustrup *et al.*, 2012). This study, however, is based on differences in expression of several hypoxia-related genes and not hypoxia directly which might increase uncertainty in the interpretation of the results.

2.2.3.2 CA IX

In the hypoxic tumour environment, the glycolytic pathway finally results in the production of lactic acids. Since the intracellular pH has to be tightly regulated to maintain the integrity of cellular mechanisms, these products are excreted into the extracellular space (Gatenby & Gillies, 2004; Chiche *et al.*, 2010a). Several mechanisms are employed by the tumour cell to ensure the constant intracellular pH. Carbonic anhydrase IX (CA IX), a transmembrane protein that catalyzes a simple but fundamental reaction, reversible CO_2 hydration to yield bicarbonate and protons. CA IX is one of the carbonic anhydrase (CA) family members to participate in a variety of fundamental biological processes, including respiration, calcification, acid-base balance, and, for example bone resorption. CA's show great diversity in tissue distribution and in their subcellular localization, CA IX, however, seems to be the only tumor-associated carbonic anhydrase isoenzyme known. Its expression and activity have been shown to directly and robustly correlate with HIF-1α function (Wykoff *et al.*, 2000; Olive *et al.*, 2001).

The correlation of CA IX with poor prognosis has been studied in many types of cancer, and most studies have found CA IX to be a negative prognostic factor of outcome. While this is true for breast cancer and lung cancer, the results found in head and neck cancer, rectal cancer, bladder cancer, and renal cancer are somewhat conflicting (for an extensive review see (Chiche *et al.*, 2010b). This might be explained by a non-straightforward correlation between CA IX expression and direct hypoxia staining found in some recent studies (Troost *et al.*, 2005; Hoogsteen *et al.*, 2009).

The antybody cG250 (Girentuximab), primarily developed for the therapeutic targeting of CA IX, has recently also been successfully used for the purpose of detection and quantification of CA IX in tumours in vivo. The main area of use for this probe is in

the detection and characterization of clear cell renal cell carcinoma (CCRCC). Characteristic of this type of cancer is the importance of the mutation of the von Hippel-Lindau gene which leads to over-expression of HIF-1α which, in turn (in about 95% of CCRCC cases), leads to over-expression of CA IX. This has resulted in a rather promising diagnostic and, at the same time, prognostic probe in this type of cancer.

2.2.4 Quantification of tumour hypoxia

Due to the growing acceptance of the important role in cancer development, several direct or indirect methods for detecting tissue hypoxia have been developed during the last decade. While direct methods aim to measure the level of oxygen in the tissue, indirect methods are based on detecting changes in tissue related to low levels of oxygen. Among indirect methods are histomorphometric studies (Mueller-Klieser & Walenta, 1993), evaluation of tissue's radiation response (Rockwell & Moulder, 1990), imaging of vascular endothelial growth factor or vascular density. These changes have a complex correlation with hypoxia and cannot be used as a simple substitute for measuring low levels of oxygen.

Measuring hypoxia also differs significantly from imaging, since the purpose of measuring is to obtain precise values of the level of oxygen present in the tissue at a certain time point (Raleigh *et al.*, 1996). This is particularly important since hypoxia is a continuous process and the border for clinically significant hypoxia is set arbitrarily (Hockel & Vaupel, 2001).

2.2.4.1 Invasive methods

The first method that allowed direct in vivo measurements of pO_2 was developed in the the 1980's using the computerized polarographic needle electrode system (Kallinowski *et al.*, 1990; Hockel *et al.*, 1991; Vaupel *et al.*, 1991). The method is based on mechanically stable O_2 sensors and is often referred to as Eppendorf® polarography after the manufacturer. It comprises the sensor in the shape of a fine needle which is positioned in the investigated tissue. The readings are made in a systematic manner with the needle held firmly in position and being automatically retracted in equal steps, resulting in a matrix-like patern of pO_2 readings and, finally, in a histogram of pO_2 distribution. The importance of hypoxia for the disease prognosis soon became clear and the method is still today considered by many to be the gold standard for evaluation of tissue oxygenation (Vaupel *et al.*, 2007). However, the method does have drawbacks that have initiated an intensive search for new methods of hypoxia quantification. The most important drawback is its invasive nature. Despite the electrode needle being very thin, it has to be inserted into the investigated tissue which, on one hand, prevents it from being of serial use, and on the other hand, limits its use to easily accessible tumours. Lymph node metastases of head and neck tumours are comparatively easily accessible and, for this reason, there are substantial amounts of data which have

established the high prevalence of low oxygen levels in this type of tumour and its importance for disease prognosis (Nordsmark *et al.*, 2005). Another important drawback is the method's inability to discriminate between hypoxic but vital and necrotic tissue. Particularly since large areas of tumours are known to be necrotic this is a relevant problem of clinical importance.

An alternative way of quantifying tissue hypoxia is by analysing tissue samples *in vitro*. Prior to obtaining the sample, the patient is given an intravenous dose of a compound which accumulates in areas with low levels of oxygen. After some time, a sample of the tissue is obtained and analysed *in vitro* using immunohistochemical methods. The most widely available and used compound in this class is pimonidazole (Varghese *et al.*, 1976; Varia *et al.*, 1998; Olive *et al.*, 2000; Kaanders *et al.*, 2002). Pimonidazole belongs to the family of nitroimidazole compounds, which have a long history of use in hypoxia research (Raleigh *et al.*, 1996). The binding of pimonidazole has been shown to correlate with oxygen levels (Arteel *et al.*, 1995; Arteel *et al.*, 1998) and with clinical outcome (Kaanders *et al.*, 2002). The binding of pimonidazole can be quantified with microscopic as well as autoradiographic analysis of the tissue samples (Wijffels *et al.*, 2000) or flow cytometry (Durand & Raleigh, 1998), with both producing reliable results. However, significant problems of tumour accessibility and sample representiveness associated with the methods mentioned above have spurred intensive investigation into non-invasive methods of hypoxia quantification.

2.2.4.2 Noninvasive methods

Non-invasive methods for measuring hypoxia *in vivo* are, understandably fewer than invasive and could be divided into nuclear medicine techniques and magnetic resonance techniques. All of these clinically relevant techniques are based on labelling of a carrier molecule with the modality specific probe. This molecule has in almost all cases been a nitroimidazole compound. This is true for scintigraphy (labelled with ^{m99}Tc) (Linder *et al.*, 1994) and SPECT (^{123}I label) (Groshar *et al.*, 1993) as well as PET (mostly ^{18}F- and ^{124}I-labelled) (Minn *et al.*, 2008) and magnetic resonance spectrometry (^{19}F-labelled) (Jin *et al.*, 1990; Li *et al.*, 1991; Cline *et al.*, 1994; Cline *et al.*, 1997).

Of these, PET with its small tracer quantities, quantitative nature and the almost limitless number of tracer possibilities has turned out to be the most promising tool for the task.

Despite having in general a lower spatial resolution than invasive methods, non-invasive methods have a crucial advantage over invasive ones: they can be used in vivo in routine clinical settings and can therefore be applied in conjunction with therapy planning of tumours in almost all parts of the body. In addition they visualise the heterogeneity of the tumour and can be used repeatedly during the course of treatment providing information on the changes in these processes and the effects of treatment, potentially enabling its adjustments.

2.3 NONINVASIVE IMAGING OF TUMOUR MICROENVIRONMENT

The tumour microenvironment can be investigated using both invasive and non-invasive methods. While invasive methods are more accurate and allow more precise characterization of tissues, these tissues or tissue samples need to be physically removed from the patient and for this reason they are not suitable for routine daily use. In addition, these methods are not able to depict dynamic physiological phenomena like blood flow. For these reasons, noninvasive methods are being developed that could successfully identify and quantify physiological processes in tumour microenvironment prior to therapy. These methods are often referred to as functional imaging, since instead of anatomical structure they depict the functions of the tissue.

Tissue functionally can be to a varying degree characterized with MRI, CT, ultrasound, SPECT, and PET. All these methods have their advantages and their weaknesses; however, PET is widely regarded as currently the most promising non-invasive tool for molecular and functional characterization of tissues *in vivo*.

2.3.1 Principles of PET

PET is a non-invasive imaging method using positron-emitting isotopes and gamma radiation to detect and quantify physiological and pathological processes *in vivo* (Valk, 2003). This is achieved with the use of compounds normally found in the body, their synthetic analogues, antibodies or receptor ligands labelled with a positron-emitting radionuclide. After being injected into the body, these compounds spread throughout the organism and take part in physiological or pathological processes taking place in the body. Due to their radionuclide label their fate can be observed with the use of a PET scanner.

Almost any molecule can be labelled with a radionuclide to form a PET tracer. The decision about which molecule to use depends on the ability of this compound to deliver meaningful information about a certain biological process in the body. This process can be, for example, blood flow (H_2O), tissues energy metabolism (FDG), expression of cell-membrane receptors, activity of brain receptor systems, tissue hypoxia, or cell proliferation rate.

Positrons are being emitted during the process of nuclear decay where a proton is converted into a neutron, a positron, and a neutrino. This happens because of the surplus of protons in the atomic nucleus and the unstable nature of such nuclei. Positrons are positively charged particles with a mass equal to that of electrons and are as such antiparticles. Positrons, like antimatter in general, react with their antiparticles electrons in a process called annihilation in which mass is converted into energy according to the equation $e=mc^2$. This energy is manifested in the form of two photons

each with an energy of 511 keV that are travelling in opposing directions from the point of annihilation at an angle of approximately 180°.

The most commonly used positron-emitting isotopes are ^{11}C, ^{13}N, ^{15}O, ^{18}F and ^{68}Ga (Table 2).

The process of annihilation takes place only once the emitted positron has lost some of its initial kinetic energy after travelling a certain distance from the point of emission from the nucleus. This distance depends on the type of medium in which the emission takes place. Since the energy of the positron varies depending on the isotope, the distances are different for different isotopes. In the human body, these are comparable to distances travelled in water which are presented in Table 1 (Valk, 2003).

Table 1 – Properties of clinically most commonly used positron-emitting nuclides

Nuclide	E_{max}(MeV)	E_{mode}(MeV)	$t_{1/2}$(min)	Range in water (mm)	
				Max	Mean
^{11}C	0.959	0.326	20.4	4.1	1.1
^{13}N	1.197	0.432	9.96	5.1	1.5
^{15}O	1.738	0.696	2.03	7.3	2.5
^{18}F	0.633	0.202	109.8	2.4	0.6
^{68}Ga	1.898	0.783	68.3	8.2	2.9

The mean range of the poisitron is an important factor from the point of image quality by presenting an objective lower limit to the resolution. This limit can be to some extent compensated for in image instrumentation and processing, but can not be entirely overcome.

The PET scanner is composed of a ring of detectors surrounding the patient, detects and registers the gamma photons of a certain time and energy window in order to separate true events from randoms and scatter to determine lines of response (LOR). The spatial distribution of annihilation events in the object/body is reconstructed using mathematical methods common to all tomographic imaging methods like CT and MRI.

The spatial resolution of the final image depends on many factors from the positron range through detector materials and electronics used in the scanner to reconstruction methods. Currently, the resolution of the whole-body PET scanners in clinical use is in the range between 4-6 mm while dedicated micro PET-cameras for use in small animals have a resolution of 1-2 mm.

Due to its relatively poor spatial resolution and due to the functional character of its images, PET has recently been combined with a CT camera to form a hybrid PET/CT system. This combines the functional information provided by PET with the superior spatial resolution and anatomical information provided by CT. PET/CT has quickly become the new clinical standard. Currently, combined PET and MRI cameras are being developed by most manufacturers.

However the innate low resolution of PET is not only a diagnostic problem, but also presents a problem in planning specific therapies where spatial distribution inside the tumour is of great importance. This might be the case also in the use of very precise irradiation techniques in the case of hypoxia-based target delineation and represents an issue which must be addressed in future studies.

2.3.1.1 Production of PET tracers

PET tracers are molecules labelled with a positron-emitting isotope. This isotope is usually one of the nuclides in the Table 1, but also other positron emitting isopotes are being used. The production of tracers is in the domain of radiopharmaceutical chemistry. Radionuclides are produced either with cyclotrons (^{11}C, ^{13}N, ^{15}O, ^{18}F, ^{64}Cu, ^{89}Z) or generators (^{68}Ga). A cyclotron is an accelerator used to propel charged particles (like protons) to energies that allow nuclear reactions, and alterations of the structure of the target nucleus. The resulting isotopes are unstable and are used to label the target molecule. In the case of ^{18}F production, enriched water ($[^{18}O]H_2O$) is bombarded with hydrogen ions creating ^{18}F. The target molecule can be almost any compound from a simple water ($[^{15}O]H_2O$) molecule to complex peptides ($[^{68}Ga]$DOTATOC).

Since the purpose of PET imaging is detection and quantification of a biological process, the use of a molecule as a PET tracer demands careful pharmaceutical, pharmacological, and biological characterization of its biological behaviour. This characterization is performed in cell cultures, animal models, and, finally, in the human organism.

2.3.1.2 PET image acquisition

As already mentioned the PET image is based on registration of the gamma photons travelling in opposite directions from the point of annihilation. They are registered using ring detectors surrounding the imaged object or subject (Figure 3).

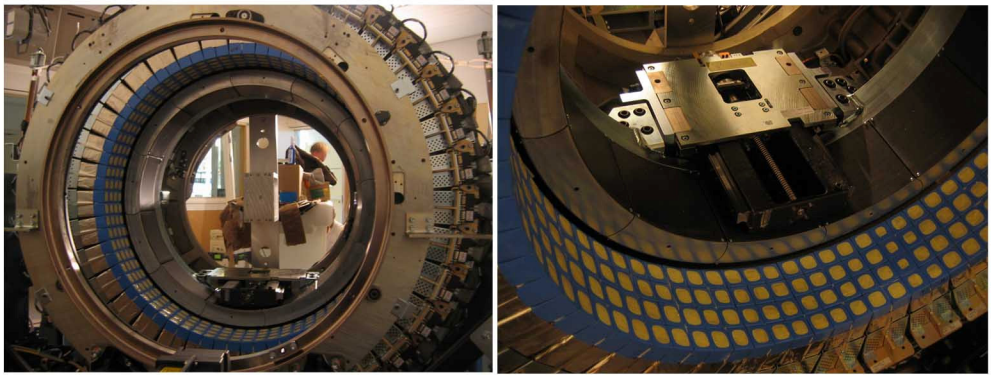

Figure 3 – Photographs of the construction of PET detector rings (Image courtesy of Mika Teräs, Turku PET Centre)

These detectors are composed of scintilator crystal and photomultiplier tubes which convert gamma rays into visible light. This light signal is in turn converted to electrical impulses by photodiodes. The electrical signal is converted into digital information using analogue-to-digital converters (ADC). This information undergoes signal processing and the process of image reconstruction in computers to obtain final tomographic images of spatial and, in the case of dynamic images, also chronological distribution of annihilation events.

There are several ways of describing the observed biological process using PET images. These reach from purely qualitative through semi-quantitative to rigorously quantitative.

The precise quantification of a biological process requires the development of mathematical models which are used as a link between the observed behaviour of the tracer in the PET image and the true, quantified values of the process. For this purpose, images are often acquired in a dynamic fashion allowing for time changes in the system to be integrated into these models. In parallel to image information, information on tracer concentration in blood is often needed for complete quantification.

2.3.2 PET imaging of tumour perfusion

Blood flow can be non-invasively quantified to a varying extent by the use of dynamic contrast-enhanced computed tomography (dCE CT), magnetic resonance imaging (MRI), ultrasound, single photon emission computed tomography (SPECT), or PET. Of these methods, PET is considered the most precise in quantification and the most widely validated (Anderson & Price, 2002). Like any other method measuring blood flow, PET has advantages as well as disadvantages.

Among the strongest advantages is its ability to precisely quantify the blood flow, resulting in direct values of ml/100g/min. This has been validated in the myocardium, kidney, brain, tumours, and several other organs. This is mostly due to the minute quantities of tracers which do not interact with the system they measure and therefore do not influence the measured parameter. The second reason is the nature of $[^{15}O]H_2O$, which is a freely diffusible molecule and, as a result, does not require complex modelling assumptions. For the same reason, variations in tumour type, patient size, vascular structure, etc. have a lesser effect on tracer behaviour and the quantification is therefore more robust (Anderson & Price, 2002).

A disadvantage is no doubt the above-mentioned relatively poor spatial resolution of the PET images, which prevent the analysis of very small regions of interest. However, in the case of perfusion imaging this has to a large degree been compensated for with the introduction of combined PET/CT machines.

The use of short-lived isotopes for labelling allows repeated studies to be performed in relatively short succession. However, these isotopes also require on-site and in the case of ^{15}O even on-line cyclotron production of the tracer, making the method expensive and logistically demanding.

2.3.2.1 PET tracers for imaging perfusion

The most common PET tracer for imaging blood flow is currently $[^{15}O]H_2O$. As already mentioned, due to its high permeability, it has several advantages compared to other tracers when it comes to modelling the data. But it also has some disadvantages. Due to its very short half-life of approximately 2 minutes (122.24 s), the tracer has to be produced on-line, meaning that the cyclotron-based production takes place virtually synchronously with the tracer's infusion into the patient. This requires the on-site presence of cyclotron which is expensive and logistically demanding. A second disadvantage is the relatively high kinetic energy of the positron produced during the decay of ^{15}O. This means that the distance travelled by its positron before being annihilated (2.5 mm) by an electron is longer than that of some other isotopes like ^{18}F (1.5 mm), potentially resulting in lower spatial resolution of the ensuing images (Valk, 2003).

Research on PET perfusion imaging is most intense in the cardiovascular field where many other tracers have been tested or validated. Among these are $[^{15}O]CO_2$, $[^{11}C]$Acetate, $[^{13}N]$Ammonia (Herzog *et al.*, 2009), ^{82}Rubidium (El Fakhri *et al.*, 2009), $[^{62}Cu]$PTSM and isotope-labelled microspheres. However, all these tracers suffer from some degree of non-linearity of uptake in correlation to blood flow values, particularly at high blood flow levels (Knuuti *et al.*, 2009).

Currently several ^{18}F-labelled tracers for imaging perfusion are being developed due to their advantages in the production and in image quality of the ^{18}F isotope as compared to short-lived cyclotron-based isotopes (Nekolla & Saraste, 2011).

Also ^{68}Ga-based tracers are being developed due to their advantages in the field of tracer synthesis and longer tracer half life (Plossl *et al.*, 2008).

2.3.2.2 Modelling and quantifying the [^{15}O]H_2O data

The purpose of the modelling of PET data is to be able to obtain precise quantitative values of a biological process based on information obtained from PET images. The PET image depends on the spatial and chronological distribution of the PET tracer, and does not always directly correlate with the magnitude of the investigated biological process. Therefore, mathematical modelling is often needed to obtain the results. A mathematical model is a tracer-, tissue- and process-specific equation used to calculate these values using image and sometimes blood information as input values. Most often a new model has to be developed and validated for each new tracer before it can be used in quantification of PET data.

The methods to measure perfusion with [^{15}O]H_2O are based on the principle of exchange of inert gas between blood and tissues. [^{15}O]H_2O is a fairly simple tracer since it is not metabolised in the body and the bond between the radionuclide and the rest of the molecule is very stable. Additionally, water is a very diffusible tracer that can freely cross cell membranes and other barriers between tissues. For these reasons a simple model comprising only a plasma compartment and a tissue compartment can be used and is therefore referred to as the two-compartment model or one tissue-compartment model. This model is used to describe the kinetics of [^{15}O]H_2O (diffusible tracer) concentration in the tissue, depending on the concentration in arterial blood, perfusion or blood flow, and the partition coefficient of water (Figure 4).

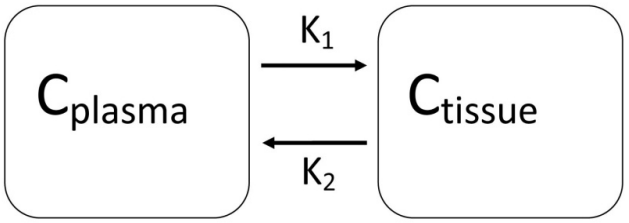

Figure 4 – A simple graphic depiction of the one tissue-compartment model

To obtain the parametric blood flow image a dynamic [^{15}O]H_2O image and the input plasma curve are needed. The duration of the dynamic image varies somewhat between methods, but usually a 5-10 minutes dynamic image with an initial 5 s framing is needed.

To minimize the inter-patient variations, automated injection methods are often used. These aim to deliver the same amount of tracer activity in the same time frame. This minimizes differences in the shape of the initial tracer peak after injection which plays a role in the subsequent modelling. The plasma curve can be obtained either invasively using arterial sampling or by arterialized venous blood sampling. Sampling is most often performed with the help of a blood pump providing a steady blood flow rate (6 ml/min) through the activity meter. This measured curve is then corrected for delay and dispersion (Iida *et al.*, 1986) before being used as the input function in model fitting.

Due to the invasive nature of the arterial sampling, several alternatives have been developed. The most commonly used are image-derived curve extractions and population-based curves.

2.3.3 PET imaging of tumour energy metabolism

Energy metabolism can be imaged using the glucose analogue [^{18}F]FDG. This is an acronym for 2-deoxy-2-[^{18}F]fluoro-D-glucose. Glucose is most often the primary source of energy (also) in tumour cells. Since 2' hydroxyl group (-OH) in normal glucose is needed for further glycolysis, [^{18}F]FDG cannot be used as an energy source. Even though phosphorylation of FDG is a reversible process, due to the high rate-constant [^{18}F]FDG is effectively trapped inside the cell. For this reason [^{18}F]FDG is well suited to evaluate glucose uptake and the energy metabolism of these cells. However there are some differences between [^{18}F]FDG and glucose which need to be taken into account when doing so.

2.3.3.1 Quantifying the [^{18}F]FDG data

As mentioned above, glucose is actively transported into cells by a group of glucose transporter proteins called GLUT. [^{18}F]FDG has a slightly higher affinity for these transporters than glucose. Once inside the cell both glucose and [^{18}F]FDG undergo phosphorylation by hexokinase which favours glucose over [^{18}F]FDG. These differences are compensated for by the use of the so-called lumped constant (Sokoloff, 1977; Wu *et al.*, 2003). This constant is, for example affected by obesity and diabetes (Peltoniemi *et al.*, 2000). In tumours this relationship between uptake and phosporylation can be deranged, and the processes of glucose transport and phosphorylation can become uncoupled somewhat decreasing the predictability and precision of quantification of glucose metabolisms by [^{18}F]FDG PET (Herholz *et al.*, 1988).

Another factor affecting the imaging properties of [^{18}F]FDG is the plasma glucose level, which primarily affects the transport of both tracer and glucose into cells. Higher plasma levels of glucose slow down this uptake, while low levels facilitate it. This needs to be taken into account particularly when comparing values between different

subjects (Minn *et al.*, 1993; Kroep *et al.*, 2003; Krak *et al.*, 2004). Blood glucose levels should be checked prior to a [^{18}F]FDG PET scan. These levels are most often normalized (4-7 mmol/L) by a standard 4-hour fast before the scan. If this is not the case and the glucose levels remain high (> 8-11 mmol/L) the scan should be rescheduled (Boellaard, 2009).

[^{18}F]FDG images can be used in several different ways with a varying degree of quantification covering the entire above-mentioned spectrum from qualitative to quantitative. Since [^{18}F]FDG is clinically most widely used tracer in PET scanning, qualitative visual interpretation is the most often used way of describing these images in clinical diagnostic work. In some cases, qualitative evaluation even has diagnostic advantages over quantitative methods (Lapela *et al.*, 2000).

Semi-quantitative methods (SUV and fractional uptake ratio or FUR) are often used in simpler applications. Since they do not require advanced image acquisition protocols or image and data manipulation, their great advantage is their simplicity. The standardized uptake value (SUV) is an example of such a simplified measure, and it is now probably the most

widely used method for the quantification of [^{18}F]FDG PET studies, although other measures have been developed as well (Hunter *et al.*, 1996; Graham *et al.*, 2000). The SUV represents the [^{18}F]FDG uptake within a tumour, measured over a certain interval after [^{18}F]FDG administration and normalized to the dose of [^{18}F]FDG injected and to a factor (such as body weight) that takes into account distribution throughout the body (22,23). The SUV normalized to body weight is given by the following equation (Equation 1):

$$\mathrm{SUV} = \frac{\mathrm{A\ (kBq/ml)}}{\mathrm{ID\ (MBq)\ /\ BM\ (kg)}} \qquad \text{Eq. 1}$$

Equation 1 – The equation for calculation of SUV: A - measured activity in the region of interest; ID - injected tracer dose; BM - body mass.

The normalization factor BM can be substituted with body surface area or lean body mass to produce more accurate results (Graham *et al.*, 2000). These methods, however, have not gained wider clinical acceptance.

SUV is commonly used in clinical imaging; however, despite its advantages it is to varying degrees affected by technical, biological, and physical factors (Reviewed in (Boellaard, 2009), and therefore standardization is required when comparing values from different time periods or centres (Westerterp *et al.*, 2007).

The most rigorous quantitative methods also require most effort in terms of image acquisition and post acquisition processing. Among these, Multiple-time graphical

analysis (MTGA) also known as Patlak analysis (Patlak & Blasberg, 1985) and compartmental model fitting are most commonly used (Reivich *et al.*, 1979). They provide quantitative measures of true physiological processes. MTGA provides a combined uptake rate of glucose while compartment model fitting provides quantitative values for each of the rate-limiting steps (included in the model) in the process of glucose uptake and metabolization. For the quantification of glucose metabolism a three-compartment model with four rate constants K_1*, k_2*, k_3* and k_4* is most often used (Minn *et al.*, 1995). The calculation of these values requires not only modified imaging protocols usually including dynamic image acquisition, but most often also blood sampling. This makes the process of obtaining these values not only more time-consuming and expensive, but also less patient-friendly. For this reason, these methods are used primarily in scientific work exploring the functioning of different tissues and tumours and much less in diagnostic work. It was also observed that these methods add little in terms of improved diagnostic differentiation between malignant and normal tissues compared to qualitative and semi-quantitative methods (Graham *et al.*, 2000; Lapela *et al.*, 2000).

2.3.4 PET imaging of tumour hypoxia

Due to its non-invasive and functional nature PET is ideally suited for imaging hypoxia in tumours and in recent years, great efforts have been invested in developing new imaging tracers, imaging protocols, and quantification methods for detection of tissue hypoxia *in vivo*.

2.3.4.1 PET tracers for imaging hypoxia

In order for a compound to be used as a PET hypoxia tracer it should have highly specific binding to viable hypoxic tissues, as well as low non-specific binding and rapid washout in normoxic tissues providing a high target-to-background signal. This is particularly important due to the relatively low spatial resolution of PET cameras, which decreases the activity of small uptake areas due to the partial volume effect.

The compound should also be able to readily diffuse between different tissues, to cross the blood brain barrier and cell membrane. This is important for the even distribution of the tracer in the body. The diffusibility is usually achieved by the high lipophylicity of a compound which is often measured using octanol-water partition coefficient or the logarithm of this value also referred to as log-P. The higher the log-P the more lipophilic a compound is. Due to differences in methodology, these values may differ in different reports; nevertheless some examples are given in Table 2.

Table 2 – Log-P values of most hypoxia tracers studied in humans (Modified based on (Gronroos, 2006)).

Tracer	***LogP***
Pimonidazole	8.5
[^{18}F]FMISO	0.40 – 2.6
[^{18}F]FETA	0.16
[^{18}F]FAZA	1.1
[^{18}F]EF1	0.35
[^{18}F]EF3	1.12
[^{18}F]EF5	5.7
[^{18}F]FETNIM	0.17

However, the high lipophilicity and the resulting high tissue penetration also mean that there is more undesirable non-specific binding to larger lipid and protein molecules which might in fact reduce the amount of freely available tracer in the blood. For these reasons, high logP values were in the recent past seen as negative characteristic of a potential PET-tracer. Wong and Pomper, for example, suggest the value of logP 5 as the upper limit (Wong & Pomper, 2003). However, recent studies have somewhat undermined this assumption and Pike suggests that high logP values may not be as important a hindrance as previously thought if other properties of the molecule are right (Pike, 2009).

In addition to lipophilicity, reduction potential (also called redox potential) also plays an important role. Redox potential decribes the tendency of a compound to acquire electrons from the environment and thereby be reduced. This is relevant since most hypoxia markers use the principle of controlled, hypoxia-dependent reduction and oxygenation as the mechanism for the detection of the oxygen levels and intracellular trapping. The higher the redox potential of a compound the greater its tendency to obtain electrons from the environment.

Another important consideration is the chemical stability of the compound. If the compound is not being metabolized by the organism, it is possible to obtain a hypoxia-specific signal even several hours after the tracer has been administered to the patient. The chemical stability of the compound is also important in the case of pharmacokinetic analysis and should be taken into account in the process of hypoxia quantification.

2.3.4.2 Nitroimidazole compounds

Imidazole compounds were initially used as antibiotics for the treatment of anaerobic bacterial infections. A member of this group, metronidazole, for example, is still to date used for the treatment of *Clostridium difficile* infections. Later, imidazoles were also used as radiosensitizers of hypoxic cells and as hypoxic cytotoxins (Varghese *et al.*, 1976). However, the high doses of these agents required to achieve a hypoxia-specific cytotoxic effect resulted in unwanted side-effects and prevented their clinical application (Dische *et al.*, 1982). Because of the much lower doses needed, it was soon proposed that these agents could, in trace amounts, be used as hypoxia markers and the use of radiolabelled nitroimidazole-based compounds for the imaging of hypoxia was proposed by Chapman as early as 1979 (Chapman, 1979).

While new, non-nitroimidazole hypoxia markers are emerging, for these historic reasons, most of the currently available PET hypoxia tracers belong to the group of nitroimidazole compounds. Nitroimidazole compounds have a common structure based on the imidazole ring which is a 5-membered planar nitroheterocycle (Figure 5).

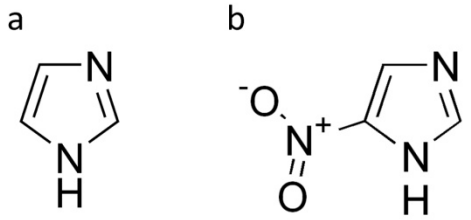

Figure 5– a) Imidazole ring structure and the b) nitro-imidazole

Nitroimidazole-based compounds enter the cell by free diffusion in which the compound's lipophilicity plays a crucial role. The more lipophilic the compound the more easily it crosses the cell membrane. The hypoxia specific binding of these compounds is achieved by intracellular reduction which, in normoxic conditions, is quickly reversed. In the absence of oxygen, however, the compound remains in its reduced state and undergoes further reductions resulting in highly reactive products (Workman, 1992). These, in turn, bind to intracellular macromolecules, probably to DNA (Edwards, 1993). However, the precise mechanism is not yet entirely clear.

[^{18}F]FMISO

The nitroimidazole was further developed to achieve better pharmacokinetic and pharmacodynamic properties, and several compounds have undergone the early stages of testing. Of these, the most extensively studied PET tracer is ^{18}F-labelled fluoromisonidazole ([^{18}F]FMISO) (Lee & Scott, 2007). [^{18}F]FMISO has been studied in animals as well as in humans and is currently the most widely used PET hypoxia tracer (Figure 6).

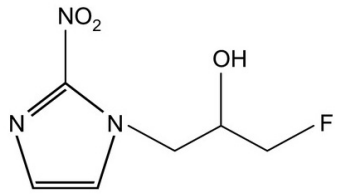

Figure 6 – The imidazole-derived structure of FMISO.

FMISO has several unfavourable characteristics that limit its performance as a hypoxia PET tracer, the most important of which are the relatively fast metabolism of the compound and the relatively slow tissue penetration (Krohn *et al.*, 2008). Due to the resulting relatively low signal-to-background ratios, it has not fully satisfied the needs of researchers and clinicians. Since these two important drawbacks are believed to be modifiable the search for better hypoxia-imaging agents has resulted in a growing number of nitroimidazole-based hypoxia-imaging agents.

[^{18}F]FETNIM

[^{18}F]Fluoroerythronitroimidazole or [^{18}F]FETNIM is a nitroimidazole compound that has been intensively studied as a potential hypoxia PET tracer in the Turku PET Centre. Due to its low log P value it was believed to have less non-specific binding and more favourable biodistribution than other more lipophylic compounds. This was partly confirmed in preclinical studies where lower uptake was observed in all normal tissues and, in particular, in subcutaneous fat tissue (Gronroos *et al.*, 2004a). Unfortunately, clinical studies showed that tumour uptake of [^{18}F]FETNIM is governed primarily by blood flow and only a weak correlation between [^{18}F]FETNIM uptake in tumours and clinical outcome could be demonstrated (Lehtio *et al.*, 2004).

[^{18}F]FETA

Etanidazole or ETA has been used primarily as a hypoxia sensitizer for radiation therapy (Overgaard, 1994; Lee *et al.*, 1995; Brown *et al.*, 2010). Due to its lower LogP-value it was, similarly to [^{18}F]FETNIM, suggested that it might serve as a better hypoxia tracer than [^{18}F]FMISO. The first synthesis was reported in 1997 (Tewson, 1997). Subsequent animal studies confirmed that the non-specific uptake in most tissues is similar to that of FMISO; however, the uptake in liver and lung was lower compared to FMISO, and the compound is also more stable with less metabolite formation (Rasey *et al.*, 1999). In the same study the authors were also able to show an oxygen-dependent level of binding in rodent cell lines, suggesting that it might be potentially suitable as a clinical hypoxia marker. These findings were confirmed by Barthel et al. (Barthel *et al.*, 2004).

[^{18}F]FAZA

Azomycin arabinoside or AZA is a nitroimidazole compound that has been shown to have more favourable biokinetic properties than FMISO. As a gamma camera/SPECT tracer it was initially developed in a radioiodinated form as [^{125}I]IAZA (Mannan *et al.*, 1991). For PET applicationes ^{125}I was initially substituted by ^{124}I (Urtasun *et al.*, 1996). However, due to its more favourable imaging characteristics ^{124}I was exchanged for ^{18}F. Mostly due to its faster background clearance, [^{18}F]FAZA was found have better biokinetic properties and higher tumour-to-background uptake ratios compared to FMISO. However, this only seems to be the case in mice, but not rats (Piert *et al.*, 2005; Reischl *et al.*, 2007). It has, for example, been used in several tumour models (Busk *et al.*, 2008; Picchio *et al.*, 2008), as well as human studies (Garcia-Parra *et al.*; Maier *et al.*, 2011), and is still considered to be a potential candidate for substituting FMISO in clinical applications.

With the shortcomings of most of these tracers in mind, a new group of etanidazole-based compounds, EF1 (2-(2-nitroimidazol-1-[H]-y)-N-(3-flouropropyl)acetamide) (Evans *et al.*, 2000), EF3 (2-(2-nitroimidazol-1-[H]-y)-N-(3,3,3-tryflouropropyl)acetamide) and EF5 (2-(2-nitroimidazol-1-[H]-y)-N-(2,2,3,3,3-pentaflouropropyl)acetamide) has been developed with the intention of improving tissue penetration by increasing lipophilicity and decrease non-specific binding by the resulting faster clearance from non-hypoxic tissues, potentially resulting in increased tumour-to-background ratio.

[^{18}F]EF3

2-(2-nitroimidazol-1-yl)-N-(3[^{18}F],3,3-trifluoropropyl)acetamide or EF3 is a similar compound to FMISO with a slightly different structure and higher lipophilicity, belonging to the subgroup of etanizols (Busch *et al.*, 2000). Based on the results of its preclinical testing in tumour models, it was believed that it might potentially offer improved biokinetic and hypoxia-imaging properties compared to FMISO (Mahy *et al.*, 2004). ^{18}F-labelled EF3 was recently tested in humans and demonstrated that the tumour-uptake dynamics were slower compared to FMISO, and that the maximum uptake was significantly lower than that of [^{18}F]FMISO. The authors therefore conclude that while it is suitable for use as a PET tracer, its hypoxia-imaging properties are not superior to those of [^{18}F]FMISO (Dubois *et al.*, 2008).

2.3.4.3 [^{18}F]EF5

The slow tissue penetration is a significant problem in the case of FMISO also because of its relatively fast metabolic decay and due to the time restrictions posed by the relatively short half-life of radionuclide labels in PET. This was in part addressed with the development of FAZA; however, only improved wash-out kinetics were observed, while tissue penetration remained problematic. EF5 (Figure 7) with its very high lipophilicity and LogP-value is an additional step, aimed at specifically improving

tissue penetration because of which it was hypothesised to have imaging properties superior to thos of FAZA (Dolbier *et al.*, 2001; Koch *et al.*, 2001; Ziemer *et al.*, 2003).

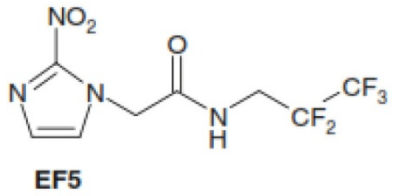

Figure 7 – 2-Nitroimidazole-based structure of EF5

The compound has been developed both as a biopsy-based (Evans *et al.*, 2006) and a PET-based agent. Radiolabelled [^{18}F]EF5 has been synthesized by Dolbier et al. (Dolbier *et al.*, 2001), as well as in our centre (Eskola *et al.*, 2011). Due to its lipophilicity, the tracer is expected to have a faster and more uniform tissue distribution. A potentially limiting step remains of course the relatively slow nature of the hypoxic trapping common to all nitroimdazoles; however, this can most likely not be modified with this family of drugs. The biodistribution of the PET tracer and the comparison of the uptake of the ^{18}F-lebelled compound to the distribution of binding of the cold EF5 have shown that the high lipophilicity and the compound's high level of stability ensure even distribution in the body and make it very suitable for clinical applications (Koch *et al.*, 2010).

[^{18}F]HX-4 – Recently, a new hypoxia tracer, 2-nitroimidazole nucleoside analogue [^{18}F]HX-4 has been presented and suggested as a potential hypoxia PET tracer (Doss et al.). It is a result of the novel, "click chemistry" approach aimed towards a generation of compounds with preferred pharmacokinetic and clearance properties. Click chemistry is based on the concept of modular units joined by standirdized reactions to form the final product/compound. This enables fast generation of new molecules with the desired properties. Initial results in a rat rhabdomyosarcoma tumour show some uptake which seems to be governed by the level of oxygen in the tissue (Dubois et al.). The first results of human studies and correlations with current hypoxia tracers have recently been presented with similar uptake T/M values to those of [^{18}F]FMISO (Chen *et al.*, 2012) in head and neck cancer. The authors of the study, however, speculate that [^{18}F]HX-4 might have higher sensitivity and specificity, faster clearance, and shorter injection-acquisition time compared with [^{18}F]FMISO, making the compound a superior PET tracer for *in vivo* use. These assumptions, however, would have to be verified in a larger study.

2.4.4.4 Other compounds

[^{64}Cu]ATSM – Copper(II)diacetyl-di(N^4-methylthiosemicarbazone) or ATSM is a copper-bisthiosemicarbazone complex that was designed and synthesized with the intention of creating a hypoxia marker (Dearling *et al.*, 1998). With its low redox potential and high membrane permeability it was shown to have a high hypoxia-specific binding in tumour cells (Obata *et al.*, 2001). Its low redox potential means that the process of reduction and intracellular trapping is enzymatically controlled. It has been demonstrated that the pO2 threshold for initiation of cellular retention is lower for Cu-ATSm than for FMISO (Lewis *et al.*, 1999; Lewis *et al.*, 2001).

Initial clinical data obtained from non-small-cell lung cancer and in cervical cancer suggested that it could be used for hypoxia detection in a clinical setting (Dehdashti *et al.*, 2003a; Dehdashti *et al.*, 2003b). However later studies demonstrated that the uptake correlated with perfusion and not hypoxia, and that the uptake did not decrease after the administration of carbogen throwing a shadow on the compounds ability to detect hypoxia (Yuan *et al.*, 2006).

Recently, a slightly different compound, generator-based ^{62}Cu-ATSM (t1/2 = 9.7 min) has been presented (Wong *et al.*, 2008) and used with the intention of detecting brain ischemia and misery perfusion, defined as decreased cerebral blood flow and decreased ratio of cerebral blood flow to blood volume in the brain typically associated with blood vessel disease (Isozaki *et al.*, 2011). The uptake of the same compound also seems to have a negative correlation with FDG uptake and a prognostic value in head and neck cancer (Okazawa *et al.*, 2011)

[^{89}Zr]cG250-F(ab')$_2$ – The above-mentioned G250 IgG is a monoclonal antibody against CA IX (Oosterwijk *et al.*, 1986). Due to the correlation of the expression of CA IX with hypoxia it has been hypothesised that it might be used as a hypoxia marker in *in vivo* studies. Recently, this compound has been labelled with ^{124}Iodine for PET use (Lawrentschuk *et al.*, 2011; Pryma *et al.*, 2011) showing promising results. Labelled with ^{89}Zr ($t_{1/2}$ = 78.4 h) it was recently tested in an animal model for head and neck cancer. The authors established that the uptake of the tracer demonstrates a significant level of correlation with CA IX expression has favourable tumour uptake characteristics, and might be suitable for use in humans. The authors suggest that the concept shows promise and further studies are warranted (Hoeben *et al.*, 2010).

The field of hypoxia imaging is currently in the focus of intense research and a large number of new candidate compounds are being presented.

2.4 HEAD AND NECK CANCER

Head and neck cancers (HNCs) form a group of malignant neoplasms of the lip, tongue, oral cavity, salivary glands, and pharynx (ICD-10 C00-C14) as well as the larynx (ICD-10 C32) and nasal cavity with paranasal sinuses (ICD-10 C30-31). Around 90% of all HNCs are squamous cell carcinomas (HNSCC). According to the Finnish cancer registry, 724 new cases (470 male and 254 female) were diagnosed in Finland in the year 2009 with the vast majority of cases occurring after the age of 50 (http://www.cancer.fi/syoparekisteri/en/). This represents 2.5% of all new cases of cancer in Finland. Due to its relatively high therapy-response rate, it accounts for a relatively small part of cancer-related deaths; 250 deaths due to HNC were registered in 2009. Treatment is based on surgery and/or chemoradiotherapy with both having a curative potential.

According to the European Cancer Observatory (http://eco.iarc.fr/), europewide (EU 27) 95,367 new cases of HNC and 39,960 deaths due to HNC were registered in 2008.

According to Siegel et al. (Siegel *et al.*, 2012), squamous-cell head and neck cancer (HNSCC) with its estimated yearly incidence of 40,250 in 2012 accounts for about 3% of all adult malignancies in the USA. Despite advances in therapy, an estimated 7,850 patients will die in the US of this disease this year.

The main risk factors for the development of HNSCC are tobacco and alcohol, which combined account for around 75% of all cases of HNSCC (Conway *et al.*, 2009). Conway et al. have also shown that a family history of HNSCC plays a role in the developing of the disease, thereby confirming the (epidemiologically minor) role of genetic background in HNSCC. The role of Epstein-Barr virus aetiology of HNSCC (nasopharingeal cancer) has been known for many years (Raab-Traub, 2002). The role of this virus also to some extent explains the higher incidence of HNSCC in south-east Asia compared to the rest of the world. Recently, a connection between human papilloma virus (HPV) and HNSCC (manly oropharingeal cancer) has been confirmed (Mehanna *et al.*, 2010), and a lot of attention has been focused on understanding the role of HPV in the etiology of HNSCC. This is particularly interesting since the HPV-related HNSCC is from an epidemiological (most cases younger non-smokers) and clinical point of view a distinct entity with a better prognosis (Ang *et al.*, 2010), and as such it may shed new light on the mechanisms underlying the development of HNSCC.

HNSCC has also been at the centre of intense investigation for reasons related to its physiology. Several studies have, namely, demonstrated that HNSCC is among the solid tumours with high levels of hypoxia (Vaupel & Mayer, 2007), and that hypoxia has a significant effect on the prognosis of this disease (Nordsmark *et al.*, 2005). The high prevalence of detected hypoxia as compared to other malignant tumours might be explained in part by the relatively easy accessibility of HNSCC which, in turn, enables

the use of invasive methods for detecting/measuring hypoxia. As such, HNSCC serves as a good model for studying the phenomenon of tumour hypoxia and its impact on resistance to therapy and disease prognosis.

2.5 PANCREATIC TUMOURS

On the basis of their pathological properties, malignant tumours of the pancreas can be divided into adenocarcinoma, inflammatory tumours, cystic neoplasms, and neuroendocrine tumours (NET). By far the most common of these is ductal adenocarcinoma, a very aggressive tumour with very poor survival rates. It spreads locally early in its development, but also distant spread is quite common for larger tumours. Others, while still malignant, are less aggressive (Li *et al.*, 2004).

In 2012, it is the 10th most common newly diagnosed cancer in the USA among men and women, representing roughly 3% of all new cancer cases. As already mentioned it has a very high death rate and while an estimated 43,920 new cases will be diagnosed in USA in 2012, 37,390 people will die in the same year due to this disease (Siegel *et al.*, 2012).

In Finland, 1,021 new cases (508 females and 513 males) of pancreatic malignancies were diagnosed in 2009, which represents about 3.6% of all new cases of malignant proliferative disease (http://www.cancer.fi/syoparekisteri/en/). This makes pancreatic cancer the 9th most common cancer according to incidence in Finland. In the same year, 1,004 deaths due to this disease were registered and due to its high mortality rate, it is the 3rd most common cancer type when it comes to cancer-related deaths. According to the Finnish Cancer Registry, the incidence of pancreatic cancer will have a slightly increasing tendency in the near future. These numbers also demonstrate the very high mortality rate typical for this malignancy with only 3 % of the patients still alive 5 years after the diagnosis (http://www.cancer.fi/syoparekisteri/en/statistics/newest-survival-ratios/).

Europewide (EU 27) the incidence of pancreatic cancer was 69,661 (9.9/100,000) and the mortality 71,116 (9.9/100,000) in 2008 (http://eco.iarc.fr/).

The well known risk factors are tobacco smoking, alcohol, family history and chronic pancreatitis. Renehan et al (Renehan *et al.*, 2008) have recently identified obesity as an additional independent risk factor for the development of the disease.

2.5.1 Imaging of Pancreatic Tumours

The objective of imaging is not only to confirm the presence of a pancreatic lesion, but also to characterize these lesions: benign, premalignant, or malignant. The potential treatment depends also on the local and distal spread of the disease in the case of

malignant lesions. In the case of benign lesions, there is also the possibility of endocrine activity and in this case surgical treatment is warranted as well.

This differentiation is also aided by the molecular markers and biochemical analyses. The most common marker associated with pancreatic adenocarcinoma is Ca 19-9 which has been observed to be elevated in about 80% of pancreatic cancers (Gattani *et al.*, 1996). As it also elevated, for example, in hepatocellular carcinoma, gastric carcinoma and ovarian cancer, it does however lack specificity with values reported as low as 43% (Ni *et al.*, 2005).

Among imaging modalities used in the diagnosis of pancreatic lesions are ultrasound, MDCT, MRI, and PET. Both MDCT and MRI are well established tools for the diagnosis of pancreatic lesions.

Due to its wide availability and fast scanning times, (Contrast Enhanced) CT is the first-line imaging modality when pancreatic pathology is suspected. The administration of intra-venous contrast agents combined with the fast imaging protocols allows image acquisition during the venous as well as the arterial phase in the course of a single session. Typically, pancreatic tumours have a slower uptake of contrast agents than the surrounding pancreatic tissue making them appear hypo-dense. This is indicative of lower vasculature compared to the highly perfused normal pancreas. However, this is not always the case and in around 10% of pancreatic malignancies an iso-dense pattern is observed. In this case indirect signs have to be identified (ductal dilatation or interruption, atrophy of the tail or abnormal shape of the pancreas) (Prokesch *et al.*, 2002).

MRI, on the other hand, is most often used as a second-line imaging tool in the cases of unclear findings in CT. As MRI imaging in general has become more technically sophisticated and complex, also MRI imaging of pancreatic lesions has advanced. Particularly with the use of stronger magnetic fields, improved coils and application of gadolinium-based contrast agents, important steps forward have been made. Typically, pancreatic tumours appear hypo-intense in T1 weighted, and iso-intense or rarely hyper-intense in T2 weighted images (Sahani *et al.*, 2008).

A meta-analysis of 68 CT and MRI studies concluded that for primary diagnosis, sensitivities of helical CT, conventional CT, MRI, and US were 91%, 86%, 84%, and 76% and specificities were 85%, 79%, 82%, and 75%, respectively, with sensitivities for MRI and US being significantly lower than that of helical CT (Bipat *et al.*, 2005). In their extensive review of pancreatic cancer imaging, Schima et al (Schima *et al.*, 2007) also onclude that MDCT is the method of choice for detecting and staging pancreatic cancer, while contrast-enhanced MRI has a role as a problem-solving tool in patients with equivocal findings on CT.

2.5.2 PET(CT) Imaging of Pancreatic Tumours

As has been the case with many other malignancies, PET has emerged as a promising imaging method also in pancreatic cancer.

Avid uptake of [^{18}F]FDG in pancreatic cancer was demonstrated in the 1990s (Reske *et al.*, 1997) and, since then, PET has been studied extensively particularly in the primary diagnosis of pancreatic adenocarcinoma (for a recent extensive review see (De Gaetano *et al.*, 2012)).

However, the sensitivity of [^{18}F]FDG PET has been repeatedly demonstrated to be similar to that of CE CT. In one of the earliest studies, Bares et al. (Bares *et al.*, 1993) have found it to be 92% versus 95% for CT. Later, Keogan et al. (Keogan *et al.*, 1998) confirmed this with a sensitivity of 88% for PET versus 75% for CT. Also Diederichs et al. found in a much larger prognostic study (Diederichs *et al.*, 2000) sensitivies of 88% for both PET and CT. Also several other larger studies, among them Kasperk et al. (Kasperk *et al.*, 2001) and Lytras et al. (Lytras *et al.*, 2005) found sensitivity and specificity values for diagnosis of pancreatic adenocarcinoma to be comparable to those of CT, while Borbath et al. found these values to be comparable to those obtained using MRI (Borbath *et al.*, 2005).

With the onset of hybrid PET/CT imaging these results had to be re-examined since it was expected that the addition of CT would have a significant impact on the diagnostic accuracy of the modality (Wahl, 2004). In line with this development, several retrospective and a few prospective studies have been conducted. Some of these studies confirmed the high diagnostic accuracy of [^{18}F]FDG PET/CT (Lemke *et al.*, 2004; Schick *et al.*, 2008), while others found the combined PET/CT significantly outperformed CT alone (Farma *et al.*, 2008). This improved performance of PET/CT has been confirmed in a recent study by Asagi et al. (Asagi *et al.*, 2012). This development has led Strobel et al. to suggest that [^{18}F]FDG PET/CT could indeed become the only required imaging modality in the assessment of resectability of pancreatic cancer (Strobel *et al.*, 2008).

These high sensitivity and specificity values, however, have not been obtained in neuroendocrine tumours (NET) of the pancreas. [^{18}F]FDG is only taken up by more aggressive NETs with high proliferation rates and low levels of differentiation (Sundin *et al.*, 2007). In these cases other, more specific tracers, such as [^{18}F]DOPA have been shown to be more successful (Rufini *et al.*, 2012).

2.6 CLINICAL IMPORTANCE OF TUMOURAL MICROENVIRONMENT

As already mentioned, the microenvironment plays a crucial role in the susceptibility of tumours to therapeutic attempts to eradicate them. This is a consequence of factors directly influencing tumour growth as well as factors influencing the efficacy of therapy.

Hypoxia has been repeatedly associated with more aggressive tumour phenotype and has a negative prognostic value also in head and neck cancer (Brizel *et al.*, 1997; Nordsmark *et al.*, 2005). Blood flow, on the other hand has a more complex role in that, on one hand, normal blood supply is necessary for the effectiveness of chemo- and radiotherapies, while, on the other hand, normal blood flow also enables the development and growth of tumour tissue. For this reason different strategies are being developed to overcome this obstacle.

2.6.1 Chemotherapy

Targeting malignant tumours with chemical agents depends greatly on the ability of the agent to reach the target cells. For this reason, tumour vasculature and blood flow play crucial roles in the effectiveness of chemotherapies regardless of their mechanisms of action.

Dysfunctional angiogenesis while being part of the cause of these problems on one hand can also be part of the solution on the other. This is particularly true for the over-expression of vascular growth factors and, in particular, vascular endothelial growth factor (VEGF). This is well demonstrated by bevacizumab, a monoclonal VEGF-A inhibitor, which has been shown to be effective in some type of colorectal cancers (Tappenden *et al.*, 2007) and gliomas (Burkhardt *et al.*, 2012).

Another approach receiving a great deal of attention is the use of hypoxia-activated prodrugs. This mechanism is based on controlled enzymatic reduction of prodrugs in hypoxic cells, resulting in active cytotoxic agents. In normoxic conditions, the reduced compound is usually re-oxidezed by oxygen. An important requirement is of course that the reduced compound is more toxic than the initial prodrug (for an extensive review see (Wilson & Hay, 2011)).

This characterist of hypoxic activation was first observed in the 1960's for the drug mitomycin C and other quinone compounds (Bachur *et al.*, 1978). This property of hypoxic reductive activation has been demonstrated for five chemical moieties: nitro groups, quinones, aromatic N-oxides, aliphatic N-oxydes, and transition metals (Chen & Hu, 2009). Very few compounds have made it to the clinical testing stage and the first results of phase III clinical trials have only recently been presented. Most

experiments have been made using aromatic N-oxydes and 2-nitroimidazoles of which Tirapazamine and TH-302, respectively, are the best known representatives (Brown, 1993; Weiss *et al.*, 2011).

Tirapazamine is the best known of these compounds and has been tested extensively in preclinical conditions. In 2006, the first results demonstrating the ability of the PET hypoxia probe [18F]FMISO to identify tirapazamine-sensitive tumours were published (Rischin *et al.*, 2006). The success of tirapazamine treatment was later not confirmed in a larger phase III study by the same group. In this study, however, the important [18F]FMISO-based stratification was not used (Rischin, 2010).

In addition to tirapazamine, a nitrobenzamide mustard prodrug PR-104A and several 2-nitroimidazole-based compounds have recently entered clinical testing and encouraging results have been reported.

PR-104 has been tested quite extensively in a preclinical setting *(Guise et al., 2007; Patterson et al., 2007; Houghton et al., 2011)* as well as in humans (Jameson *et al.*, 2010), and currently the first phase-I trial results are being reported (McKeage *et al.*, 2011; McKeage *et al.*, 2012).

Also two 2-nitroimidazole compounds, TH-302 (Liu *et al.*, 2012; Sun *et al.*, 2012) and CEN-209 (Hunter *et al.*, 2012; Wang *et al.*, 2012) are currently showing promising potential and are entering clinical testing.

This is an exciting and very rapidly evolving field; however, results of larger clinical trials are still awaited and judgement on the efficacy of such treatments has yet to be passed. The fast evolution of the field, nevertheless, only emphasises the need for pre-treatment identification of hypoxic tumours.

2.6.2 Radiotherapy

Radiotherapy used in cancer treatment works by damaging the cell's DNA. The damage can be caused directly by photons or indirectly by charged particles or free radicals. Direct damage is produced by photons hitting DNA and causing either single-strand breaks or double-strand breaks. Most single-strand breaks can be, and most often are, successfully repaired by the cell's DNA repair mechanisms. Double-strand breaks, on the other hand, are more damaging to the cell, since repair mechanisms do not have a repair template provided by the opposing, intact DNA strand, and are therefore unable to repair them. These double-strand breaks, however, are very rare.

In general, the damage caused by radiation can be classified into lethal, sub-lethal, and potentially lethal. While lethal damage causes instant cell death, sub-lethal changes cause delayed cell death, but only if they could not have been successfully repaired. Potentially lethal damage to DNA, on the other hand, does not cause direct cell death,

but instead causes damage that is initially repairable, but results in genotype mutations that later change the cell's functionality.

Most of the damage caused by radiation is produced indirectly by free radicals through interaction of radiation photons and small molecules in the cell, in most cases water, the most abundant molecule in the cell. A proton is knocked from the water molecule by the photon, producing highly reactive hydroxyl radicals. These free radicals react with DNA (and other macromolecules) and thereby damage it. This damage, however, accumulates with time and only becomes obvious when cells are unable to produce a vital protein or are unable to pass through the process of division. By binding to the exposed reactive sites and thereby stabilizing or "fixing" them, reactive oxygen radicals play an important role in the accumulation of DNA damage caused by free radicals by preventing the repair of this damage, thereby making it permanent. Consequently, cells in an anoxic (complete absence of oxygen) environment are almost three times more resistant to radiation damage than cells in the presence of oxygen (Steel, 2002). As described above, hypoxia is a common phenomenon in malignant tumours and oxygen or more precisely the lack of it has been at the centre of oncologic research ever since Thomlison and Gray pointed to its potential role in radiotherapy (Thomlinson & Gray, 1955).

For this reason, different strategies for modifying the levels of oxygen in malignant tumours have been investigated (Horsman & Overgaard, 2002). Since the level of oxygen in tissue is dependent on the level of red blood cells, anaemia is usually corrected before the start of radiotherapy, even though there no direct correlation between anaemia and locoregional control in radiotherapy has been established. A way of compensating for the lack of oxygen is the use of radiosensitizers, chemical agents that, to some, albeit a lesser extent than oxygen, intensify the effect of radiation on cells. These compounds accumulate in all, not only hypoxic, cells. During radiotherapy they act in a similar fashion to oxygen by fixing the DNA strand breaks. For this reason, they have no significant effect in normoxic tissues where the same role is performed by oxygen. The best known radiosensitizer is misonidazole, a compound from the large group of nitroimidazoles (Brown & Siim, 1996). Misonidazole has shown promising results in cell cultures, but was less effective in clinical trials where its usability was strongly limited by the compound's pronounced neurotoxic effects.

Other compounds from the same group are metronidazole, nimorazole, and etanidazole. This strategy was demonstrated to be beneficial in head and neck cancer in some trials (Overgaard *et al.*, 1998) and, in Denmark, it is even being used as part of standard HNSCC treatment.

An additional strategy for overcoming the hypoxic barrier is the use of carbogen gas (95% O_2 plus 5% CO_2) breathing during irradiation to combat the diffusion-limited (chronic) hypoxia with the addition of nicotineamide, a vasoactive agent combating the

acute or perfusion-limited hypoxia (Chaplin *et al.*, 1990; Martin *et al.*, 1993; Bussink *et al.*, 1999). A Danish study recently demonstrated that the use of nimorazole resulted in improved outcome in patients with confirmed hypoxic tumours but not in patients with normoxic tumours (Toustrup *et al.*, 2012).

A way of turning the presence of hypoxia in tumours into a potential therapeutic target is the use of hypoxic cytotoxins. These compounds are only toxic in an environment of low oxygen concentration, where they are transformed into the effective, toxic form. A very promising compound in this group was tirapazamine (Gandara *et al.*, 2002). It showed very good results when used in hypoxic tumours in the first clinical study published in 2006 (Rischin *et al.*, 2006). In 2010, the results of the same group demonstrated that the use of tirapazamine, in patients with advanced head and neck cancer not selected for the presence of hypoxia, does not improve the overall survival of patients (Rischin *et al.*, 2010). In addition, as in misonidazole, strong toxic effects were observed that prevent it from being used on a larger scale.

Hypoxic toxins are a field of intensive research and new tirapazamine-related compounds are being investigated for potential clinical applications. Some of these are Q39 (Zhu *et al.*, 2010), NLCQ-1 (Papadopoulou *et al.*, 2011), and the most recent and most promising agent, TH-302 (Sun *et al.*; Liu *et al.*, 2012).

Nevertheless, the results of both tirapazamine (hypoxic toxin) and nimorazole (hypoxic sensitizer) studies demonstrate the importance of selective use of these toxins in hypoxic tumours and emphasize the role of pre-treatment hypoxia detection.

With the development of new radiotherapy techniques, the precision of dose delivery has improved significantly and higher levels of radiation can be delivered to smaller areas without affecting the surrounding tissues, thereby reducing the side-effects of therapy. This higher dose can also be three-dimensionally moulded and the approach is known as intensity-modulated radiotherapy or IMRT. Since hypoxic areas would need higher irradiation doses to achieve the same therapeutic effect, IMRT could be combined with imaging information on tumor microenvironment to identify the most resistant/hypoxic areas of the tumour and, accordingly, to deliver higher doses to these areas. This, currently only experimental approach is sometimes also refered to as “dose painting” and will be discussed in more detail later.

2.7 INTEGRATION OF FUNCTIONAL IMAGING AND THERAPY IN HNC

Delineation of dose delivery in radiotherapy has for a long time been based on the morphological information provided by conventional imaging techniques, mostly on CT. However, as discussed above, the role of functional characteristics (blood flow,

metabolic activity, oxygenation, etc.) in diagnosis, prognosis and treatment response is gaining importance, emphasising the need to incorporate this information into treatment planning. However, the delivery of the therapeutic irradiation dose has been to a great extent limited by the poor spatial resolution of the irradiation technology. During the last decade, technical progress in this field, with the development of intensity modulated radiotherapy (IMRT), has enabled a greater precision of spatial dose delivery (Kuppersmith *et al.*, 1999; Teh *et al.*, 1999). With this possibility of delivering higher doses of irradiation to particular areas of the tumours, the question of functional tissue heterogeneity inside the otherwise morphologically uniform tumour mass has emerged (Grosu *et al.*, 2009). This, however, is an area where morphological imaging cannot provide the necessary information, and functional target volume delineation is gaining importance (Bentzen, 2005).

While the benefits of FDG PET/CT in diagnosing and particularly in staging HNC are well established, its role in the planning of radiotherapy is far from simple (MacManus *et al.*, 2009). While it does provide good diagnostic sensitivity and specificity, its integration into IMRT is rather complex (Koshy *et al.*, 2005; Paulino *et al.*, 2005). The reliability of FDG PET/CT-based GTV-delineation compared to CT-based GTV (current gold standard) varies greatly (Wang *et al.*, 2006) making it hard to draw any clear conclusions. This is mostly due to PET's relatively low spatial resolution and high noise in images which together make automatic volume definition or segmentation very demanding (Thorwarth & Schaefer, 2010). Currently, the most commonly used method is visual contouring of PET images; however this method has a high level of inter-individual variability posing problems of repeatability and reliability. To solve this problem, several different approaches have been developed ranging from using fixed absolute (usually SUV of 2.5 (Hellwig *et al.*, 2007)) or relative (usually 40% or 50% SUVmax (Erdi *et al.*, 1997; Ford *et al.*, 2006) threshold values through methods integrating background uptake values (Daisne *et al.*, 2003) all the way to very complex iterative segmentation methods (van Dalen *et al.*, 2007) and segmentation based on dynamic data (Janssen *et al.*, 2009). The methods are also reported to have greater correlation with histo-pathological findings (Daisne *et al.*, 2004) and applicability in fields of non-FDG PET imaging, particularly in hypoxia imaging (Thorwarth *et al.*, 2007).

Despite this great research interest, there is no clear consensus on the methodology and the extent of FDG PET use in radiotherapy planning in HNC at the moment (Minn *et al.*, 2010). To achieve this, larger clinical studies with correlation to histological findings and clinical outcome are needed (Thorwarth & Schaefer, 2010). Therefore, the use of FDG PET is currently limited to smaller experimental projects and plays a supporting role to CT-based contouring. A lot of work is still needed before it can be routinely incorporated into therapy planning. The same is true for the use of other PET tracers (such as hypoxia tracers) where the way to this goal is even longer (Astner *et*

al., 2010; Thorwarth & Alber, 2010; Troost *et al.*, 2010). However, as already mentioned, a recent study emphasized that the effects of non-selective use of radiosensitizers are insignificant, so identification of hypoxic tumours might be of crucial importance for the success of such treatment (Rischin *et al.*, 2010).

3 OBJECTIVES OF THE STUDY

Microenvironment plays a crucial role in determining the phenotype of malignant tumours and in the response of these tumours to therapy.

The purpose of this work was to investigate and develop new non-invasive PET methods for imaging tumour blood flow, energy metabolism, and hypoxia and to evaluate their impact on patient prognosis.

The specific aims of the four performed studies were:

1. To evaluate 2-(2-nitro-H-imidazol1-yl)-N-(2,2,3,3,3-pentafluoropropyl)-acetamide (EF5) labeled with ^{18} F-fluorine to image hypoxia in patients with squamous cell carcinoma of the head and neck (Study I).

2. To non-invasively quantify the BF and metabolic activity of pancreatic tumours using [^{15}O] H2O and [^{18}F]FDG PET/CT imaging, to compare these findings in malignant tumours to those in normal pancreatic tissue and benign lesions, as well as to assess the effects of these functional variables on the survival of patients with confirmed cancer (Study II).

3. To prospectively compare the accuracy of [^{18}F]FDG PET/CT, MDCT and MRI in the diagnosis, staging, and assessment for surgery in patients with suspected pancreatic malignancy (Study III).

4. To develop a simple non-invasive method of measuring blood flow (BF) using [^{15}O]H_2O PET/CT for the head and neck area applicable in daily clinical practice (Study IV).

5. To determine the predictive value of pre-treatment PET/CT imaging using [^{18}F]FDG, the hypoxia tracer [^{18}F]EF5, and the perfusion tracer [^{15}O]H_2O in patients with squamous cell cancer of the head and neck treated with chemo-radiotherapy (Study V).

4 SUBJECTS

All studies were performed after approval by the Ethical Board of Turku University Central Hospital and in accordance with the Helsinki Declaration. Informed consent was obtained from each patient. Permission to use [^{18}F]EF5 in human studies was granted by the Finnish Medicines Agency (Fimea). Patients participating in these studies were recruited through the Department of Oncology and Radiotherapy of the Turku University Hospital (Studies I, III and IV) and the Department of Abdominal Surgery of the Turku University Hospital (Study II).

In studies **I** and **IV**, 15 patients (11 male and 4 female) with newly diagnosed, untreated HNSCC referred to Turku University Central Hospital for chemoradiotherapy between December 2005 and January 2007 participated in this study. The average patient age was 55.5 ± 14 years (24 – 77). Detailed information about patients participating in studies I, III and IV can be found in Table 3.

Table 3 - Detailed information on patient demographics, tumour location, TNM, Stage, and histological grade.

Number	Gender	Age	Weight	BMI	Tumour location		TNM	STAGE	Grade
1	M	45	65	21.2	Base of tongue	Oropharynx	4/1/0	IV a	II
2	M	58	72	24.3	Base of tongue	Oropharynx	2/1/0	III	II
3	F	58	50	21.6	Tonsilla	Oropharynx	1/2b/0	IV a	II
4	M	62	67	22.4	Supraglotis	Larynx	2/2b/0	IV a	II
5	F	39	68	21.5	Supraglotis	Larynx	4/2c/0	IV a	III
6	M	43	100	27.7	Maxillary gingiva	Oral cavity	4/0/0	IVa	I
7	M	68	70	26	Base of Tongue	Oropharynx	2/1/0	III	II
8	F	46	59	22.5	Nasopharynx	Nasopharynx	1/2/0	III	III
9	M	53	76	24.8	Supraglotis	Larynx	3/2b/0	IV a	II
10	M	23	129	39.8	Tongue	Oral cavity	3/2b/0	IV a	I
11	M	70	92	27.8		Oral cavity	1/0/0	I	II
12	M	57	77	25.7	Base of Tongue	Oropharynx	1/2b/0	IVa	III
13	M	65	98	29.6	Nasopharynx	Nasopharynx	2a/1/0	II b	III
14	M	68	64	22.7	Base of tongue	Oropharynx	1/2b/0	IV a	III
15	F	78	52	22.2	Maxilla	Paranasal sinus	4/1/0	IVa	II
16	M	57	99	27.7	Base of tongue	Oropharynx	3/2b/0	IV a	III
17	M	61	130	40.1	Oropharynx	Oropharynx	2/2/0	IVa	III
18	M	51	65	19	Floor of mouth	Oral cavity	2/1/0	III	II
19	F	61	80	29.4	Retromolar	Oral cavity	3/2b/0	IVa	II
20	M	54	70	23.4	Hypopharynx	Hypopharynx	4a/1/0	IV a	III
21	M	60	80	25	Tongue	Oral cavity	2/0/0	II	II
22	M	53	91	32.2	Tonsilla	Oral cavity	3/2c/0	IV a	II

In study **II**, 26 consecutive patients (14 male, 12 female, age 64.8±12.5 years) with clinical suspicion of pancreatic malignancy were, prior to any treatment, prospectively enrolled in the study between September 2006 and October 2007. Criteria for enrolment in PET/CT imaging was a suspicion of malignant biliary stricture at ERCP (n=15), or a suspicious pancreatic lesion on US or CT in a referring centre (n=11). Validation of diagnosis was based on the findings at operation with biopsy (n=11), operation without biopsy (n=4), percutaneous/cytological brush biopsy (n=2), autopsy (n=1), or follow-up of a median of 20.1 months (range, 16-27 mo) (n=8). Patients were divided into three groups as follows: Group A, no anatomical tumour (n=7); Group B, benign lesion (n=8), and Group C, malignant pancreatic tumour (n=11). More detailed information on patients in Group C can be found in Table 4.

Table 4 – Gender, age, and TNM status of patients with malignant lesions in Study II (Table adopted from publication II).

Patient No.	Gender	Age	pTNM/cTNM
1	F	68	T4N1bM0
2	F	69	T3-4NXM1
3	M	64	T4NXM0
4	F	59	Insufficient
5	M	62	No histology
6	F	74	T2-3N1M0
7	F	69	TXNXM1
8	F	67	Insufficient
9	M	77	T2-3N1M0
10	M	56	High-grade NET
11	M	76	Low-grade NET

In study **III**, out of a total of 40 enrolled patients with pancreatic cancer, 38 were included in the final analysis. Of these patients, 26 also participated in study II. Alongside the PET imaging all the patients underwent both comparative MDCT and MRI imaging. The therapeutic work-up was performed according to the usual procedures of our institution (Figure 8). Results of these imaging methods were compared to operative and histopathological findings or follow-up.

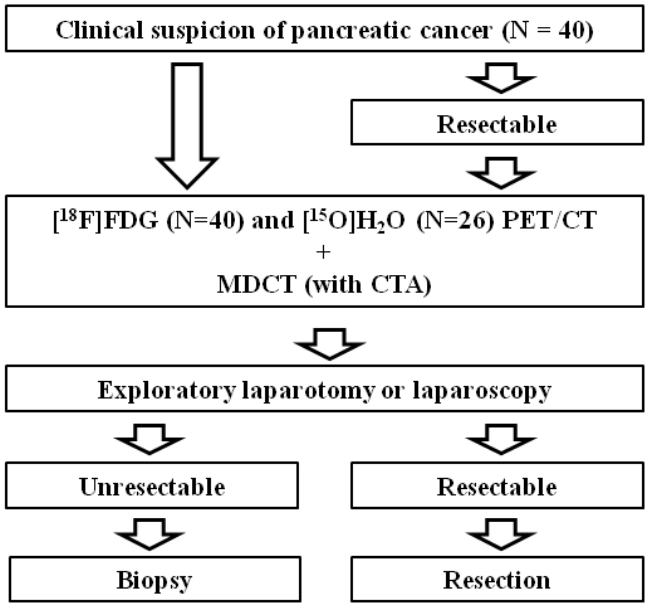

Figure 8 – The diagnostic work-up of patient participating in study III (Figure adopted from publication III).

In study **V**, in addition to the 15 patients with HNSCC studied in study I, 7 new patients were recruited according to the same inclusion criteria. For details see Table I (Patients 16 – 22). In total, 22 patients were scanned and followed for a median period of 40 months (range 3 – 53).

5 METHODS

5.1 POSITRON EMISSION TOMOGRAPHY

All studies were performed on a Discovery VCT PET/CT scanner (General Electric Medical Systems, Milwaukee, USA) which combines a helical 64-slice CT scanner and a Bismuth Germanate Oxide (BGO) block PET tomography. The PET scanner part consists of 13 440 BGO crystals arranged in 24 rings yielding 47 transverse slices spaced axially by 3.27 mm. The PET imaging field of view (FOV) was 70 cm in diameter and 15.7 cm in axial length. Attenuation correction was performed using a low-dose ultra-fast CT protocol (80 mAs, 140 kV, 0.3 mSv per FOV). The voxel size of the PET image is 3.5 x 3.5 x 3.27 mm. The 128 x 128 matrix size was used in all PET images. For detailed scanner performance data see Teräs et al. (Teras *et al.*, 2007)

5.1.1 Tracer Production

5.1.1.1 [^{15}O]H_2O

A low-energy deuteron accelerator Cyclone 3 (IBA Molecular, Louvain-La-Neuve, Belgium) was used for production of ^{15}O. To synthesize radiowater for blood flow imaging, a diffusion membrane technique in a constantly working water module was applied (Radio Water Generator, Hidex Oy, Finland). For each examination, an online radioactivity recording of products was performed using a low voltage ionization chamber.

5.1.1.2 [^{18}F]EF5

[^{18}F]EF5 (^{18}F--2-(2-nitro-1*H*-imidazol-1-yl)-*N*-(2,2,3,3,3-pentafluoropropyl)-acetamide) was synthesized from 2-(2-nitro-1*H*-imidazol-1-yl)-*N*-(2,3,3-trifluoroallyl)-acetamide using high specific radioactivity ^{18}F-F_2 as the labelling reagent (Bergman & Solin, 1997). The specific radioactivity of [^{18}F]EF5, decay corrected to the end of synthesis, exceeded 3.7 GBq/µmol. Radiochemical purity was higher than 98.5 % in every production. For a more detailed description of [^{18}F]EF5 synthesis see Eskola et al. (Eskola *et al.*, 2011).

5.1.1.3 [^{18}F]FDG

[^{18}F]FDG was synthesized from mannosyl triflate using a nucleophilic method. Radiochemical purity exceeded 95% and specific radioactivity was approximately 74 GBq/µmol at the end of the synthesis.

5.1.2 Imaging protocols

Study **I** - Measurement of tumour blood flow with [^{15}O]H_2O was followed by PET/CT imaging with [^{18}F]EF5. On a separate day, [^{18}F]FDG PET/CT was performed. Both studies were performed in random order within an average of 6 days (range, 1 -16 days). The sequence of events for the combined [^{15}O]H_2O [^{18}F]EF5 study is shown in the flow-chart (Figure 9).

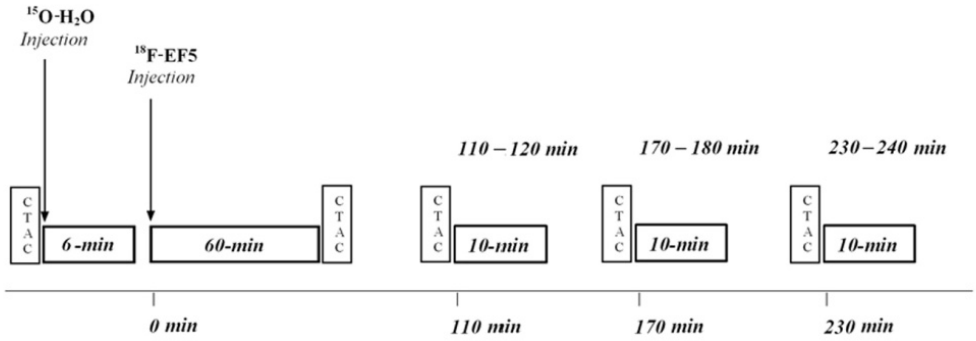

Figure 9 – Time sequence of acquisition of [^{15}O]H_2O and [^{18}F]EF5 images (Figure adopted from publication I).

All patients fasted at least 6 hours prior to tracer injection. A venous line was inserted in the forearm for injection of the tracer and another catheter was placed in the contra-lateral radial artery for the frequent blood sampling during the image acquisition. Patients were positioned on the tomograph couch in supine position, arms alongside the body, with a head support (combined [^{15}O]H_2O and [^{18}F]EF5 study) or a custom-made thermoplast mask used in radiotherapy (RT; FDG study) stabilizing the head.

The study began with CT imaging followed by an injection of [^{15}O]H_2O (median dose 1205 MBq or 16.8 ± 3.2 MBq/kg) and an immediate 6 minute dynamic emission image acquisition. Arterial blood was withdrawn with a pump (Alitea, Stockholm; Sweden) at a speed of 6 ml/min to obtain the input function. Blood radioactivity was measured with an online detector (GE Medical Systems, Uppsala, Sweden). After the completion of the [^{15}O]H_2O blood flow study, a slow (approximately 15 seconds) bolus of [^{18}F]EF5 was injected (median dose 250 MBq or 3.9 ± 1.5 MBq/kg). In six patients, following the tracer injection, a set of dynamic images over 60 minutes was acquired to demonstrate the early tracer distribution, after which patients were removed from the scanner. Late images (2 frames of 300 s) were acquired at 2, 3, and 4 hours after the tracer injection. Patients were allowed to relax quietly in the preparation room between these late acquisitions.

During the [^{18}F]EF5 image acquisition, 28 blood samples were obtained through the arterial catheter to measure the time-course of tracer concentration and presence of any tracer metabolites in plasma. A total of 9, 14, 15 and 3 images were acquired at 1h, 2 h, 3h, and 4h post-injection, respectively.

The [^{18}F]FDG study was performed according to the routine [^{18}F]FDG protocol used for RT planning in our centre (Minn *et al.*, 2010). The median injected FDG dose was 369 MBq (4.8 ± 0.9 MBq/kg) and a static image was acquired approximately one hour after the tracer injection.

In study **II**, all patients fasted at least six hours and their plasma glucose (GlcP) was measured before the start of the acquisition. Measurement of tumour BF with [^{15}O]H_2O was followed by PET/CT imaging with [^{18}F]FDG. Patients were positioned on the tomography couch in supine position, arms alongside the body. The study started with CT imaging for attenuation correction followed by a bolus injection of [^{15}O]H_2O (mean dose 1100±81 MBq, range 960–1280 MBq) and an immediate dynamic emission image acquisition of 6 minutes (26 frames). After this the patient was removed from the scanner. [^{18}F]FDG images were acquired according to a standard diagnostic scanning protocol 57±5 (range 49-70) minutes post-injection (mean dose 367±17 MBq, range 316-386 MBq).

In study **III**, PET imaging was done using the Discovery [^{18}F]FDG PET/CT STE scanner (General Electric Medical Systems, Milwaukee, WI) at Turku PET Centre. Patients fasted 6 hours before the study. Plasma glucose levels ranged from 5 to 11 (mean: 6.7 ± 1.8) at the time of intravenous FDG injection (366 ± 15 MBq). Approximately 60 minutes after injection, static [^{18}F]FDG PET/CT imaging in 3D covering the upper torso from eyebrows to mid-thighs (3-minute emission scan/position) started. Attenuation correction was performed using a low-dose ultra fast CT protocol (80 mAs, 140 kV, 0.3 mSv/FOV). In addition, delayed PET emission images of the upper abdomen were acquired at approximately 110 minutes. Transaxial, coronal, and sagittal images for visual and semi-quantitative analysis of the data were corrected for deadtime, decay, and photon attenuation, and reconstructed in a 128 x 128 matrix. Images were reconstructed using 2 iterations and 28 subsets with a 6.0 mm FWHM postfilter and a fully 3D maximum likelihood ordered subset expectation maximization reconstruction algorithm. Any focal tracer accumulation exceeding normal regional tracer uptake was considered a pathological finding (tumour manifestation). PET images were analyzed visually and semiquantitatively by calculating mean and maximum standardized uptake values (SUVs) defined as the ratio of activity per milliliter of tissue to the activity in the injected dose corrected by decay and by patient's body weight. The region of interest with a diameter of 1 cm (0.77 cm^3) was placed on the area of the lesion with the highest FDG uptake, and when there was no uptake in the normal pancreas, the region of interest was placed on the region of

suspected lesion based on referral. The retention index (RI) SUV was calculated from the results of 1-hour (early scan) and 2-hour (delayed scan) imaging, according to the following equation: RI = (SUV[delayed scan] – SUV[early scan]) x 100/SUV[early scan].

In study **IV**, the same [^{15}O]H_2O images as acquired in Study **I** were used. Framing for the dynamic image acquisition is as follows 12 x 5 s, 6 x 15 s, and 7 x 30 s.

In study **V**, [^{18}F]EF5 images were acquired according to a simplified protocol only 3 hours after the tracer injection.

5.1.3 Image processing

In studies **I**, **II** and **V**, dynamic 2D [^{15}O]H_2O images were reconstructed using two iterations, 20 subsets, a 6.0 mm FWHM (full-width half-maximum) postfilter, and a 5.47 mm loop filter.

Parametric blood flow images were calculated using the one-tissue or two-compartment model, which was linearized (Blomqvist, 1984). Lawson-Hanson non-negative least squares analysis was used to solve general linear least squares functions. The input function for the tissue was corrected for the measured external dispersion in the tubing by deconvolution with an exponential function. The delay was corrected by fitting the input curve into the measured tissue curve (Meyer, 1989; van den Hoff et al., 1993).

[^{18}F]FDG and [^{18}F]EF5 images were reconstructed using two iterations and 28 subsets with a 6.0 mm FWHM postfilter and a fully 3D maximum likelihood ordered subset expectation maximization (ML-OSEM) reconstruction algorithm.

In study **II**, the [^{18}F]FDG activity concentration values were corrected for radioactive decay, and standardized uptake value (SUV) was calculated as SUV=activity concentration in a ROI / (injected dose / body mass). The resulting values were normalized to GlcP levels according to the formula SUV*(GlcP/5) [21]. Finally, SUV_{max} normalized to GlcP was divided by BF to obtain the SUV/BF ratio.

In study **IV**, one invasively obtained (Blood-IF) and two non-invasive, population-based curves were compared (SUV-IF and BSA-IF). The Blood-IFs were corrected for physical decay. Equation 2 was used for the calculation of BSA (Mosteller, 1987).

$$\mathrm{BSA} = \sqrt{\frac{\mathrm{BM}(kg) \times \mathrm{Height}(cm)}{3600}} \qquad \text{Equation 2}$$

In order to calculate the population-based curves (SUV-IF and BSA-IF), measured activity curves were first converted to standardized uptake values (SUV) and BSA-corrected values according to equations 3 and 4, respectively.

$$\text{SUV - IF} = \frac{\text{BM}(g) \times \text{Activity}(Bq/mL)}{\text{ID}(Bq)} \qquad \text{Equation 3}$$

$$\text{BSA - IF} = \frac{\text{BSA}(m^2) \times \text{Activity}(Bq/mL)}{\text{ID}(Bq)} \qquad \text{Equation 4}$$

These converted curves were realigned to ensure the same time position of the ascending slope in all curves. Using these realigned curves, average SUV-IF and BSA-IF curves were then calculated. The two curves were rescaled back to activity (kBq/ml) values using each patient's BM and injected dose (ID) in the case of SUV-IF and BSA and ID in the case of BSA-IF.

The IFs of all three methods were individually corrected for tissue delay by using the same tissue curve in all three cases. After delay correction, dispersion correction was performed for each curve (Iida *et al.*, 1986). BF images were calculated using a linearized one-tissue compartment model (Blomqvist, 1984) using the three evaluated input functions. The Lawson-Hanson non-negative method was used to solve general linear least squares functions (Lawson & Hanson, 1987).

5.1.4 Image analysis

Study I

Calculation of Metabolically Active Tumour Volume (MATV), Hypoxic Subvolume (HS) and percent hypoxic area (PHA)

The manufacturer's proprietary software ADW (Advanced Workstation 4.3, GE Healthcare, Buc, France) was used for the analysis of tumour volumes, uptake volumes for FDG and [^{18}F]EF5 tracers, and calculation of percent hypoxic area (PHA).

a) FDG images – Metabolically active tumour volume (MATV) was identified visually on the basis of anatomical CT guidance and FDG accumulation. 3D regions of interest (ROI) were positioned to cover the entire FDG-avid volume of the uptake region. These ROIs were drawn manually in all planes in which the accumulation was visible and then automatically summed to create one 3-dimensional ROI and obtain the metabolically active tumour volume.

b)[^{18}F]EF5 images –ROIs generated from the FDG study were transferred to the combined blood flow and [^{18}F]EF5 study by carefully aligning the corresponding image planes of the two PET/CT acquisitions using non-commercial research imaging software (Vinci, Max-Planck-Institut für neurologische Forschung, Cologne, Germany; http://www.mpifnf.de/vinci/). Using this software, we were able to draw equal-sized ROIs and position them in the same portion of the tumour in images obtained with all three tracers. [^{18}F]EF5 tumour-to-muscle uptake ratios (T/M) at 1, 2, and 3 hours were determined as the ratio between the resulting 3D tumour ROI and a large ROI covering a dorsal neck muscle area contralateral to the tumour in three consecutive planes. Maximum T/M for all time points was defined by comparing the highest activity in a tumour ROI against a whole muscle ROI. In the 6 patients receiving dynamic [^{18}F]EF5 scans, the same ROIs were applied throughout the long acquisition protocol. The [^{18}F]EF5-avid volume at 3 hours was determined using three arbitrarily selected T/M thresholds: 1.4, 1.5 and 1.6, which were evaluated against the voxel-by-voxel correlation between the blood flow and [^{18}F]EF5 images (see below). The thresholds formed cut-off values for 3D tumour regions presumably presenting significant hypoxia within the MATV. The PHA was calculated by dividing the summed volume of voxels above the selected T/M threshold by the MATV.

Analysis of Blood Flow Images, Correlation between [^{15}O]H_2O,[^{18}F]EF5 and [^{18}F]FDG, Time Course of [^{18}F]EF5 uptake

A comparative analysis of the global uptake of the tracers in the corresponding regions of tumours was performed with Vinci software. The size and location of ROIs was of particular importance in this comparative analysis, since a larger (MATV/FDG-sized) ROI in [^{18}F]EF5 and [^{15}O]H_2O images would result in much lower average values. Under these circumstance, the information regarding the potentially different localization of high-uptake areas inside the tumour could not be accurately extracted. A ROI was therefore drawn according to visible [^{18}F]EF5 uptake and then copied onto FDG and [^{15}O]H_2O images for each patient. In case there was no visible sub-region of [^{18}F]EF5, the [^{18}F]FDG image was used to determine the size and position of ROI in [^{18}F]EF5 and [^{15}O]H_2O images.

Voxel-by-voxel analysis was also performed in order to determine the relationship between spatial distributions of tumour blood flow as measured by [^{15}O]H_2O scan and [^{18}F]EF5 uptake, presumably representing hypoxia. The co-localization of blood flow and hypoxia images was the primary method used to validate an appropriate threshold for calculation of PHA. The voxel-by-voxel analysis was performed using the freely available open source image analysis tool AMIDE (Loening & Gambhir, 2003). Both blood flow and hypoxia images were carefully aligned using the CT image, and an identical ROI covering the whole tumour was positioned on both images. The individual voxel values (including the localization information) were extracted from

both images and the values for each voxel compared. [^{18}F]EF5 tumour values were divided by the average [^{18}F]EF5 muscle value of the respective image to obtain T/M ratios for each voxel. Voxel values for both tracers including all 18 lesions were plotted on one graph to obtain an expression of the relationship between blood flow and hypoxia in HNSCC, as evaluated with [^{15}O]H_2O and [^{18}F]EF5 PET.

Study II

Images were analysed on computer using the same Vinci software as in study I. Perfusion and [^{18}F]FDG values for different tissues were obtained by positioning a round 3-plane region-of-interest (ROI) with a diameter of 1 cm (0.77 cm^3) on the area of the lesion with the highest [^{18}F]FDG uptake and copied onto the corresponding region in the perfusion image using the CT image as anatomical reference. This was facilitated by the good co-registration of PET and CT images from the PET/CT scanner.

One example of the SUV/BF image (Figure 10) was calculated by careful realignment of tumours in both images and re-slicing. To obtain the resulting ratio image, the individual [^{18}F]FDG SUV voxel values were divided by the BF values of voxels of the same anatomical position in the BF image.

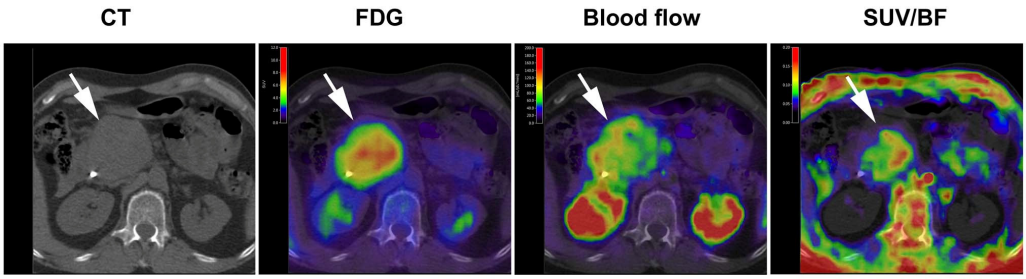

Figure 10 - Combined axial BF and [^{18}F]FDG PET images superimposed on corresponding CT slice in a patient with high-grade neuroendocrine carcinoma. Tumour located in the head of the pancreas is indicated with white arrow. Note the differential pattern of regional uptake in images representing metabolism ([^{18}F]FDG), BF and the SUV/BF ratio illustrating the incremental information provided by each functional measurement (Figure adopted from publication II).

Study III

Diagnostic [^{18}F]FDG PET images were qualitatively analysed using the scanner-manufacturer's own dedicated work station ADW (Advanced Workstation 4.3, GE Healthcare, Buc, France), by the nuclear medicine specialist.

Study IV

The parametric perfusion images were analyzed using Vinci software. Perfusion values for tumour, cerebellum and muscle tissues were obtained by positioning a 3-plane region-of-interest (ROI) over each tissue, identified using the corresponding patient's CT image. The tumour ROIs were positioned in order to cover the whole area of the tumour visible on the CT image. The same size and position of ROI were used for each of the three images from the same patient. The muscle values were obtained from the dorsal neck muscles usually visible in the same image plane as the tumour, and the cerebellum values from the part of the cerebellum in the field of view.

Study V

The perfusion images were calculated using the same compartment model and methodology as in study I. In addition, [^{18}F]EF5 and [^{18}F]FDG images were co-registered with the CT-based radiotherapy treatment plan delineated by an experienced oncologist.

To gain information about hypoxia, the tumour-to-muscle ratio 1.5 (T/M 1.5) was determined. This was achieved by delineating the neck muscle on the [^{18}F]EF5-CT image, moving the ROI to the [^{18}F]EF5-PET-image and inspecting the average activity of the tissue ROI. This value was then multiplied by 1.5, and the resulting value was regarded as the threshold of the hypoxic regions. Because the PET and CT images were acquired subsequently with the same patient positioning, the images shared the same DICOM coordinates and no image fusion was required.

The T/M 1.5 region was then delineated using the auto segmentation tool in iPlan 4.5 and the threshold value described above. After auto segmentation, an experienced oncologist removed parts that were not pathological from the structure. The resulting structure was regarded as the hypoxic area.

5.2 COMPUTED TOMOGRAPHY IMAGING

In study **III**, diagnostic abdominal MDCT with a dedicated pancreas protocol was performed according to clinical routine. A 4-phase MDCT examination was performed with a 64-slice PET/CT scanner (GE medical Systems, Milwaukee, WI) as follows: non-enhanced MDCT of the upper abdomen with 5-mm section thickness and 5-mm spacing. Intravenous contrast agent (Iomerol 400 mg/mL, 1.5 mL contrast/kg patient weight) was administered at 3.5 to 4 mL/s, and arterial phase imaging of the upper abdomen started half-automatically using the bolus tracking method. Arteriography (CTA) and pancreatic parenchymal phase imaging were scanned with collimation of 64 ± 0.625 mm, while venous imaging used 5 mm slice thickness and a scan area from

above the diaphragm to below the symphysis. Tube voltage was 120 kV, while current was determined individually using an automated modulation system.

5.3 MAGNETIC RESONANCE IMAGING

MRI of the pancreas and MRCP in study **III** were performed using a 1.5 T system (Gyroscan Intera Nova Dual, Philips Medical System, Best, The Netherlands) with a 4-channel SENSE-body surface coil. T1-weighted coronal and axial fast field (dual) echo images were obtained. In addition, axial T2-weighted fat-saturated images and coronal 2D- and 3D-MRCP were acquired before contrast agent administration, all using a turbo spin echo technique. Axial T1weighted fast field echo 3D-images of the pancreas were obtained before and after administration of a routine dose of gadolinium contrast media (0.2 mL/kg patient weight, Dotarem; Guerbet, Aulnay-sois-bois, France). Dynamic contrast-enhanced imaging was performed in 3 phases (arterial, parenchymal, and venous) concentrating on the pancreatic parenchyma.

5.4 STUDY ENDPOINTS

In studies **II** and **V**, statistical correlation of PET findings and clinical parameters was performed.

Eleven patients in study **III** with pancreatic malignancy were followed for at least 13 months after the diagnosis, and five of these patients were alive at the time of analysis. One patient with low-grade NET died due to complications related to surgery, and therefore we excluded him from the survival analysis. The remaining ten patients were divided into two groups using survival at 12 months after diagnosis as cut-off point.

In study **III**, the diagnostic accuracy of the PET studies was assessed by analyzing the operative findings or histopathological reports and when these results were unavailable, by consensus based on the other imaging procedures and follow-up examinations. Data on primary tumour site and diameter were collected from the pathology reports and/or operative findings and from other imaging studies. UICC TNM classification (Sobin, 2002) was assessed using findings from each of the imaging methods, and these were compared with histopathological (pTNM) and clinical TNM classification. Analysis and TNM classification of [^{18}F]FDG PET/CT were based on consensus of two independent observers (M.S. and S.K.) with no knowledge of the MDCT or MRI findings. MDCT and MRI/MRCP images were interpreted blindly by an abdominal radiologist from a different institute (I.RK). All the readers had the same referral information on the patients. Validation of diagnosis was based on the findings at operation without biopsies (n = 4), operation with biopsies (n = 19), percutaneous/cytologic brush biopsies (n = 3), autopsy (n = 3), and follow-up (n = 9).

Clinical TNM classification was based on the description of the tumour at operation or on the histologic specimen.

In study **V**, overall survival and local control were used as the end-points. Local control was defined as sterilization of primary tumour and/or metastases by radiochemotherapy (RCT). Local relapse was determined. The overall survival was calculated for the period between the first scan of the patient and the conclusion of the follow-up period. The median follow-up time was 40 months (range 3 – 53).

5.5 STATISTICAL ANALYSIS

In study **I**, Student's t-test was used to test the difference between the [^{18}F]EF5 SUVs at different time points. Pearson's correlation coefficient was calculated to test the correlation between the uptake values of different tracers.

In study **II**, Pearson's correlation coefficient was calculated to test the correlation between BF values of different parts of the pancreas. Unpaired Student's t-test was used to test the difference between SUV_{max}, BF values and SUV/BF ratio of normal pancreas, benign, and malignant lesions. $P<0.05$ was considered statistically significant. All statistical analyses were performed with Statview (version 5.0; SAS Institute, Cary, NC).

In study **III**, sensitivity, specificity, positive predictive value (PPV), and negative predictive value, as well as accuracy of [^{18}F]FDG PET/CT, MDCT, and MRI were evaluated. Specificity and sensitivity of PET for pancreatic tumour detection were calculated using pathology results and clinical follow-up as the gold standard using a 2 x 2 contingency table. A McNemar test was performed to compare [^{18}F]FDG PET/CT, MDCT, and MRI findings. For the receiver operating characteristic (ROC) analysis, sensitivities and specificities for different cut-off points were calculated within the group of patients with pancreatic adenocarcinoma and patients with a benign tumour or a normal pancreas. $P < 0.05$ was considered statistically significant. All statistical analyses were performed with SAS (Version 8.2; SAS, Cary, NC).

In study **IV**, the input curves were compared in terms of area under the curve (AUC). To create a slightly more detailed picture of the possible differences in the shapes of the curves, AUC values were compared for the whole duration, the first 90 s, and the period of 90-350 s.

After obtaining the BF values from the images, these were compared using the Pearson's correlation coefficient, and the difference between the values was compared using the paired Student's t-test. The agreement between the two non-invasive methods and the Blood-IF method was tested using Bland-Altman analysis (Bland & Altman,

2003). $P<0.05$ was considered statistically significant. All statistical analyses were performed using StatView (Version 5.0; SAS Institute, Cary, NC).

In study **V**, the Shapiro-Wilk test was used to test the distribution of the data. Due to the non-normal distribution of the data, Spearman correlation coefficients were calculated to determine the correlations between the uptake of FDG, EF5, and blood flow. The differences between the groups were determined using the non-parametric Wilcox signed-rank test. For the survival analysis, the Log-rank test and the Cox proportional hazards model were used. Positive predictive value (PPV) and negative predictive value (NPV) of pre-treatment PET uptakes were calculated in the analysis of localization of local relapses. Kappa-coefficient was calculated to determine the relationship between the ideal and observed division between the groups of recurrent and non-recurrent tumours. P-values of less than 0.05 were considered statistically significant. SAS Version 9.2 software was used to perform the statistical tests (SAS Institute Inc., Cary, NC).

6 RESULTS

In study **I** (15 patients), a total of 18 lesions were identified and further analyzed. These included 13 primary tumours and 5 lymph node metastases. In one patient (No. 2) only the lymph nodes could be imaged because the primary tumour was excised prior to scanning. Additionally, in patient No. 12, a radiologically and clinically undetectable, but histologically confirmed mass, designated as a T1 lesion in the base of the tongue, was not seen on the FDG scan (nor the [^{18}F]EF5 scan) and was therefore excluded from quantitative analysis. Furthermore, FDG positive lymph node metastases measuring < 1 cm in four patients were considered too small for quantitative analysis and four more patients had undetectable nodal micrometastases found only at elective neck dissection after RT.

As mentioned above in study **II**, 26 patients were divided into three groups as follows: Group A, no anatomical tumour (n=7); Group B, benign lesion (n=8), and Group C, malignant pancreatic tumour (n=11).

In studies **IV** (n = 15) and **V** (n = 22) only the primary tumours were included in further analyses.

6.1 Blood flow of tumours of head and neck and of pancreas

In study **I** In all patients except No. 12 the primary or metastatic lesion was clearly visible on both the blood flow ([^{15}O]H_2O) and FDG images (Figure 11).

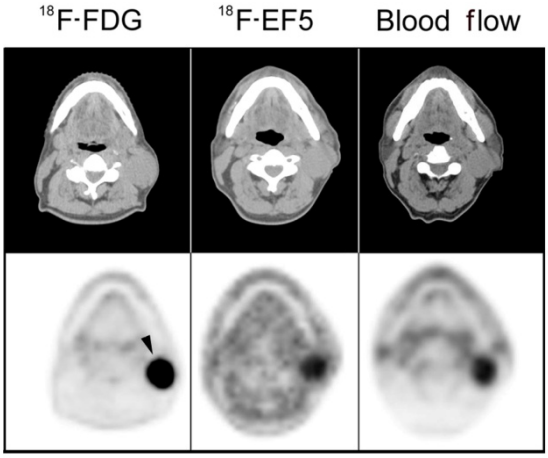

Figure 11 - Examples of both PET and CT images for all three tracers for three patients. [^{18}F]EF5 images are obtained at 3 hours post injection. Arrow indicates the primary tumour (Figure adopted from publication I).

Tumour blood flow and uptake of [^{18}F]FDG and [^{18}F]EF5 are presented in Table 5 below.

Table 5 - Tumour blood flow, metabolism expressed as Standardized Uptake Value (SUV) of FDG, and hypoxic fraction (PHA) as a percent of voxels above tumour-to-muscle uptake ratio (T/M) = 1.5 three hours after injection of [^{18}F]EF5. LN designates the lymph node metastasis of the preceding patient (Table adopted from publication I).

		[18F]FDG		[18F]EF5 3h p.i.		
No.	**Blood flow** (ml/100g/min)	**Max SUV**	**Mean SUV**	**Mean T/M**	**Max T/M**	**PHA**
1	54.84	4.80	3.74	1.49	1.75	34.70
2 (*LN*)	78.55	4.13	2.53	1.20	1.39	0.00
3	70.72	12.67	8.58	1.05	1.15	0.00
4	28.09	5.35	2.33	1.27	1.52	66.70
5	39.64	22.06	14.08	1.20	1.20	0.00
6	36.69	5.71	2.70	1.46	1.64	29.90
7	52.33	10.84	7.69	1.21	1.35	0.00
LN	35.26	8.39	6.33	1.84	2.29	64.30
8	25.92	6.35	4.74	1.38	1.74	7.60
LN	43.53	5.17	3.67	1.37	1.62	8.00
9	23.26	7.98	6.49	3.34	4.07	86.80
LN	30.96	5.45	3.93	1.90	2.63	44.90
10	40.24	10.56	7.16	1.51	1.90	20.80
LN	29.66	8.48	4.68	1.37	1.74	34.50
11	31.87	4.56	3.56	1.33	1.65	11.10
12	30.96	7.46	4.90	1.37	1.91	40.00
13	49.56	9.12	7.68	1.76	2.02	50.40
14	*	8.66	6.10	1.70	2.26	49.30

** Patient No. 2 had the primary tumour excised prior to scanning*
*** The Input curve was lost due to technical difficulties*
SUV = Standardized Uptake Value; PHA = Percent Hypoxic Area

The average mean blood flow measured in all analysed lesions was 41.3 ml/100g/min (SD = 15.4) with median being 36.7 ml/100g/min and the range 23.3 – 78.6 ml/100g/min. When looking only at the primary lesions the average mean value was 40.3 ± 14.1 ml/100g/min (median 38.3).

In study **V**, we concentrated only on the maximum blood flow values. In the 22 analysed patients the mean blood flow of the primary tumours was 102.5 ± 52.2

ml/100g/min with values ranging from 31.9 to 207.2 ml/100g/min. Median value was 92.8 ml/100g/min.

The results of average blood flow in malignant and benign pancreatic lesions, as well as in normal pancreatic tissue obtained in study **II** are presented in Table 6 and graphically in Figure 12.

Table 6 - Blood flow (BF) values for normal pancreas, benign lesions and malignant lesions, as well as values for the non-tumoural part of the pancreas in the respective patient groups (Table adopted from publication II).

	Normal pancreas	**Benign lesions**		**Malignant lesions**	
		Lesion	*Non-tumoural part*	*Lesion*	*Non-tumoural part*
BF (ml/100g/min)	113.8±48.2	59.0±26.7	87.5±32.7	45.7±18.2	59.6±40.8

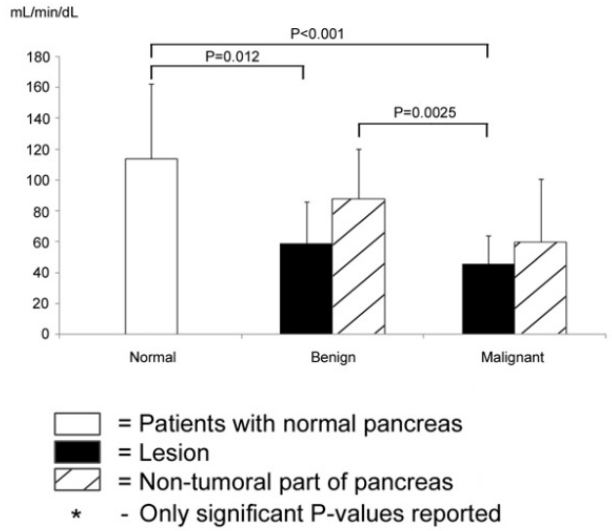

Figure 12 – Blood flow values for normal pancreas, benign lesions, and malignant lesions, as well as values for the non-tumoural part of the pancreas in the respective patient groups with statistically significant differences indicated (Figure adopted from publication II).

6.1.1 Differences between the invasive and the noninvasive methods (Study III)

In study **III**, the blood flow of 15 tumours, posterior neck muscles and cerebellum was measured using three different methods. The invasive method was used as reference method and the values obtained with it are equal to those obtained in study **I**.

6.1.1.1 Individual input curves

Comparing the AUC of individual curves (as opposed to the compared average curves above) of the three methods reveals, that on average, both non-invasive methods slightly overestimated the peak values. The average percentage increase in the total AUC of individual SUV-IFs and the corresponding Blood-IFs was 3.6% ± 19.9%, while the total AUCs (from 0 to 350 seconds) of BSA-IFs were on average greater by 2.1% ± 14.8% than the respective Blood-IFs. This difference for the first 90 seconds after injection, which represents the period of the peak value, was 4.7% ± 22.9% and 3.6% ± 18.2% for SUV-IFs and BSA-IFs, respectively. Slightly smaller average differences were observed for the period from 90 to 350 seconds after injection (3.8% ± 21.0% and 2.0% ± 15.8% for SUV-IFs and BSA-IFs). As evidenced by the relatively large SD values, the relative differences varied substantially.

Because of these substantial variations, we also performed basic correlation testing for the AUC values (Figure 13). We observed fairly good correlations between the invasive and the two non-invasive methods, with SUV-IF showing slightly steeper slopes and BSA-IF stronger correlation coefficients. However, all the P-values were below the limit of statistical significance.

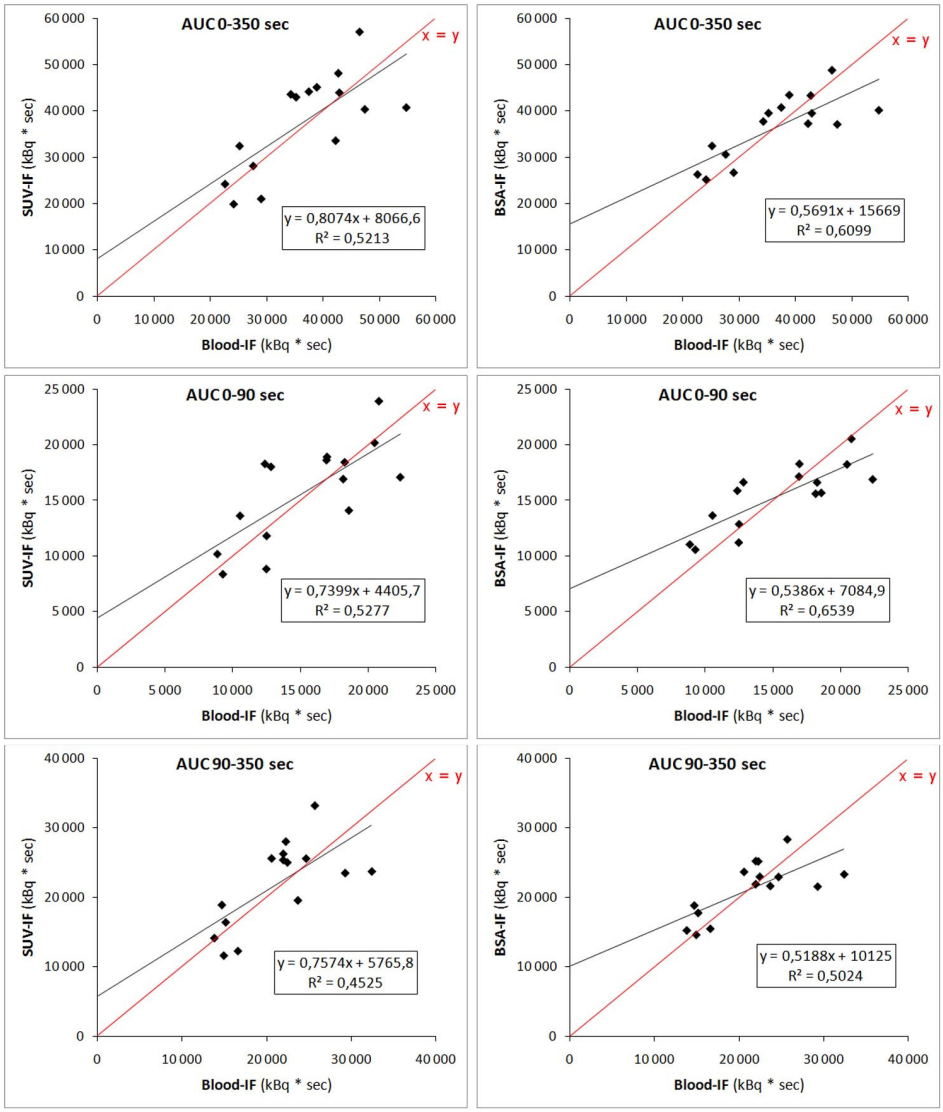

Figure 13 - Correlation of AUC of individual curves between the invasive Blood-IF method on the X-axis and SUV-IF (left column) and BSA-IF (right column) on the Y-axis. Top row represents the AUC for the whole duration of the study, the middle row the time from injection to 90 s, and the bottom row the time between 90 s post-injection to the end of the study (Figure adopted from publication IV).

6.1.1.2 Comparison of perfusion values

Due to their higher perfusion, tumours were clearly distinguishable from the surrounding muscle tissue in the parametric perfusion images of all three methods as

demonstrated in Figure 14. Also, heterogeneity within the tumours was clearly visible, but this heterogeneity was not quantified.

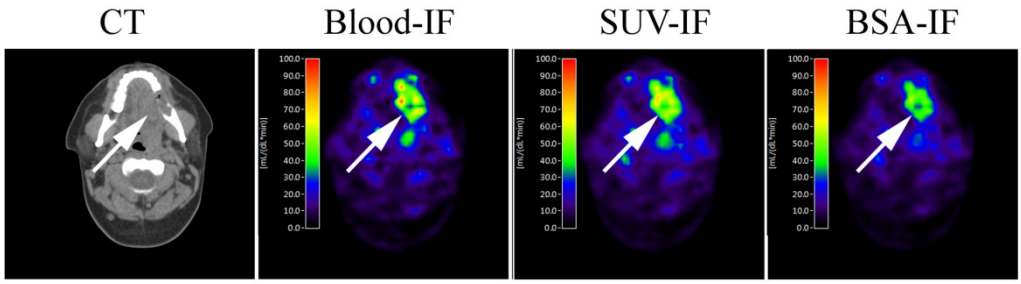

Figure 14 - Sample images of one patient obtained using all three input functions. A clear contrast between muscle and tumour tissue is visible, as well as intra-tumoural heterogeneity (Figure adopted from publication IV).

The median and range of BF values for all three methods in the three analysed tissues are presented in Table 7.

Table 7 - Median blood flow and range of values measured with the invasive (Blood-IF) and the two non-invasive methods in all 15 patients (Table adopted from publication IV).

	Blood-IF (ml/100g/min)		**SUV-IF** (ml/100g/min)		**BSA-IF** (ml/100g/min)	
	Median	Range	Median	Range	Median	Range
Tumour	57.6	45.58 – 106.18	61.57	28.50 – 110.16	61.6	34.15 – 119.73
Muscle	7	2.05 – 13.44	5.85	2.70 – 12.21	6.19	2.75 – 14.32
Cerebellum	53.85	36.99 – 79.03	54.75	33.34 – 77.46	57.82	32.20 – 86.59

Graphical analysis of values obtained in all tissues indicates that both non-invasive methods produce statistically significant correlations with the invasive method. However, BSA-IF (R^2=0.813 and P<0.0001) seems to perform slightly better than SUV-IF (R^2=0.786 and P<0.0001) (Figure 15). The paired T-test did not reveal any significant differences between the values measured with the Blood-IF method and those of the two non-invasive methods (P=0.259 for Blood-IF vs. SUV-IF and P=0.326 for Blood -IF vs. BSA-IF).

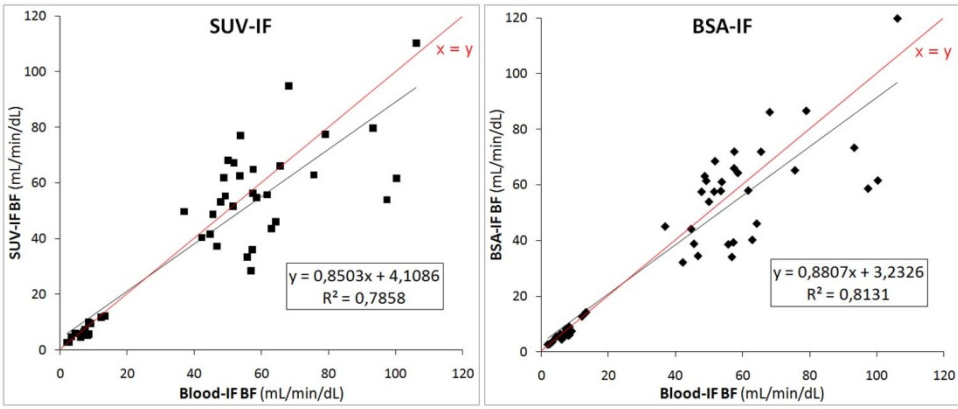

Figure 15 - Blood flow values of all tissues obtained with both non-invasive methods (Y-axis) plotted against the values obtained using the invasive method (X-axis). A tendency towards greater scattering can be observed with the increasing values (Figure adopted from publication IV).

Looking at the correlations for individual tissues, we noticed the strongest correlation in resting muscle (Figure 16). In this tissue, both SUV-IF (R^2=0.810 and P<0.0001) and BSA-IF (R^2=0.863 and P<0.0001) showed statistically significant correlations. In contrast, in tumour and the cerebellum, only BSA-IF correlated significantly with the gold standard of Blood-IF (tumour R^2=0.307, P=0.032 and cerebellum R^2=0.441, P=0.007).

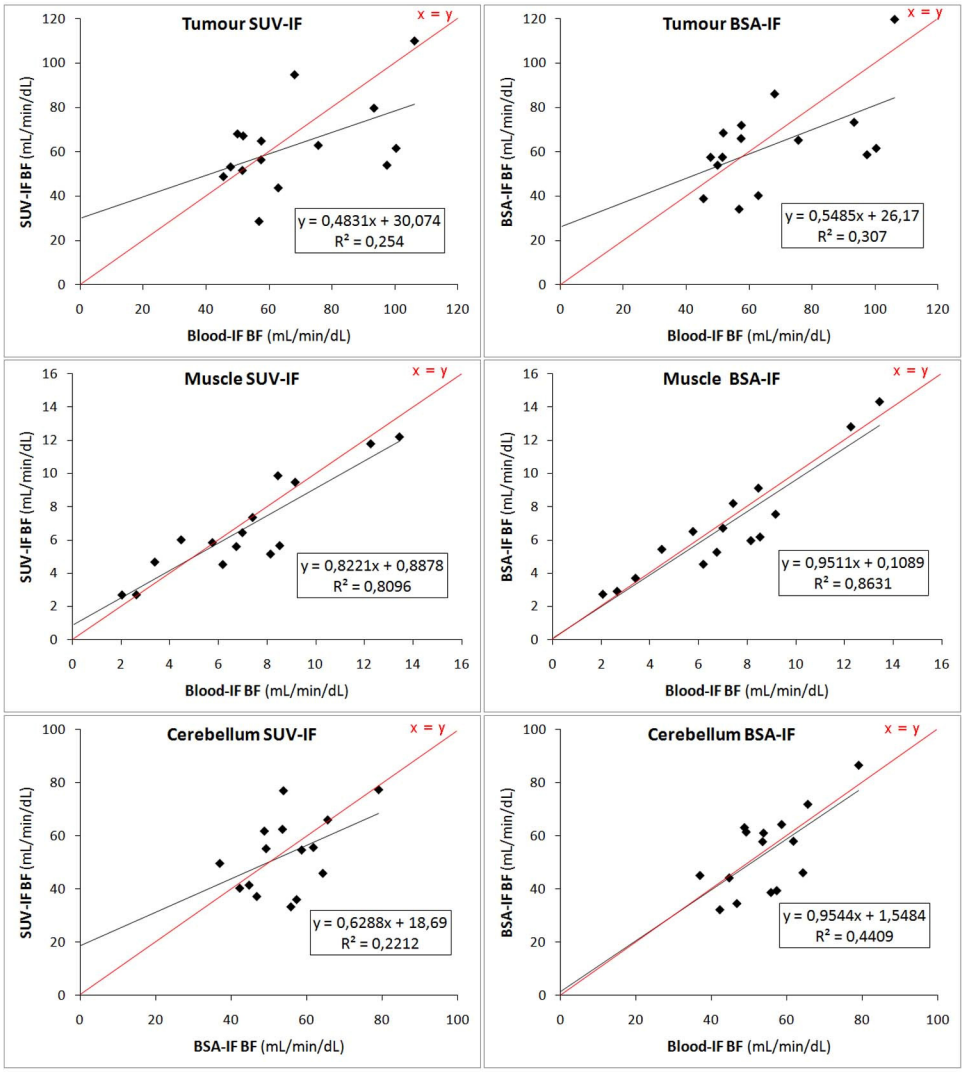

Figure 16 - Scatter charts of non-invasively obtained values plotted against those obtained invasively for tumour (top), muscle (middle), and the cerebellum (bottom). The correlation is weakest for tumour tissue in both methods (Figure adopted from publication IV).

Plotting the relative difference against the mean value of the invasive method and either SUV-IF or BSA-IF (Figure 17) did not reveal any value-dependent bias, as indicated by extremely low correlation coefficients (R^2=0.0007 for SUV-IF and R^2=0.0001 for BSA-IF) and highly insignificant P-values (P=0.863 for SUV-If and P=0.937 for BSA-IF) in both methods. Also, BSA-IF performs slightly better than SUV-IF with most values within 20% of the average.

We observed a similar, if somewhat weaker trend when looking solely at the tumour tissue values (R^2=0.0011 with P=0.905 for SUV-IF and R^2=0.0018 with P=0.880 for BSA-IF) (Figure 17, red dots).

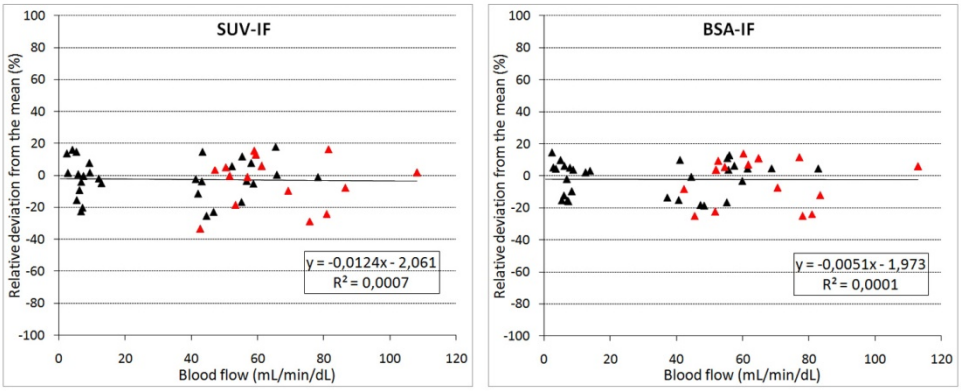

Figure 17 - Bland-Altman plots depicting relative deviation of the non-invasive value from the mean of both non-invasive method and the invasive method plotted against this mean value for all values. The relative deviation does not change with the magnitude of the mean value as witnessed by the low R^2 and high P-value of their correlation. Red dots represent tumour values (Figure adopted from publication IV).

6.2 Metabolic activity of pancreatic and head and neck cancer

The metabolic activity was studied using the [^{18}F]FDG PET (Studies **I, II, III and V**).

Due to its simplicity and wide familiarity in clinical applications we used the semi-quantitative method of standardized uptake value (SUV).

The results obtained in Study **I** are presented in Table 8.

The average maximum SUV (SUV_{max}) was 8.21 ± 4.22 g/ml with the range between 4.8 and 22.06 g/ml. Median SUV_{max} value was 7.72 g/ml. The average mean SUV value (SUV_{mean}) was 5.61 ± 2.85 g/ml with the range between 3.74 and 14.08 g/ml. Median SUV_{mean} value was 4.82 g/ml.

The results obtained in study **V** with the five additional patients and the total number of 22 are presented in Table 8 (all the PET values). The average SUV_{max} here was 12.56 ± 6.92 g/ml with the range between 2.97 and 32.66 g/ml. The median SUV_{max} value was 11.74 g/ml.

Table 8 – All the PET values obtained in study V.

	[18F]FDG			[18F]EF5				Blood Flow	
Number	ID (MBq)	SUVmax	Volume (cm^3)	ID (MBq)	T/Mmax	Volume (cm^3)	HFA (%)	ID (MBq)	Max (mL/min/dL)
1	368	10.00	12.32	319	1.81	2.15	17.45	1290	124.71
2	389	6.25	4.50	348	1.73	1.27	28.22	1339	160.93
3	257	8.15	7.24	322	1.43	0.00	0.00	1176	86.78
4	369	16.42	4.69	200	1.56	0.10	2.13	1218	95.95
5	359	20.29	20.83	363	1.60	1.07	5.14	1205	171.10
6	375	8.96	0.98	364	1.49	0.00	0.00	1001	48.11
7	376	32.66	7.04	326	1.59	0.39	5.54	1176	63.38
8	363	12.29	10.56	363	1.84	1.66	15.72	1069	69.34
9	375	13.69	13.40	244	3.74	21.52	100.00	1320	31.89
10	377	16.30	16.14	250	2.06	10.56	65.43	1061	97.60
11	355	7.38	1.07	181	1.46	0.00	0.00	1328	44.06
12	350	3.71	3.91	189	1.95	3.52	90.03	1405	52.48
13	372	12.71	2.05	196	2.10	0.78	38.05	1358	79.14
14	358	2.97	1.17	216		0.00	0.00	1065	37.90
15	375	15.32	44.99	250	2.47	28.85	64.13	1051	72.72
16	200	26.00	22.42	297	2.50	22.39	99.87	1150	158.86
17	372	10.91	3.03	247	1.89	0.98	32.34	1129	89.55
18	361	12.69	1.17	212		0.00	0.00	1168	100.67
19	290	12.34	5.18	175	1.67	0.10	1.93	1160	186.20
20	369	7.17	12.71	377	1.95	0.71	5.59	1170	105.25
21	254	11.18	3.91	297	1.98	0.59	15.09	1071	207.15
22	366	8.97	4.21	366	1.46	0.00	0.00	1157	171.68

In study **II**, glucose metabolism of pancreatic benign and malignant lesions was evaluated using SUV_{max}. The [18F]FDG average values obtained are presented in Table 9.

Table 9 - FDG values obtained in malignant and benign lesions of the pancreas, as well as normal pancreatic tissue (Table adopted from publication II).

	Normal pancreas	Benign lesions		Malignant lesions	
		Lesion	*Non-tumoural part*	*Lesion*	*Non-tumoural part*
FDG (SUVmax)	2.7 ± 1.3	2.9 ± 1.0	1.8 ± 0.4	8.0 ± 4.9	2.4 ± 1.4

Average SUV_{max} for normal pancreas was 2.7±1.3 (range, 1.8 – 5.1). SUV_{max} values for malignant lesions were significantly higher compared to those for normal pancreas (P=0.01) or benign lesions (P=0.01). Instead, SUVs of benign lesions were not significantly different compared to those for normal pancreas (Figure 18). The GlcP values were 6.7±1.7, 5.6±0.6 and 7.1±1.8 mmol/L for patients with normal pancreas,

benign, and malignant lesions, respectively. Only the difference between GlcP values of patients with benign and malignant lesions was statistically significant (A *vs*. B, P=0.11; A *vs.* C, P=0.61; B vs. C, P=0.03). To account for this difference, SUV_{max} was normalized to GlcP levels as explained above. The GlcP-normalization had the strongest effect on the statistical differences between groups A and B (non-GlcP P=0.12), but less effect on other values. The time between injection of [^{18}F]FDG and start of imaging did not differ significantly among the three groups (A: 58.1±5.9; B: 56.5±3.0; C: 57.2±5.7 min, respectively).

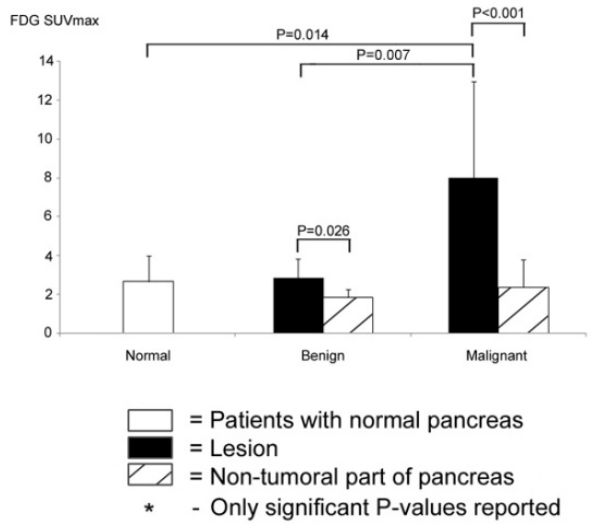

Figure 18 - FDG values obtained in malignant and benign lesions as well as in normal pancreas. Statistical significance of the differences is indicated above the bars (Figure adopted from publication II).

6.3 [^{18}F]EF5 (Studies I and V)

6.3.1 Dynamics of [^{18}F]EF5 uptake and maximum T/M ratios

In the very early phase (minutes post-injection) we observed a pattern in the[^{18}F]EF5 uptake resembling the [^{15}O]H_2O blood flow images. This was most likely due to the high concentration of tracer in the blood and consequently also in the hyperperfused areas of the tumours. The activity in these areas decreased over time and a slow but steady increase of the activity in other tumour regions became visible (Figure 19).

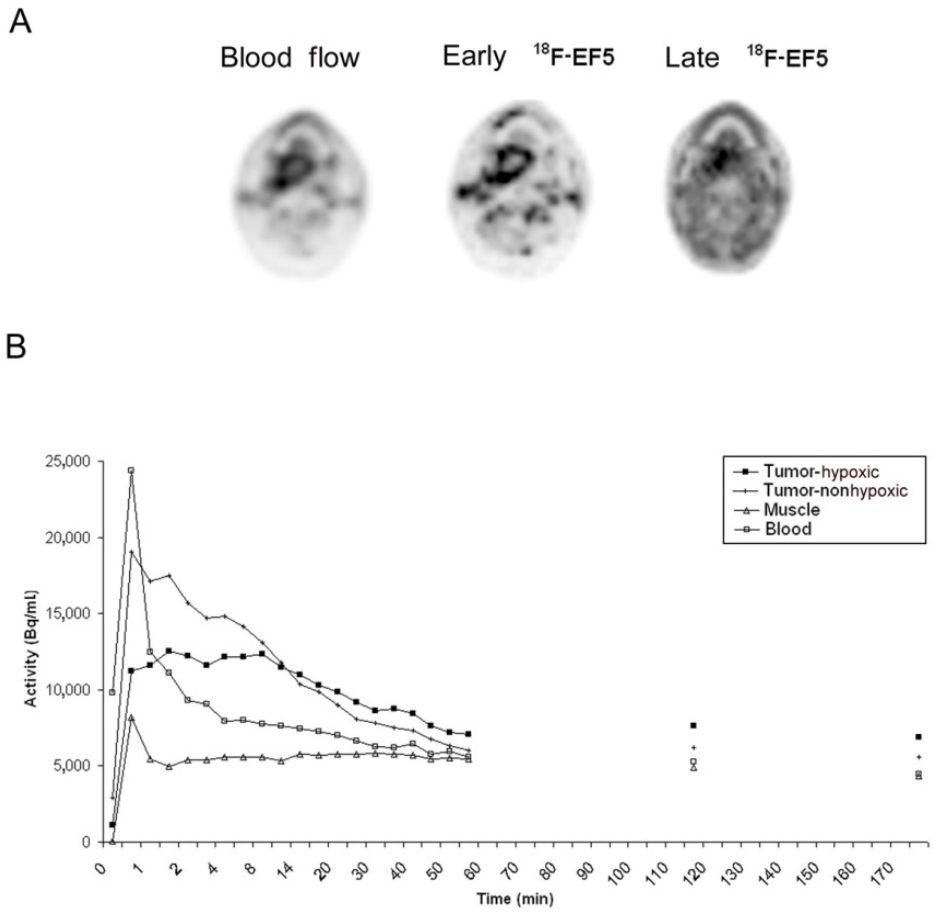

*Figure 19 - Combined blood flow and early and late (3 hours from injection) [^{18}F]EF5 images (**A**) in patient No. 1 who presented with a right T4N0 base of tongue HNSCC. Note the similarity of blood flow and early [^{18}F]EF5 images (2 minutes from injection) showing a doughnut-like appearance of tracer uptake in tumour. In contrast, the [^{18}F]EF5 image obtained 3 hours post-injection shows uptake in the central, less perfused area. Time Activity Curves (**B**) from the same tumour demonstrating the differential uptake kinetics of [^{18}F]EF5 of the peripheral (non-hypoxic) and central (hypoxic) parts of the tumour. In the well-perfused area, initial uptake of [^{18}F]EF5 is higher than in the more hypoxic area; after the first 15 minutes, the reverse is the case. With the exception of the first 90-second image, the uptake in dorsal neck muscle and arterial blood remains lower than that in both tumour parts throughout the 3-hour acquisition time (Figure adopted from publication I).*

We also observed a similar early-stage, presumably blood-flow-dependent, pattern in tumours that did not show [^{18}F]EF5 uptake at later time points.

To determine the optimal imaging time point, we compared the [^{18}F]EF5 T/M for all the static emission image acquisition time points after injection (1, 2, and 3 hours) (Figure 20).

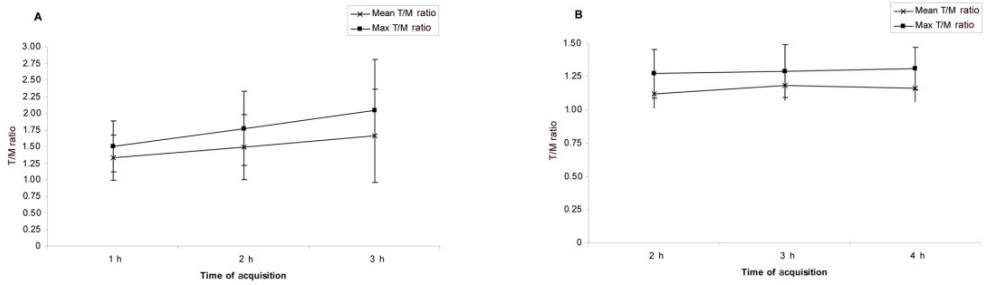

Figure 20 – Maximum and mean [^{18}F]EF5 T/M ratios over all static emission image acquisition time points. Mean T/M ratios increase from 1 through 3 hours post-injection (A). Higher max T/M ratio and lower mean T/M ratio at 4 h p.i., when compared to 3 h p.i. could be explained by the increasing image noise (and decreasing overall image quality) (B) (Figure adopted from publication I).

Due to a steady increase of T/M values from 1 to 2 hours (mean T/M p=0.005; max T/M p<0.001) and from 2 to 3 hours (mean T/M p=0.01; max T/M p=0.005), a decision was made to scan three additional patients at 4 hours post-injection. In these three patients, we observed a small decrease in the mean T/M ratio (p=0.29), a small increase in max T/M ratio when compared to 3 hours images (p=0.32, Figure 3b) and a noticeable degradation of overall image quality.

6.3.2 Hypoxic sub-volume and Percent hypoxic area (PHA)

To determine the MATV, a "brush" tool was used and the entire visible tumour was selected in all planes and summed. The average measured MATV was 9.02 cm^3 (0.4 – 55.35 cm^3). Because of to the lack of previous clinical experience using ^{18}F-EF5, three T/M thresholds were applied in the ^{18}F-EF5 images. The volumes composed of voxels above this threshold were considered hypoxic and these volumes varied with the applied thresholds (Figure 21). The lowest threshold of 1.4 resulted in the largest HS (average HS 48.9%; range 25% – 97%) such that 14 out of 18 tumours (78%) displayed some degree of hypoxia. As expected, these values decreased with the increased thresholds. For the threshold of 1.5, the average HPA was 30.5% (range 8% - 87%) and the percentage of hypoxic tumours remained at 78%. With the highest threshold of 1.6, the average HPA dropped to 16% (range 1% - 74%) and areas above this threshold were found in 11 out of 18 lesions (61%). Comparison of individual thresholds with the blood flow data depicted in Figure 5 supported the T/M threshold

of 1.5 as representing clinically significant hypoxia, since all tumour regions with high blood flow fell below this value.

In lesions with areas above the T/M ratio of 1.5, no correlation between the size of the lesion and the HPA was observed.

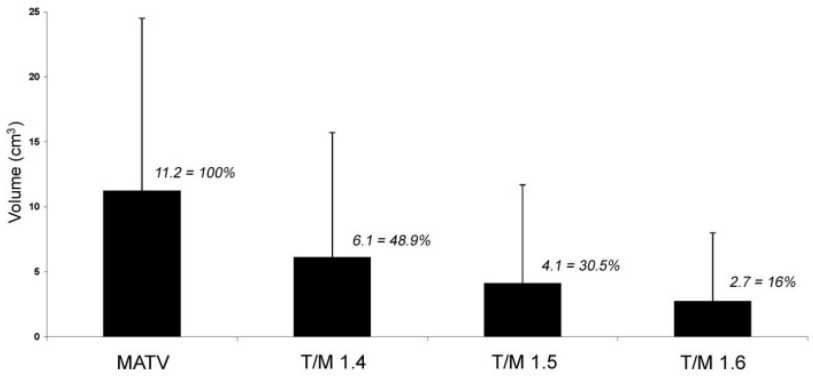

Figure 21 - Comparison of percentages of tumour sub-volumes representing HPA using three different T/M ^{18}F-EF5 uptake threshold values. Metabolically active tumour volume (MATV) is determined from FDG study performed on a separate day (Figure adopted from publication I).

6.4 Correlations between [^{18}F]EF5 uptake, metabolic activity and blood flow

Study I

The lesion uptake values for FDG and blood flow, as well as for [^{18}F]EF5 at 3 hours p.i. are shown in Table 8.

The global tumour uptake did not show significant correlation between any of the three tracers although the patterns of regional uptake in the blood flow and early [^{18}F]EF5 images were similar. Voxel-by-voxel analysis revealed a complex picture of the relationship between tumour blood flow and tumour hypoxia, as monitored by [^{18}F]EF5. Three visually distinct trends were observed. All regions with high blood flow had T/M <1.5 (Figure 22, region A) and showed a positive correlation between blood flow and [^{18}F]EF5 T/M ($R = 0.621$, $P<0.0001$). In regions with blood flow values less than 30 ml/100g/min (Figure 22, region B), we observed a negative correlation ($R = -0.042$, $P=0.259$) between blood flow and [^{18}F]EF5 T/M. Between these two expected extremes (Figure 22, regions C), blood flow and hypoxia increased at approximately the same rate ($R = 0.295$, $P<0.0001$). Analysis of all the tumour voxel values above T/M = 1 showed an inverse relationship between the two tracers ($r = -0.2$).

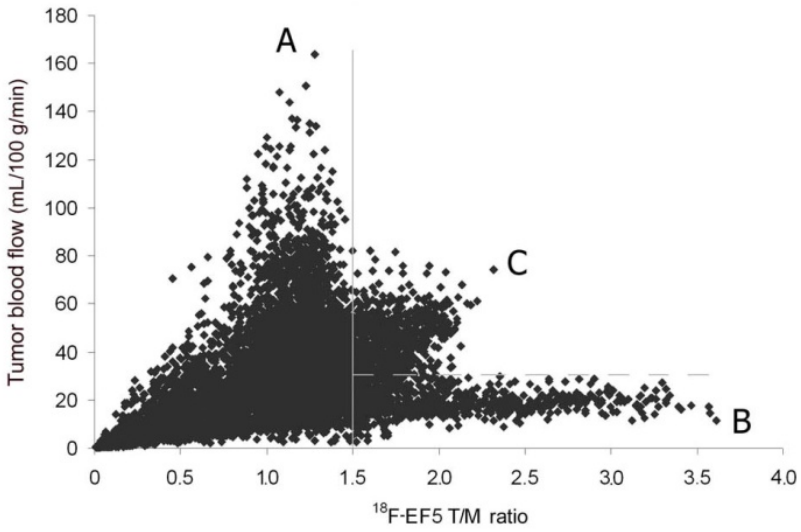

Figure 22 - Relationship between uptake of 18F-EF5 at 3 hours expressed as T/M and blood flow on a voxel-by-voxel basis in all 18 primary and metastatic tumours. The y-axis indicates the threshold value of 1.5, tentatively representing the PHA. The x-axis indicates the perfusion value of 30 ml/100 g/min, which represents the border between poorly and well perfused areas. As a result, areas of high perfusion with good oxygenation (trend A), low perfusion with low oxygenation (trend B), and the intermediate (trend C) (Figure adopted from publication I).

Also in study **V** with the additional five patients we did not observe any significant correlations between any of the relevant PET parameters.

In study **II**, SUV_{max} values were also divided by BF to obtain the SUV/BF ratio. The values for this parameter are presented in Figure 23.

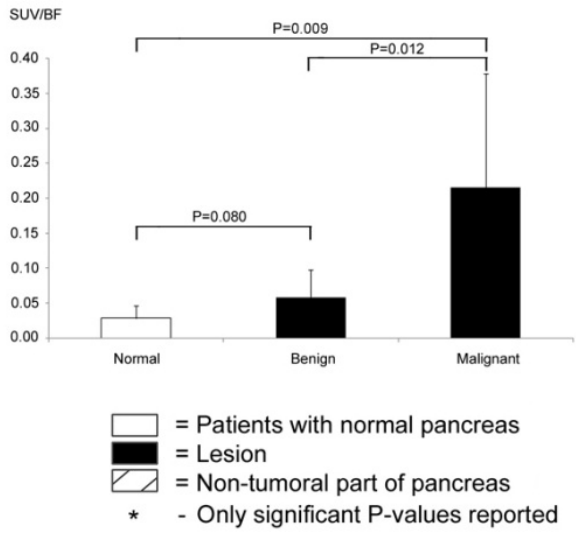

Figure 23 – SUV/BF values obtained in malignant and benign lesions, as well as in normal pancreas. Statistical significance of the differences is indicated above the values (Figure adopted from publication II).

We did not observe any significant correlation between [^{18}F]FDG uptake and BF measured in any part of the pancreas.

As expected, the SUV/BF ratio was significantly different between normal pancreas and malignant lesions (P=0.01), as well as between benign and malignant lesions (P=0.01). In contrast, no difference was observed between SUV/BF of normal pancreas and benign lesions (P=0.08) (Figure 23). When we plotted the SUV_{max} against the BF values of the same lesion we observed a clustering of values according to the lesion pathology (Figure 24). However, there were no significant correlations between [^{18}F]FDG SUV_{max} and BF in any of the three groups.

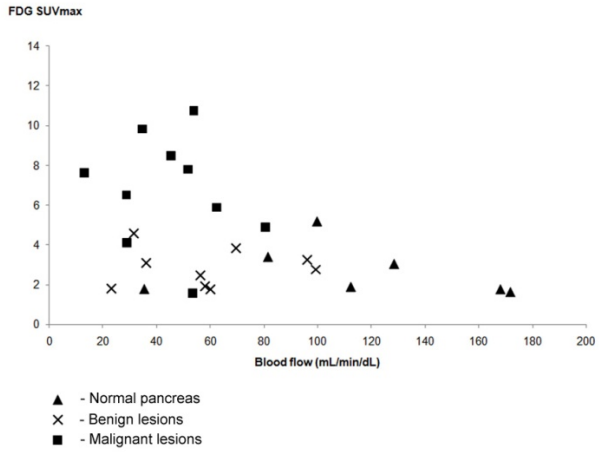

Figure 24 - The relationship between uptake of [^{18}F]FDG and BF in individual patients presenting with a malignant lesion (squares), benign lesion (crosses), and normal pancreas (triangles) (Figure adopted from publication II).

6.5 The correlation between pre-treatment tumour characteristics and PET values (Study V)

Table 10 – Most relevant information regarding tumour location and therapy in Study V

											Radiotherapy Doses and Fractions			
Number	Gender	Age	Weight	BMI	Tumor location		TNM	STAGE	Grade	Chemotherapy (Cys)	Accumualtive Cys dose	Def CRT (Gy)		CRT + Srg	
1	M	45	65	21.2	Base of tongue	Oropharynx	4/1/0	IV a	II	40mg/m2/wk x6	420 mg (228mg/m^2)			62.9	25
2	M	58	72	24.3	Retromolar/Base of Tongue	Oropharynx	2/1/0	III	II	40mg/m2/wk x6	435 mg (231 mg /m^2)			66.5	26
3	F	58	50	21.6	Tonsilla	Oropharynx	1/2b/0	IV a	II	40mg/m2/wk x3	171 mg (118mg/m^2)			68.1	27
4	M	62	67	22.4	Supraglotis	Larynx	2/2b/0	IV a	II	40mg/m2/wk x6	420 mg (233mg/m^2)			68.8	26
5	F	39	68	21.5	Supraglotis	Larynx	4/2c/0	IV a	III	40mg/m2/wk x5	380 mg (200mg /m^2)			70.3	26
6	M	43	100	27.7	Tuber maxillae (gingiva) l. sin	Oral cavity	4/0/0	IVa	I	40mg/m2/wk x6	540 mg (234mg/m^2)			62.7	26
7	M	68	70	26	Base of Tongue	Oropharynx	2/1/0	III	II	40mg/m2/wk x4	380 mg (160mg/m^2)	68.4	26		
8	F	46	59	22.5	Nasopharynx	Nasopharynx	1/2/0	III	III	40mg/m2/wk x6	375 mg (231mg/m^2)	70.3	26		
9	M	53	76	24.8	Post.aryt.glottic	Larynx	3/2b/0	IV a	II	40mg/m2/wk x6	420 mg (223 mg/m^2)			60.8	26
10	M	23	129	39.8	Tongue	Oral cavity	3/2b/0	IV a	I	40mg/m2/wk x4	320 mg (135mg/m^2)			61.66	26
11	M	70	92	27.8		Baseos oris	1/0/0	I	II	40mg/m2/wk x5	380 mg (179mg/m^2)	66.5	26		
12	M	57	77	25.7	Base of Tongue	Oropharynx	1/2b/0	IVa	III	40mg/m2/wk x6	390 mg (210mg/m^2)			62.3	33
13	M	65	98	29.6	Nasopharynx	Nasopharynx	2a/1/0	II b	III	40mg/m2/wk x6	480 mg (219mg/m^2)	57.2	34		
14	M	68	64	22.7	Base of tongue	Oropharynx	1/2b/0	IV a	III	40mg/m2/wk x6	400 mg (235mg/m^2)			63.7	34
15	F	78	52	22.2	Maxilla		4/1/0	IVa	II	40mg/m2/wk x6	330 mg (231mg/m^2)			64.6	34
16	M	57	99	27.7	Base of tongue	Baseos linguae	3/2b/0	IV a	III	100mg/m2/wk x2	375 mg (169mg/m^2)			62.4	33
17	M	61	130	40.1	Oropharynx	Oropharynx	2/2/0	IVa	III	40mg/m2/wk x6	480 mg (196mg/m^2)			65.5	35
18	M	51	65	19		Baseos oris	2/1/0	III	II	40mg/m2/wk x6	440 mg (233mg/m^2)			59.9	30
19	F	61	80	29.4	Retromolar	Retromolaris	3/2b/0	IVa	II	40mg/m2/wk x2	140 mg (74mg/m^2)			59.9	30
20	M	54	70	23.4	Hypopharynx	SCC Hypopharyngis	4a/1/0	IV a	III	40mg/m2/wk x6	420 mg (232mg/m^2)	69.3	33		
21	M	60	80	25	Tongue	Linguae dex	2/0/0	II	II	ND	ND			60	30
22	M	53	91	32.2	Tonsilla	SCC Tonsillae	3/2c/0	IV a	II	40mg/m2/wk x6	440 mg (222mg/m^2)	55.68	32		

Dividing the patients into two groups according to disease stage (I+II + III vs. IV) did not result in any significant difference in any of the PET parameters. When dividing

patients according to the T-classification (T1+T2 vs. T3+T4), only MATV values of the two groups were significantly different (p=0.009); however, none of the most relevant uptake parameters (FDG SUVmax, EF5 T/M max and Blood Flow) showed statistically significant differences between the groups. These results are graphically presented in Figure 25.

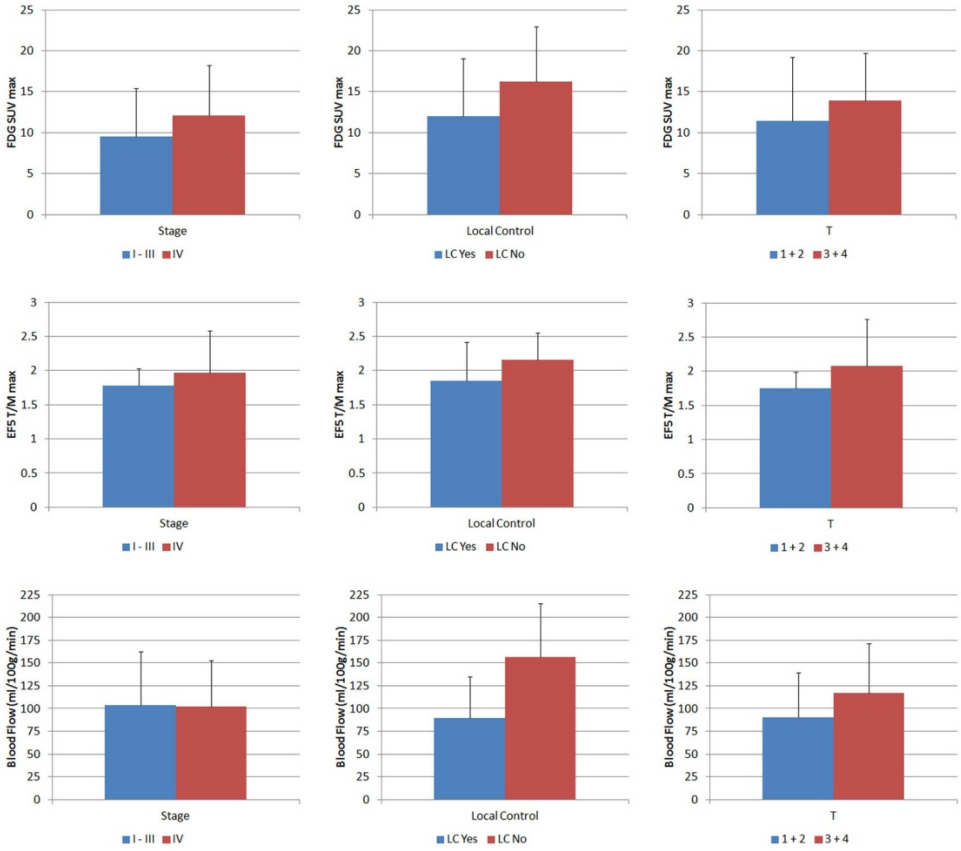

Figure 25 – Even though there was a visible trend for higher Stage, larger T-value and tumours with post-treatment local control failure to have higher values of all three PET parameters, the differences were not statistically significant.

No significant results were observed between these compared groups with regard to received treatment.

6.6 Correlations between uptake of PET tracers and Clinical end-points (Studies II and V)

The results obtained in studies **II** and **V** were also correlated with the clinical end-points.

6.6.1 Correlation between PET parameters and overall survival in pancreatic cancer (Study II)

The PET parameters and the survival of patients in study II are presented in Table 11.

Table 11 - Blood flow (BF), [^{18}F]FDG uptake and survival of patients with malignant pancreatic lesion (Figure adopted from publication II).

Patient No.	**Gender**	**Age**	**Blood flow** (mL/min/dL)	**FDG** (SUVmax)	**FDG/BF Ratio**	**Size of Tumor** (cm)	**pTNM/cTNM**	**Survival** (months)	**Therapy** (duration months)
1	F	68	28.9	6.5	0.23	4.7	T4N1bM0	3	no resection / no oncological treatments
2	F	69	34.8	9.8	0.28	5.0	T3-4NXM1	8	no resection / G (6)
3	M	64	13.2	7.6	0.58	7.5	T4NXM0	3	no resection /G (0.5)
4	F	59	80.6	4.9	0.06	3.0	Insufficient	20*	no resection / G + radiotherapy (7)
5	M	62	29.1	4.1	0.14	6.5	No histology	19*	no resection / G (10)
6	F	74	45.4	8.5	0.19	3.5	T2-3N1M0	6	R1 resection / G (2) + capecitabine
7	F	69	48.9	20.6	0.42	3.5	TXNXM1	5	no resection / reduced G (1)
8	F	67	62.5	5.9	0.09	2.5	Insufficient	14*	no resection / G (12)
9	M	77	53.9	10.8	0.20	5.0	T2-3N1M0	13*	R0 resection / G (8)
10	M	56	51.7	7.8	0.15	8.0	High-grade NET	23*	no resection / somatostatin-analog (13) carboplatin/etoposide+streptozocin/ 5-fluorouracil
11	M	76	53.6	1.6	0.03	2.8	Low-grade NET	PO†	-

*; Alive at close-out
†; Died post op
G; gemcitabine
pTNM; pathological TNM classification
cTNM; clinical TNM classification
SUVmax; maximal standardized uptake value

Eleven patients with pancreatic malignancy were followed for at least 13 months after the diagnosis, and five of these patients were alive at the time of analysis. One patient with low-grade NET died due to complications related to surgery, and therefore he was excluded from the survival analysis. The remaining ten patients were divided into two groups using survival at 12 months after diagnosis as cut-off point. The SUV_{max} or BF between the groups living less or longer than 12 months was not significantly different (10.6±5.7 *vs.* 6.7±2.7, P=0.20 and 34.2±14.3 ml/100g/min *vs.* 55.6±18.7 ml/100g/min, P=0.08, respectively). In contrast, when the SUV/BF ratio was compared between these two groups, a high SUV/BF was associated with poorer prognosis (0.3±1.6 *vs.* 0.1±0.5; P=0.02, Figure 26).

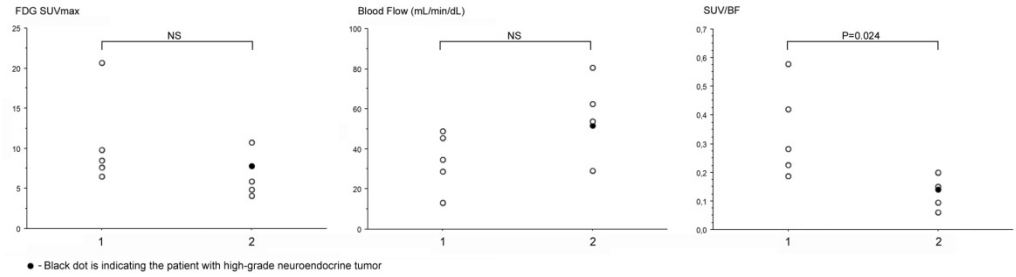

Figure 26 - [^{18}F]FDG SUVmax, BF and the SUV/BF ratio in patients with pancreatic adenocarcinoma that had died (Group 1) and those still alive at the time of analysis (Group 2) (Figure adopted from publication II).

6.6.2 Correlation between PET parameters and local relapse and overall survival in HNC (Study V)

Dividing the patients into two groups according to Local control (+ vs. -) at follow-up, PET values of the two groups did not differ significantly (Figure 25).

When divided into two groups according to the median value of each of the pretreatment PET parameters, the groups did not have significantly different overall survival. The difference was closest to significant when the two groups were formed according to the median EF5 T/M (Log-rank, p=0.109). (Figure 27).

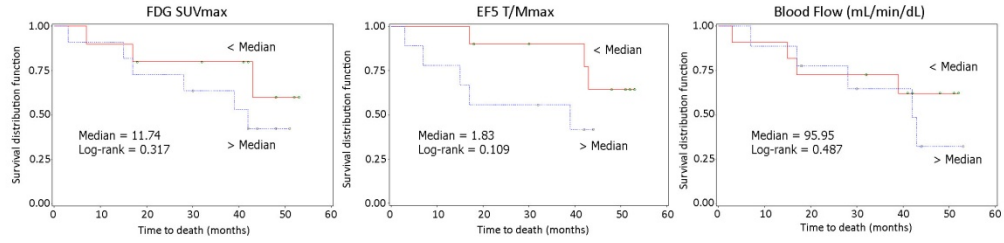

Figure 27 – Log-rank charts for the three tracers/parameters. Patients were divided into two groups based on the median value. Red line represents the patients with values above the median and blue line the patients with uptake values below the median.

Analyzed using Cox proportional hazards model, only MATV (p=0.008; HR=1.11), EF5 T/M (p=0.015; HR=4.08) and HTV (p=0.005; HR=1.12) had significant correlation with overall survival. None of the other PET values crossed the threshold of statistical significance.

6.7 Diagnostic accuracy of [^{18}F]FDG PET compared to MDCT and MRI (Study III)

6.7.1 [^{18}F]FDG PET/CT, MDCT, and MRI /MRCP in the Diagnosis of Primary Pancreatic Tumour (T-Staging)

In the diagnosis of primary tumours, [^{18}F]FDG PET/CT achieved a sensitivity of 85% and a specificity of 94%. Corresponding sensitivities and specificities for MDCT were 85% and 67%, and for MRI 85% and 72%, respectively (Table 12).

Table 12 – The performance of the three different imaging modalities in the diagnosis of primary pancreatic tumor (n = 38) (Figure adopted from publication III).

	Imaging Modality			McNemara (p)	
Parameter	**[^{18}F]FDG PET/CT**	**MDCT**	**MRI**	**[^{18}F]FDG PET/CT Vs. MDCT**	**[^{18}F]FDG PET/CT Vs. MRI**
Sensitivity	85% (17/20)	85% (17/20)	85% (17/20)	1.0	1.0
Specificity	94% (17/18)	67% (12/18)	72% (13/18)	0.025	0.046
Accuracy	89% (34/38)	76% (29/38)	79% (30/38)	0.096	0.157
PPV	94% (17/18)	74% (17/23)	77% (17/22)		
NPV	85% (17/20)	80% (12/15)	81% (13/16)		

When three patients with neuroendocrine tumour (NET) were excluded, [^{18}F]FDG PET/CT accurately detected 16 out of 17 cases with both pancreatic adenocarcinoma (n = 17) and benign tumours (n = 18) with a sensitivity of 94% and a specificity of 89%, while sensitivities and specificities were 82% (14/17) and 66% (12/18) for MDCT and 82% (14/17) and 72% (13/18) for MRI; repsectively. [^{18}F]FDG PET/CT was significantly more accurate in detecting pancreatic adenocarcinoma than MDCT (P = 0.008) or MRI (P = 0.014). Twenty-one patients with jaundice underwent ERCP by experienced endoscopists, and in all cases the stricture was suspected to be malignant. [^{18}F]FDG PET/CT T was able to distinguish between a benign and a malignant stricture with a sensitivity of 85% and with a PPV of 92% (Table 13).

Table 13 – Positive (PPV) and negative (NPV) predictive values of [^{18}F]FDG PET/CT for malignant biliary stricture (Figure adopted from publication III).

	Lesion		
[^{18}F]FDG PET/CT	Malignant	Benign	
Positve	11	1	PPV = 92%
Negative	2	7	NPV = 78%
	Sensitivy = 85 %	Specificity = 88%	

The corresponding sensitivities of MDCT and MRI were 77% and 86%, respectively. In 12 cases out of 17 with malignant disease, clinical T-staging could be assessed on the basis of either operative findings or histopathologic analysis (clinical TNM-stage) (Table 14).

Table 14 – Alterations in TNM Status (Different Imaging Methods vs. Clinical/Pathological TNM Staging) in 17 Patients with malignant disease. T-staging: assessment was possible in 12 patients based on operative findings (n = 8) and histopathological analysis (n= 4). N-staging: assessment was possible in 8 patients based on operative findings (n =2) and histopathological analysis (n = 6). M-staging: assessment was possible in 14 patients based on operative findings (n = 7) and histopathological analysis (n = 7) (Figure adopted from publication III).

	T	N	M
[^{18}F]FDG PET/CT			
Unchanged	3	3	13
Overestimated	1		
Underestimated (or no tumour detected)	7(1)	5	1
MDCT			
Unchanged	6	3	10
Overestimated	1		
Underestimated (or no tumour detected)	2(3)	5	3
MRI			
Unchanged	5	2	10
Overestimated	1		
Underestimated (or no tumour detected)	3(3)	6	3

Clinical T-stage was altered in nine patients after [^{18}F]FDG PET/CT (8 underestimated, 1 overestimated), in six patients after MDCT, and in seven patients after MRI. None of the four patients with mass-forming chronic pancreatitis had uptake in [^{18}F]FDG PET/CT. In addition, in six patients with cystic lesions of the pancreas, [^{18}F]FDG PET/CT accurately detected four out of five benign cysts and one malignant cystic lesion (Figure 28).

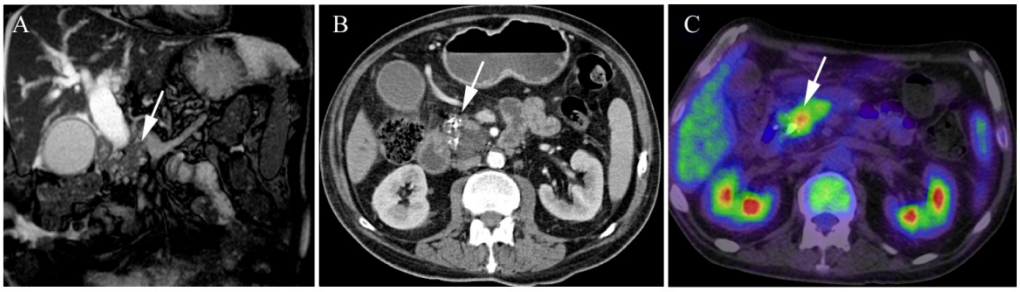

Figure 28 - A representative patient with malignant cystic lesion of pancreas seen on [^{18}F]FDG PET/CT: A 56-year-old man, who had been treated for diabetes and had had excessive alcohol consumption for several decades. He developed jaundice, and suspected malignant stricture was observed on ERCP. Serum tumor markers (CA19-9, CEA) were normal. Several cystic lesions were seen in head of pancreas on MRI (arrow) (A) and also calcification on MDCT (arrow) (B). Both MRI and MDCT findings were considered to be caused by pancreatitis. Instead, [^{18}F]FDG PET/CT showed focal uptake in head of pancreas (arrow) (C). Physical condition of the patient was very poor, and therefore operation was not possible. He died 14 months later, and autopsy verified pancreatic adenocarcinoma grade 2, as well as metastatic lesions in liver (Figure adopted from publication III).

In one patient with pancreatitis-related cystic lesions of the pancreas, all three imaging methods produced a false positive result. The patient was operated on and laparoscopy revealed benign findings. This has been reconfirmed by follow-up of 26 months without evidence of malignancy. Further, there were three false negative findings on [^{18}F]FDG PET/CT; two patients had a diagnosis of low-grade NET in the pancreas, while one patient showed inoperable adenocarcinoma in the head of the pancreas. Distributions of SUVs in the normal pancreas, benign and malignant pancreatic lesions are shown in box-blots (Figure 29). The SUVs were significantly higher in malignant lesions (4.85 ± 2.77) compared with benign lesions (2.25 ± 0.75) or the normal pancreas (2.02 ± 0.57). Retention index of SUV was borderline significant between the groups (P = 0.071).

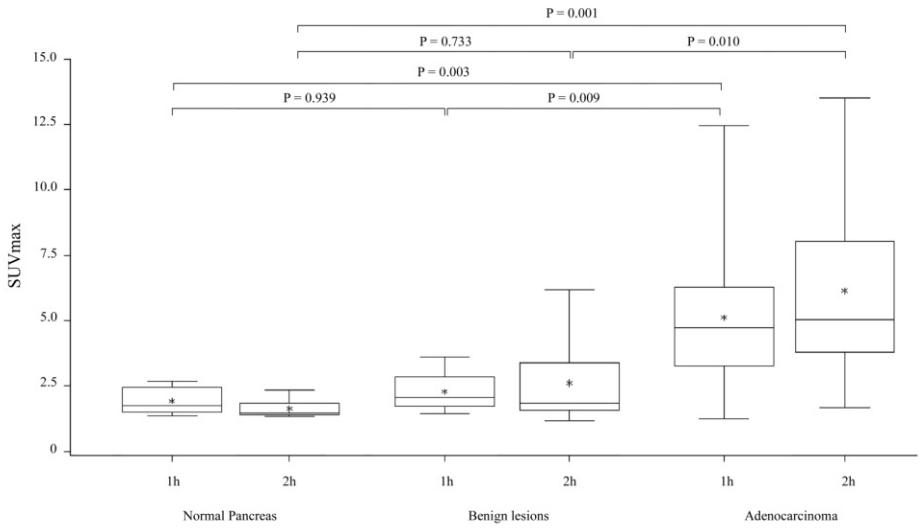

Figure 29 - Distributions of FDG SUVmax in early and delayed images in pancreatic normal pancreas, benign lesions, and pancreatic adenocarcinoma (Figure adopted from publication III).

A cut-off point of 2.6 for the SUV_{max} of the primary tumour showed the best discriminative value in receiver operating characteristic analysis (Figure 30).

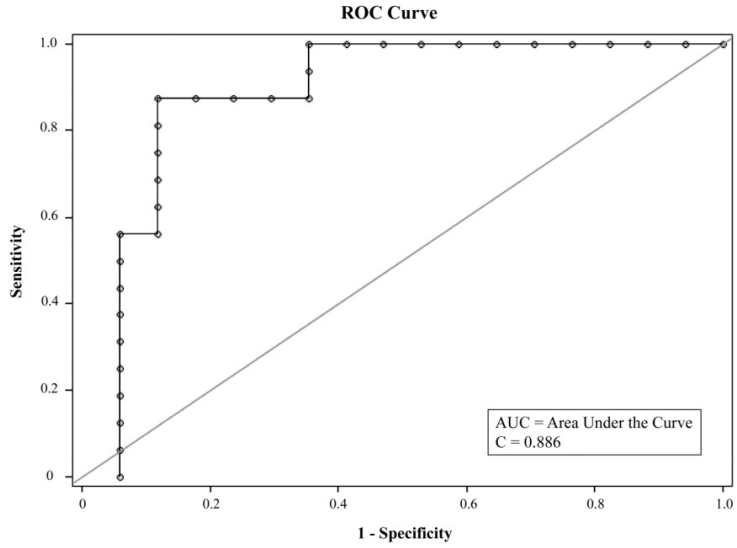

Figure 30 - Receiver operating characteristic (ROC) analysis comparing pancreatic adenocarcinoma (n = 17) with benign lesion or normal pancreas (n = 18). With cut-off of SUVmax 2.6, sensitivity was 83.3% (CI: 66.1–100) and specificity 86.7% (CI: 69.5 – 100) (Figure adopted from publication III).

6.7.2 [^{18}F]FDG PET/CT, MDCT, and MRI in the Diagnosis of Metastatic Disease (N-Staging and M-Staging)

All 17 patients with pancreatic adenocarcinoma had disseminated disease. Clinical N-stage changed in five out of eight patients after [^{18}F]FDG PET/CT or MDCT and in six patients after MRI, based on either operative findings or histopathological analysis (Table 13). Instead, [^{18}F]FDG PET/CT correctly identified the presence of distant metastasis in the liver in six out of seven patients (88%), while both MDCT and MRI only demonstrated liver metastasis in three patients. One of the liver lesions with a diameter of 1 cm was not detected in any of these imaging methods. In addition, [^{18}F]FDG PET/CT showed focal uptake in the region of the splenic flexure which was not detected on MDCT or MRI, although histological verification of this lesion was not carried out. Overall, clinical M-staging was falsely estimated in one of 14 patients after [^{18}F]FDG PET/CT compared with four patients after MDCT and MRI.

6.8 Impact of [^{18}F]FDG PET on treatment of patients with pancreatic malignancy (Study III)

In 10 out of 38 patients (26%) with suspicion of pancreatic cancer, the result of the preoperative [^{18}F]FDG PET/CT scan would have significantly influenced treatment protocol when compared with conclusions from the findings of MRI, and in 11 patients (29%) when compared with the findings of MDCT. Six patients' operations would have been avoided (3 benign lesions, 3 liver metastases), if [^{18}F]FDG PET/CT findings had been relied on. Two patients with adenocarcinoma had correctly positive [^{18}F]FDG PET/CT, but showed false negative MDCT and MRI. In two other patients with biliary stricture, both MDCT and MRI revealed a tumour in the head of the pancreas, while [^{18}F]FDG PET/CT was negative. These patients are still well without operation and no signs of malignancy have been observed during the 14 and 16 months of follow-up. If [^{18}F]FDG PET/CT had been used as a first-line imaging method, the additional use of conventional imaging would have had a positive impact on management in only two patients (5%) with low-grade NET.

7 DISCUSSION

PET is currently considered to be the most suitable imaging method for quantifying the function of tissues *in vivo*. With the use of short-lived radioisotopes, the radiation exposure of the studied subjects is comparable to exposure in modern radiological tomography studies. However, the relatively short half-life also limits the time period in which good quality images can be obtained. For this reason, it is crucial that the optimal imaging protocol is determined prior to the routine use of a new tracer. Another disadvantage of PET is the relatively long acquisition times required to achieve good image quality. This is usually in the range between 2 and 5 minutes for static, "snap-shot" images acquired several hours (1-3) after the tracer injection for [^{18}F]-labelled tracers. All imaging sessions were also part of multi-tracer studies, with some images being acquired on separate days, and some of the acquisitions being accompanied by blood sampling. Despite this and despite the very long imaging protocols lasting up to several hours (required for reasons mentioned above), the patients tolerated the imaging protocol quite well and none of the imaging sessions was interrupted due to patient discomfort or lack of compliance.

Relatively low numbers of patients have been studied in all studies. This is a particular problem concerning follow-up studies correlating pre-treatment findings with clinical end-points or even survival as we did in studies II and V. However, this was done, on one hand because we wanted to obtain multi-tracer information on the same tumour which requires multi-tracer, long imaging protocols and are therefore difficult to perform in larger cohorts. On the other hand this has invariably decreased the statistical power of our study. Multi-tracer protocols are costly, resulting in low number of patients studied.

The aim of this study was to explore the microenvironment of malignant tumours of the pancreas and head and neck in vivo using positron emission tomography (PET), and to test a new hypoxia PET tracer [^{18}F]EF5 in humans. With this in mind, five separate studies were performed each of them concentrating on a particular aspect of these issues.

In study I, we performed the first *in vivo* PET studies of tumour oxygenation using a new tracer [^{18}F]EF5. We evaluated the tumour uptake dynamics of the tracer and determined the most appropriate imaging protocol for the tracer. We also established that the tracer is safe for use in human subjects and appropriate for routine clinical use. In addition, we also compared the uptake of this tracer to the uptake of [^{18}F]FDG and blood flow.

In study II, we imaged patients with strong clinical suspicion of pancreatic malignancy using [^{18}F]FDG and [^{15}O]H_2O. We compared the uptake of glucose and blood flow in

malignant to those in benign pancreatic lesions and in normal pancreas. Study III was designed to compare, in a prospective fashion, the diagnostic properties of [18F]FDG PET/CT, MD(CE)CT, and MRI in patients with suspicion of pancreatic malignancy.

In study IV, we aimed to develop a new non-invasive, population-based method for blood flow quantification using [^{15}O]H_2O PET in head and neck cancer.

And in the final study (V), we compared the uptake of [^{18}F]EF5, [^{18}F]FDG, and blood flow in head and neck cancer to the clinical end-points, and tried to determine the prognostic value of pre-treatment PET imaging with [^{18}F]EF5.

7.1 Uptake of [^{18}F]EF5 in head and neck cancer (I and V)

In our study, patients with untreated HNSCC were studied with the novel tracer [^{18}F]EF5 as a hypoxia imaging agent. Our data corresponded to previously published results in cells, animals, and humans using quantitative immunohistochemical detection of non-^{18}F-labelled EF5 (Evans *et al.*, 2007; Ljungkvist *et al.*, 2007), and supported our hypothesis that [^{18}F]EF5 would be an accurate PET marker of hypoxia with uniform access to all tissues, dominantly excreted via the kidneys, and having no detectable metabolism. These observations had been previously confirmed in preclinical studies we conducted where an almost complete absence of [^{18}F]EF5 metabolites in blood was demonstrated (Gronroos *et al.*, 2004b). Based on these preclinical PET studies and many studies based on immunohistochemical detection of EF5, we predicted that [^{18}F]EF5 would display very favourable biokinetic properties for a PET tracer to be used in humans (Laughlin *et al.*, 1996; Koch *et al.*, 2001). Since there was very limited information on uptake of [^{18}F]EF5 in human tissues, our study included a long scanning protocol. Specifically, we sought to determine an optimal time point for detection of specific binding in hypoxic tissues; we predicted that 2 – 4 hours from injection would be optimal, based on previous data from other 2-nitroimidazole compounds. Our data showing increasing T/M over the first three hours and slight degradation of the image quality at four hours supports the recommendation that three hours after the injection of [^{18}F]EF5 is the optimal acquisition time for clinical protocols.

This allowed us to modify the scanning protocol when we were scanning seven additional patients included in the follow-up study (IV) where we only acquired static images at three hours p.i. We believe this to be a simple protocol that can be applied routinely in clinical practice, not unlike a typical [^{18}F]FDG scan.

7.2 Correlations between [^{18}F]EF5 uptake and [^{18}F]FDG and Blood flow (I and V)

In addition to [^{18}F]EF5 imaging, blood flow studies with [^{15}O]H_2O and [^{18}F]FDG imaging were performed to evaluate the interrelationship between tumour blood flow and metabolic activity. The measured blood flow values for tumours were significantly higher than those found in muscles of adjacent neck areas, varying between 23 and 78 ml/100g/min, while the muscle values remained considerably lower, between 2.5 and 12 ml/100g/min. These results are in accordance with previous studies in HNSCC performed in our centre (Lehtio *et al.*, 2001).

As expected, we could not find any significant correlation between the three tracers either in studiy I or in study IV with the slightly higher number of patients. This again emphasizes the need for a multi-tracer approach through which relevant information can be obtained on different aspects of tumour biology.

7.3 Relationship between glucose metabolism and blood flow in pancreatic tumours (II)

In study II, the focus of our investigation was the relationship between glucose metabolism and blood flow in malignant and benign pancreatic lesions. To our knowledge, this was the first prospective study where BF and metabolism were measured in parallel using [^{15}O]H_2O and [^{18}F]FDG PET/CT in such lesions. We found average BF to be significantly decreased and metabolism significantly increased in malignant pancreatic lesions compared to normal pancreas. Based on our initial findings, we hypothesise that a high ratio of metabolism to BF may predict survival better than either functional measurement alone.

At a time when the possibilities and limitations (Nalluri *et al.*, 2008) of new therapeutic agents targeting angiogenic mechanisms of tumours are being recognized, it is becoming obvious that careful classification and selection of patients prior to treatment is necessary for these therapeutic strategies to be successful. This is of particular importance in malignancies with a low likelihood of response, such as pancreatic cancer (Longo *et al.*, 2008). In this respect, tumour perfusion and metabolism seem to be among the most relevant clinical parameters (Hoekstra *et al.*, 2002; Miles & Williams, 2008). Several methods have been proposed for non-invasive measurement of pancreatic perfusion in humans. Contrast-enhanced US (Sofuni *et al.*, 2005; Bize *et al.*, 2006) and DCE-CT (Miles *et al.*, 1995) have been used to assess pancreatic perfusion in inflammatory and malignant lesions with encouraging results. Park et al. observed that high perfusion in pancreatic cancer detected on DCE-CT was associated with increased response to chemo-radiotherapy. Also the role of DCE-MRI has evolved in the field of perfusion imaging, and several groups have used it in evaluating

the perfusion of benign and malignant pancreatic lesions (Coenegrachts *et al.*, 2004; Tajima *et al.*, 2004; Bali *et al.*, 2008; Lee *et al.*, 2008). Nevertheless, [^{15}O]H_2O PET has been studied more extensively than either DCE-CT or MRI and is regarded by some authors as a gold standard in perfusion imaging (Rajendran & Mankoff, 2007). As previously demonstrated (de Langen *et al.*, 2008; Lodge *et al.*, 2008), it is a reproducible and reliable method for the quantification of BF in tumour and other tissues such as brain and heart. In addition, CT combined with PET studies has provided the added benefit of precise anatomical localization, the lack of which was often used as an argument against PET in studies of inaccessible abdominal organs like the pancreas. The recent developments have also enabled extraction of the input curves directly from the images, making the procedure more patient-friendly compared to previously used invasive arterial blood sampling (Liukko *et al.*, 2007). This new non-invasive technique has been found to be suitable for routine clinical applications, and the findings of pancreatic tumour BF obtained in our study are in line with some of the previous studies of BF in abdominal tumours with [^{15}O]H_2O PET (Wells *et al.*, 2003). Also the results from the normal pancreas seem to be in line with BF measurements obtained in some other highly perfused abdominal organs such as the spleen (Wells *et al.*, 2003). The higher uptake of [^{18}F]FDG in malignant tumours compared to benign lesions and normal pancreas is well established and seen also in the current study.

Relative to other techniques, there are some advantages in measuring tumour perfusion using [^{15}O]H_2O PET. First, PET is currently the most quantitative and best validated method with applications in several tissue and tumour types. An additional advantage of PET imaging is the possibility to concurrently measure metabolic activity using [^{18}F]FDG. Studies on the relationship between metabolism of tumours and their BF have provided quite variable results. Some of the studies were not able to demonstrate any correlation between these two parameters (Hoekstra *et al.*, 2002), while others found a positive (Zasadny *et al.*, 2003) or a negative (Hirasawa *et al.*, 2007) relationship, depending on tumour type and grade. In the current study, we were not able to demonstrate any correlation between these two parameters. The diverse findings in different tumour types and sizes reflect the heterogeneity of malignant tissues and also the limited specificity of [^{18}F]FDG to depict neoplastic transformation.

7.4 Impact of [18F]FDG PET imaging on diagnosis and treatment of pancreatic cancer (III)

This is, to our knowledge, the first prospective study that has compared combined [^{18}F]FDG PET/CT to both dedicated MDCT and MRI in the detection and assessment of pancreatic malignancies. In this study of 38 patients, the accuracy of PET/CT was 89%, compared with 76% and 79% for MDCT and MRI, respectively. In 17 patients with advanced pancreatic adenocarcinoma, one adenocarcinoma was missed on

[^{18}F]FDG PET/CT and a sensitivity of 88% was achieved for M-staging while three adenocarcinomas were missed on both MDCT and MRI, when sensitivities were 38% for M-staging. Furthermore, the clinical management of 10 patients (26%) was changed after [^{18}F]FDG PET/CT. Due to the restrictions of the different imaging modalities, tissue diagnosis, staging, and assessment of pancreatic tumor resectability are all currently carried out during primary exploratory laparotomy. During this procedure, determination of the pathological stage and the relationship of the tumour to adjacent vessels, as well as resectability are estimated (Fritscher-Ravens *et al.*, 2005). In this context, whole-body PET imaging is an interesting imaging modality, and several studies have already shown [^{18}F]FDG PET without CT to be more accurate than conventional imaging techniques for initial diagnosis of pancreatic cancer, although conflicting results have also been published (Sendler *et al.*, 2000; Lytras *et al.*, 2005).

In our study, [^{18}F]FDG PET/CT had a sensitivity of 85% and a high PPV of 92% in differential diagnosis of biliary stricture. In agreement with our findings, Wakabayashi et al. reported a sensitivity of 91% and a specificity of 78% in evaluating malignancy in 30 patients with biliary stricture by [^{18}F]FDG PET. Our study included only four patients with mass-forming pancreatitis, and in all cases, no uptake was observed in [^{18}F]FDG PET/CT images. A study conducted to investigate the differential diagnosis of chronic pancreatitis by [^{18}F]FDG PET/CT showed that in 77 patients with long-standing chronic pancreatitis without carcinoma, [^{18}F]FDG PET was negative in 67 cases (van Kouwen *et al.*, 2005). Concerning the usefulness of [^{18}F]FDG PET in early-stage pancreatic malignancy, encouraging results have been reported in the diagnosis of intraductal papillary mucinous neoplasms of the pancreas with better sensitivity than conventional imaging (Sperti *et al.*, 2007). In addition, a study by Seo et al. (Seo *et al.*, 2008) showed a high sensitivity of 91% for the detection of resectable pancreatic cancer using [^{18}F]FDG PET, while among tumours with a diameter of less than 2 cm, the sensitivity exceeded 81% In our study, using additional [^{18}F]FDG PET/CT was not able to assess the resectability of the tumor any better than MDCT or MRI. This was caused by the poor sensitivity to show local invasion of disease due to the high signal intensity of the primary tumour, and the low sensitivity to detect small lymph-nodes. In line with this, there are no previous data supporting the usefulness of [^{18}F]FDG PET in detecting local spread of pancreatic cancer because of the lack of detailed anatomical information (sensitivities: 46%–71%, specificities: 63%–100%) (Bares *et al.*, 1994; Diederichs *et al.*, 2000; Wakabayashi *et al.*, 2008).

In our study, [^{18}F]FDG PET/CT detected distant disease with a sensitivity of 88%. In support of our results, several studies (Jadvar & Fischman, 2001; Nishiyama *et al.*, 2005; Wakabayashi *et al.*, 2008) have shown that whole-body [^{18}F]FDG PET has a complementary role in M-staging. [^{18}F]FDG PET leads to a more accurate preoperative diagnosis and avoids unnecessary non-curative operations with sensitivities ranging

from 70% to 81.8%, and specificities from 95% to 98.4% (Diederichs *et al.*, 2000; Nishiyama *et al.*, 2005).

In addition to its diagnostic relevance, several studies have shown a correlation between high SUV in pancreatic tumour and poor survival (Nakata *et al.*, 2001; Sperti *et al.*, 2003). In contrast, in a recent study, Wakabayashi (Wakabayashi *et al.*, 2008) did not observe any correlation between histology and SUV. They did, however, report a statistically significant difference in the SUV between patients with resectable and non-resectable disease. Our sample size was considered to be too low to draw reliable conclusions concerning survival and resectability with respect to SUV.

Recently, the [^{18}F]FDG PET/CT era has brought significant improvements also to the diagnostic imaging of abdominal organs. In 2000, Hosten et al (Hosten *et al.*, 2000) reported a case study of a patient with adenocarcinoma in the head of the pancreas seen in retrospective fusion of PET and CT images. Later, the same group (Lemke *et al.*, 2004) evaluated the clinical benefit of retrospective [^{18}F]FDG PET/CT image fusion in the diagnostic workup of pancreatic cancer. In their retrospective study, 104 patients with suspected pancreatic lesion underwent preoperative MDCT and [^{18}F]FDG PET. The sensitivity of the MDCT and PET imaging was 77% and 84%, respectively, and with retrospective fusion of these two imaging modalities, the sensitivity rose to 89%. So far, only two prospective studies have been conducted to evaluate the value of combined [^{18}F]FDG PET/CT in the diagnosis of pancreatic malignancy. In his study group of 59 patients, Heinrich et al. (Heinrich *et al.*, 2005) demonstrated a PPV of 91% for [^{18}F]FDG PET/CT, but a negative predictive value of only 64% for pancreatic cancer, they still, however, estimated that [^{18}F]FDG PET/CT was a cost-effective method in this patient group. Later, Schick et al. (Schick *et al.*, 2008) prospectively compared [^{18}F]FDG PET/CT, EUS, ERCP, and US in a series of 46 patients. [^{18}F]FDG PET/CT CT had a sensitivity of 89% and a specificity of 74% in the evaluation of solid pancreatic lesions of over 1 cm in diameter, a finding which was not significantly different from conventional imaging methods. According to the recent study by Strobel et al. (Strobel *et al.*, 2008), in assessing the resectability of pancreatic cancer, contrast-enhanced [^{18}F]FDG PET/CT seemed to be superior to non-enhanced [^{18}F]FDG PET/CT, or PET alone. Moreover, it was observed that the frequency of severe artefacts in the area of the diaphragm can be decreased by half if optimized breath-holding protocols are used (Beyer et al., 2003). A new gating technique to account for respiratory motion during the PET/CT scan could further improve the diagnostic accuracy of pancreatic imaging, although prospective studies have not yet been done. In addition, former studies have shown the advantage of delayed scanning in the differentiation of malignant and benign lesions (Nakamoto *et al.*, 2000; Lyshchik *et al.*, 2005); our also study showed a borderline significant difference in the retention index between the groups. In future, [^{18}F]FDG PET/CT CT could prove to be a reliable method among patients with suspicion of malignant biliary stricture and inconclusive

findings in conventional imaging. At the moment, based on this and previous studies, [^{18}F]FDG PET/CT combined with contrast-enhanced MDCT could be used as a first-line imaging method in patients with suspicion of pancreatic cancer to detect optimally unexpected metastatic lesions and [^{18}F]FDG-negative histological types (i.e. low-grade NETs).

7.5 Suitability of [^{18}F]EF5 for imaging of tumour hypoxia (I)

To validate [^{18}F]EF5 as a hypoxia marker, we compared both global and regional blood flow in tumour with the uptake of the radiolabelled 2-nitroimidazole during early and late phases of biodistribution. Both [^{18}F]FMISO and [^{18}F]FETNIM show some degree of positive correlation with blood flow within the first minutes after injection; this was also the case for [^{18}F]EF5 (Lehtio *et al.*, 2001). In 12 out of 15 patients, [^{18}F]EF5 distribution changed over time from highly perfused into less perfused areas of the tumour. This is in accordance with the cumulative character of covalent binding of [^{18}F]EF5 in hypoxic cells, which is typical for all 2-nitroimidazole-based compounds. As expected, global blood flow did not show any distinct relationship with uptake of [^{18}F]EF5 during the period of hypoxia-specific binding. We therefore performed a voxel-by-voxel analysis for evaluation of regional differences in blood flow and hypoxia 3 hours after injection of [^{18}F]EF5. During this time period, regions of several tumours showed high uptake, consistent with the presence of hypoxia. The cumulative findings from all 18 tumours showed striking correlation between blood flow and hypoxia. Under circumstances of low blood flow and high [^{18}F]EF5 binding (hypoxia) and high blood flow and low [^{18}F]EF5 binding (normoxia), a clear inverse correlation could be seen; the slopes of the best fit lines for these relationships were significantly different. Interestingly, in tumour regions where the [^{18}F]EF5 T/M was between 1.5 and 2.2, a relationship with an intermediate slope was identified where slightly increased blood flow and moderate PET values were observed.

Since all tumour regions with high blood flow fell below [^{18}F]EF5 T/M of 1.5, we propose this level as a cut-off point for determination of PHA. Of course, this T/M value as an indicator of significant hypoxia in head and neck cancer (and other tumour types) needs further validation, especially in outcome studies, before it can be generally accepted. The intermediate zone in our study suggests a more complex and heterogeneous relationship between blood flow and hypoxia, and may signify the presence of hypoxia in some well-perfused tumour regions. A number of biological explanations for this phenomenon have been proposed including acute changes in blood flow, plasma flow without red blood cells, retrograde flow, longitudinal gradients and flow in arteriovenous malformations. Interestingly, a similar observation was made by Thorwath et al. who used [^{18}F]FMISO to evaluate both blood flow and

hypoxia at the same time point but using different data modelling approaches than those described here (Thorwarth *et al.*, 2005).

7.6 Reliability of noninvasive blood flow measurement in tumours (IV)

In study **IV**, we aimed to develop and validate a simple, non-invasive method of measuring blood flow using [^{15}O]H_2O PET/CT in malignant tumours of the head and neck area. We believed this to be of importance and relevance based on the invasive nature of current methods, making them unsuitable for routine use in diagnostic imaging. In addition, it is well documented that angiogenesis plays an important role in the progression of cancer, and the validation of methods monitoring changes in blood flow is important for the development of drugs targeting the vasculature. Third, radiation oncology may also benefit from volumetric maps of tumour blood flow, especially when they are combined with metabolic maps such as [^{18}F]FDG PET images. Due to the need for patients to wear immobilization masks during radiation therapy planning studies, it is essential to keep patient comfort as high as possible to minimize patient movement due to discomfort.

Our approach was to apply two population-based methods to derive the input function, which were based on patients' injected dose and body weight (SUV-IF) and injected dose and body surface area (BSA-IF). We were able to demonstrate a fairly good correlation between the population-based methods and measured Blood-IF, in particular for BSA-IF, which resulted in $R^2 = 0.8131$ and $P<0.05$. This method performed best in resting muscle tissue, which has relatively low blood flow, but it also produced statistically significant correlations in tumours and the cerebellum. Bland-Altman analysis did not reveal any value-dependent change in the size of relative deviation from the mean, while paired T-tests did not show any significant differences between the values of the compared methods, thus offering additional support for the use of this non-invasive approach.

The focus of this study was to compare blood flow values, and as such the comparison of individual input curves was considered less important. We did, however perform a basic analysis of individual input curves, which offers some insight into the basic differences in the shape and size of the input curves obtained by the three methods. The curves were similar in shape; however the non-invasive methods did on average slightly overestimate the peak values, BSA-IF by 3.6%, and SUV-IF by 4.7%.

Based on the results of the current study we believe that, keeping the limitations of the method in mind, BSA-IF may be useful for monitoring acute or short-term changes in tumour blood flow when repeated cannulation of radial or other forearm artery is inconvenient. The non-invasive nature of the procedure is a big step forward for the routine use of blood flow measurement for planning and evaluating the effects of

therapy in patients with head and neck cancer. This is particularly important given the increasing number of drugs targeting the tumour's vasculature and angiogenesis, as well as the advances made in intensity modulated radiation therapy (IMRT). Furthermore, when comparing the same patient's images during the course of therapy, the relative differences due to a constant BSA and other physiological parameters influencing the shape of the curve might be decreased; this would make the non-invasive methods even more reliable.

Another advantage of the presented method over image-derived methods arises from the fact that it is independent of the image reconstruction method. Different reconstruction methods deal differently with the above-mentioned partial-volume and spill-over effects, and can therefore strongly affect blood activity values in smaller vessels (Brix *et al.*, 2002). Since the population-based IFs used in this study are calculated using blood data rather than image-derived data, the values are independent of the method used for image reconstruction.

One limitation of the non-invasive methods is the need for a repeatable injection procedure with the same speed and volume of injection, providing a similar shape of the arterial input curve. A high level of repeatability is achieved using computer-controlled injection as in our case. Without computer control, the variability of injection procedures might introduce a significant change in the shape of the average curves, which might in turn produce perfusion values with a lower degree of correlation and lower reliability, and thus reduce the benefit provided by constant BSA in the follow-up of patients.

As already mentioned in the introduction, a similar approach was developed by Tsuchida et al. (Tsuchida *et al.*, 1999; Shiozaki *et al.*, 2000) to calculate the metabolic rate of glucose. This is important because the shape of the input curve of glucose is influenced by more factors than the $[^{15}O]H_2O$ input curve, which is metabolically rather simple. Another similarity between our findings and those from glucose metabolism lies in the semi-quantitative nature of the standardized uptake value (SUV) itself. SUV, while being a very simple value, provides good levels of correlation with tissue glucose metabolism. For this reason, it is very often used as a substitute for other parameters of tissue glucose consumption, which are more precise but require more complex imaging protocols and data analysis (Boellaard, 2009). The level of correlation between the simple SUV and more complex glucose measurements is similar to those between BSA-IF and Blood-IF in our study (Eary & Mankoff, 1998). This level of correlation, despite being statistically significant, is not optimal and could therefore be described as semi-quantitative.

In contrast to tissue, we found very good correlations of both non-invasive methods in resting muscle. This might also be true for other tissues with similar levels of blood flow such as subcutaneous and visceral fat tissues, which have become the focus of

intense investigative efforts in recent years due to their role in metabolic syndrome and other disorders (Viljanen *et al.*, 2009). This, however, would require further validation.

Finally, with the increased use of dynamic contrast-enhanced computed tomography (dCE-CT) for the purpose of blood flow imaging, our results should be compared with the performance of dCE-CT. Although the extraction of the input curve in CT may be superior to that in PET, given the superior resolution and negligible partial-volume effect and spill-over, the quantification of blood flow with dCE CT is inferior to that with [^{15}O]H_2O PET. CT contrast agents are intravascular tracers and BF quantification is based on first-pass kinetics, which is inferior to the kinetic modelling of dynamic PET imaging of freely diffusible [^{15}O]H_2O.

7.7 Correlations between uptake of PET tracers and clinical end-points (II and V)

7.7.1 Pancreas (II)

Recently, several studies have combined findings on metabolic activity and perfusion to demonstrate their impact on prognosis in different types of cancer. Mankoff et al. (Mankoff *et al.*, 2002) have described, in patients with breast cancer, the importance of the relationship between BF and metabolic activity of the tumour for treatment outcome. Recently, Groves et al. (Groves *et al.*, 2008) demonstrated that combining [^{18}F]FDG PET and perfusion measurement helps to predict the histological grade of breast tumours. In accordance with this, Hermans et al. (Hermans *et al.*, 2003) reported that high glucose metabolism and low vascularity measured by [^{18}F]FDG PET and DCE-CT, respectively, predicted poor local control in head and neck cancer. Our results provide new evidence that pancreatic tumours with high metabolic activity and relatively low BF are aggressive and may be more refractory to treatment than those with higher perfusion. We suggest that high metabolic activity combined with low BF indicates adaptation of tumours to a hypoxic microenvironment. Hypoxia, in turn, has been shown to be an important factor of selection in the development of aggressive phenotype (Smalley *et al.*, 2005). This is also demonstrated by differential regional distribution of areas of high perfusion, high [^{18}F]FDG uptake, and high SUV/BF ratio within the tumour (Figure 1), with areas of overlap where the ratio is high being potential targets for hypoxia-directed radiotherapy. In addition to its prognostic value, our study demonstrated that the SUV/BF ratio could provide a potentially useful tool for differentiating benign pancreatic dysfunction and normal pancreas, which otherwise show substantial overlap in uptake of [^{18}F]FDG.

What is common to all studies applying diverse methodologies is the observation that perfusion in normal pancreas is higher than in pancreatic tumours. An early CT study investigating the vascularity of pancreatic lesions showed that malignant lesions are

hypovascular compared to normal pancreas (Hosoki, 1983). We observed that BF in benign lesions is significantly reduced compared to normal pancreas. However, benign lesions do not seem to have a similar detrimental effect on the BF of the non-tumoural parts of the pancreas as malignant lesions do. As first reported by Kubo et al. (Kubo *et al.*, 1991), this reduction seems to be present only in the case of lesions located in the head of the pancreas as confirmed by our findings. This finding might be explained by the fact that tumours located in the head of the pancreas can cause obstruction of the pancreatic duct, followed by formation of fibrotic tissue with low BF in the body-tail – region of the pancreas.

Since some parameters related to BF have been shown to correlate with microvascular density (Folkman, 2002), the use of drugs targeting angiogenesis could be optimized by pre-treatment measurement of BF. Both BF and vascularisation of tumours vary greatly, and therefore poor selection of patients might also explain why many clinical trials have failed to demonstrate any significant benefit of antiangiogenic therapies in the case of pancreatic malignancy. Recently Jain et al. reported that when antiangiogenic therapy is given, tumour vessel permeability and, subsequently, peritumoural edema decrease. These changes lead to improvement in the effectiveness of tumour perfusion in a process called vessel normalization (Jain, 2005). Other authors have also suggested that normalizing the tumours' vasculature might improve the response to oncological therapy (Stockmann *et al.*, 2008).

7.7.2 Head and neck cancer (V)

The results obtained from studying 22 patients indicate that the metabolically active tumour volume (MATV) is an important prognostic factor. This value is similar to anatomical tumour size, which was also confirmed in our study by the significant influence of T-classification on MATV. This is in line with previous findings (Haerle *et al.*).

We also explored the correlations between individual PET parameters, as well as pretreatment tumour characteristics, and PET parameters. The most relevant results, however, were obtained in the analysis of the correlation between PET parameters and clinical end-points, in our case overall survival. With Log-rank test we observed only a borderline significant effect of pretreatment [^{18}F]EF5 uptake and over-all survival. However, using the Cox proportional hazards model we detected a significant correlation between [^{18}F]EF5 maximum pretreatment uptake and over-all survival of patients.

While previous studies have established the importance of hypoxia in disease progression and treatment outcome, this is the first study, to our knowledge, to detect a positive correlation between a non-FMISO hypoxia PET tracer and survival of patients.

We believe this to be an interesting and important finding, particularly since neither of the other two PET tracers showed similar correlations. This is of course in line with the lack of correlation between the PET parameters and once again emphasizes the need for multi-tracer imaging in pretreatment tumour evaluation and treatment planning. We are, however, also aware of the very low number of patients investigated in this study which might affect the results. In particular, [^{18}F]FDG PET uptake values have been shown to have a positive correlation with treatment outcome in studies with a large number of patients, and it is reasonable to speculate that a similar correlation would have emerged also in our study had we been able to increase the number of patients.

While we are aware of these limitations, on the other hand, one could also speculate that the small number of patient in our study only further emphasizes the importance of the significant correlation between [^{18}F]EF5 uptake and over-all survival. This, however, remains a speculative statement; for any definitive conclusions regarding a potential routine clinical use of [^{18}F]EF5, a far greater number of patients needs to be investigated.

7.8 Problems of using PET imaging in therapy planning and other open issues

Study I – Perhaps the most important drawback of this study is the lack of direct quantification of the level of tissue hypoxia which would enable a clearer correlation between the uptake of [^{18}F]EF5 and the tissue oxygenation. However, as already mentioned, these methods are also very much operator-dependent and a correlation between them and the PET findings is far from straightforward.

When investigating tumour hypoxia, time always plays a role. As mentioned above, there are several mechanisms of tumour hypoxia and it is reasonable to assume that unless images are acquired at the same time point some changes in the distribution of hypoxia within the tumour has taken place. When looking at the correlations between different tracers in images not acquired at the same time point (as [^{18}F]EF5 and [^{18}F]FDG in our case) this should be kept in mind.

Study II - Among the limitations of our study are the small sample size and the heterogeneous group of patients with malignant lesion, including two patients with NETs. It is well known that NETs have a different biology and better prognosis compared to pancreatic adenocarcinoma. We included only one patient with high-grade NET in the survival analysis since the second patient with low-grade NET died from postoperative complication after imaging. As observed in former studies, especially less aggressive forms of NETs show a lower uptake of [^{18}F]FDG and might not be detected on [^{18}F]FDG PET/CT (Adams *et al.*, 1998). The lowest SUV_{max} of the malignant lesions in the current study (1.6) was indeed observed in a low-grade NET.

Additionally, it has been shown that hyperglycemia (Zimny *et al.*, 1998; Delbeke *et al.*, 1999) affects the uptake of [^{18}F]FDG. In spite of the requirement of a six-hour fast, we found a significantly higher glucose concentration in patients with pancreatic malignancy compared to other patients. As suggested by others (Kroep *et al.*, 2003; Krak *et al.*, 2004), we therefore consider the normalization of [^{18}F]FDG SUVs to plasma glucose to be of particular importance when using [^{18}F]FDG SUVs to quantify the metabolic activity of malignant and benign pancreatic lesions. This might not be needed in purely diagnostic imaging but may be helpful if serial imaging is performed to monitor treatment effects.

For the purpose of this study we decided to use a fixed small-size ROI in comparison between regional perfusion and metabolism. This was a pragmatic decision and necessary to limit errors associated with organ movement and transfer of ROIs from one image set to another where differential analytic software was applied.

Study III – Also this study is limited by the fairly heterogeneous and the relatively small group of patients with malignant lesions (n = 20). Additionally, only one patient had R0-resection, one patient had R1-resection, and two patients R2-resection. Twenty-five of the 38 study patients had histological confirmation of the disease, although it is ethically unfeasible to do extensive sampling in the case of strong suspicion of either benign or disseminated disease. The study protocol also did not include endoscopic US. This was mostly due to the lack of experience in this field in our institute, while the benefit of EUS is based on extensive usage of this method. As observed in former studies, both hyperglycaemia (Zimny *et al.*, 1998; Delbeke *et al.*, 1999) and inflammation (van Kouwen *et al.*, 2005), including pancreatitis accompanied by tumour or stricture could affect the sensitivity of [^{18}F]FDG PET. In addition, an increased rate of glucose intolerance represents a potential limitation to [^{18}F]FDG PET in the diagnosis of pancreatic lesions. This was indirectly also observed in Study II. On the other hand, all patients in this study had normal C-reactive protein and amylase levels before [^{18}F]FDG PET/CT scanning.

Study IV – One of the most important drawbacks of the current study is no doubt the lack of direct comparison of the population-based methods with the image-derived method. While it does represent a potentially essential reference point, such a method would probably require a high level of modelling making it unsuitable for simple clinical applications.

Another potential problem is the lack of quantification of BF heterogeneity produced by the three methods. Also this is related in part to the general aim of the study which is to offer the clinician a simple method for quantification of BF not unlike SUV in FDG imaging. This method is used mostly in a semi-quantitative, semi-visual manner.

Study V – Again, the low number of patient must be mentioned as an important drawback of this study. While we did aim for a higher number of patients than in study I, we only had the possibility to include a further seven patients. Although this is far from enough to draw any significant conclusions, we do believe the study adds additional weight not only to the role of hypoxia in tumour biology, but also confirms the suitability of [^{18}F]EF5 as a hypoxia tracer.

Additionally, a direct comparison with another hypoxia tracer, preferably [^{18}F]FMISO, would be beneficial in demonstrating any potential advantages (or disadvantage) in tumour uptake.

7.9 Future perspectives

Blood flow, metabolic activity and hypoxia all play an important part in tumourigenesis and tumour susceptibility to cytotoxic tumour therapy. Our studies show that functional imaging of malignant tumours in vivo is feasible not only in the diagnostic workup of patients with cancer, but might in the near future also become a part of tumour characterisation and treatment planning. This is true for chemotherapy and application of biological targeted therapy but, first and foremost, it is true for radiotherapy and in particular IMRT.

Before these principles and techniques can be translated into routine clinical practice, further tracer development, optimization of imaging protocols, and image quantification will most likely be necessary.

With our work we have tried to address some of these issues and I believe we have made a step towards this goal. Nevertheless, important questions remain unanswered, the most import of which would be the direct comparison of currently available hypoxia tracers with regard to their target-to-background ratios and upake kinetics. This should be studied in vivo within a short time window due to the dynamic nature of tumour blood flow and hypoxia. These studies should no doubt also be expanded to include larger numbers of patients with possibly different tumour types. A multi-centre setup would need to be included as well.

With regard to blood flow imaging in routine clinical practice, it would, in my opinion, be necessary to strive for even further simplification of imaging protocols and image analysis. Due to the poor availability of [^{15}O]H_2O generators, a comparison between PET and DCE CT should be performed in order to determine the feasibility of using widely available CE DC as a substitute for the more precise [^{15}O]H_2O PET. For the same reason, the possibility of extracting, and maybe even quantifying, blood flow information from the early-stage [^{18}F]EF5 images should be explored.

8 SUMMARY AND CONCLUSIONS

Clinical evaluation of [^{18}F]EF5 showed that it is a safe PET tracer with favourable biokinetic properties suitable for use in human subjects. Its uptake properties in head and neck cancer demonstrate that it is governed by low tissue oxygen levels or hypoxia. The uptake of this new tracer was also shown to be indicative of a negative prognostic factor for overall survival and local control in this type of cancer. We also demonstrated that [^{18}F]FDG PET is a viable alternative to other imaging modalities in diagnosis and staging of pancreatic cancer, and that the mismatch between glucose metabolism and blood flow is a negative prognostic factor in this type of cancer. This suggests that cancer cells that are able to maintain high glucose metabolic levels despite low blood flow and, consequently, presence of hypoxia signals a more aggressive phenotype. This provided us with an additional motive to develop a simple method for quantifying blood flow using [^{15}O]H_2O PET which we believe might be of use in routine clinical settings.

Functional imaging of tumours and in particular of tumour hypoxia using PET remains an extremely interesting field of research and many questions remain open. The search for an optimal hypoxia PET tracer is far from over.

The specific conclusions of the studies are:

I. The first human study of [^{18}F]EF5 PET hypoxia marker was successfully conducted. We compared uptake of [^{18}F]EF5 with blood flow as measured by radioactive water, and metabolism measured with [^{18}F]FDG in patients with HNSCC. Our data suggest that the initial uptake of [^{18}F]EF5 is governed by blood flow, while in the later phase, uptake and binding seem to be hypoxia specific. The [^{18}F]EF5 binding distributions and patterns in primary tumours and cervical lymph node metastases are heterogeneous, which is consistent with clinical expectations and previously published data using immunohistochemical analyses of EF5. Uptake of [^{18}F]EF5 increased until 3 hours p.i. after which time the quality of the image decreased. We propose that the 3-hour time point is the optimal time for detecting hypoxia-specific binding in human head and neck cancer. By comparing regional blood flow and [^{18}F]EF5 T/M at 3 hours we identified T/M= 1.5 as an appropriate threshold for determining the presence of clinically significant hypoxia.

II. The differences in BF and its relationship to metabolic activity both in pathological pancreatic lesions and normal pancreas have been evaluated for the first time using combined [^{15}O]H2O and [^{18}F]FDG PET/CT. We found both malignant and benign lesions to be associated with decreased perfusion and, in patients with malignant disease, a high ratio of metabolism to BF seemed to

predict poor survival. Our preliminary findings in this study with a limited number of patients may shed light on the general resistance of pancreatic cancer to oncological treatments. Finally, we suggest the implementation of combined imaging of perfusion and metabolism in pre-treatment evaluation in clinical trials where anti-angiogenic targeting is planned.

III. We found [^{18}F]FDG PET/CT a highly useful method to characterize suspicious pancreatic masses in patients with inconclusive MDCT or MRI. [^{18}F]FDG PET/CT influences the surgical strategy in a quarter of patients by revealing metastases that are not observed by MDCT and MRI, or by identifying primary tumours not identified by MDCT or MRI. It was also useful in patients with biliary stricture and tumour suspicion on MDCT or MRI. [^{18}F]FDG PET/CT was not, however, able to assist in the evaluation of resectability of malignant lesions. On the basis of the encouraging results of our study, combined whole-body [^{18}F]FDG PET/CT together with contrast-enhanced MDCT is promising as an 'all-in-one' imaging technique for the detection of primary tumour, and for showing the distant metastases of pancreatic cancer. Optimized scanning protocols including control of blood glucose and motion of organs in the upper abdomen can further improve the diagnostic sensitivity of [^{18}F]FDG PET/CT and might enable more accurate detection of early-stage pancreatic cancer, although more extensive studies are needed to confirm the results of this study.

IV. Blood flow in low-perfusion tissues in the head and neck area (resting muscle) can be quantified using both of the non-invasive methods presented here. The higher and more variable BF of malignant tumours and the cerebellum makes the use of non-invasive techniques more challenging, yet the BSA-IF method seems to perform reasonably well even considering the limited number of patients in our study. This method also seems to perform best in all three tissues studied. Despite its relative simplicity, it allows the safe determination of high and low perfusion areas inside the tumour and a fairly reliable comparison with the surrounding muscle tissue. This makes the method suitable for the planning of therapies and the evaluation of treatment response.

Our initial experience warrants further validation of the non-invasive methods with the emphasis on repeatability over time and over treatment-induced changes.

V. Despite the small number of patients that participated in our study, the results clearly show that hypoxia represented as [18F]EF5 uptake seems to be a negative prognostic factor, possibly predictive of radioresistance. As such, [18F]EF5 remains a strong potential candidate for pretreatment patient stratification and treatment planning. However, definite clarification of this question would require a larger study. Also [18F]FDG showed a trend that might

have been significant had the number of patients been higher. On the other hand, the lack of correlation between the uptakes of the three evaluated tracers confirms the need for multi-tracer imaging in order to obtain all the significant information on tumour biology.

ACKNOWLEDGEMENTS

The work presented in this thesis has been carried out during the years 2006 – 2011 in Turku PET Centre and partly also in the Department of Oncology and Radiotherapy and the Department of Surgery of the Turku University Hospital. I would therefore like to thank Professor Juhani Knuuti, director of the PET Centre, Professor Jaakko Hartiala, head of Clinical Phisiology and Nuclear Medicine Department, Professor Seppo Pyrhönen, head of the Oncology and Radiotherapy Department, as well as Docent Timo Savunen, head of the Department of Surgery for providing the facilities and the complex infrastructure required in modern multidisciplinary research.

My deepest gratitude goes to the supervisors of this thesis, Professor Heikki Minn and Adjunct Professor Marko Seppänen, not only for their formal work of supervising and guiding this project, but also for their support and guidence at the beginning of my scientific career and for giving me the opportunity to work in their reaserch group. Heikki, your insightful understanding of the vast and fast-evolving field of cancer research as well as that of *in vivo* cancer imaging has helped me stay on track even when things seemed overwhelmingly complex. And Marko, your meticulous attention to detail and passion for nuclear medicine have been inspirational. I consider myself priviledged to have worked with both of you.

I would like to acknowledge the reviewers of this thesis Adjunct Professor Eva Brun of the University of Lund and Adjunct Professor Morten Busk of the University of Aarhus for their constructive criticism. With their thorough knowledge of the field they have helped me to improve this work. Without their comments, this thesis would have been much less consistent and some important details would have been written in a less clear fashion. On the other hand, their observations have also made me think of the big picture and not just the separate pieces of data obtained in the research.

I wish to thank all my excellent co-authors without whome this work would not have been possible. I would like to thank Professor Pirjo Nuutila whose knowledge, determination, organizational skills and support have been invaluable in the completion of this thesis. Your knowledge on one hand and your genuine curiosity on the other hand are admirable and something to aspire to. I wish to aknowledge Saila Kauhanen for her work on two of the included projects. Your efficiency and determination were inspiring. Hannu Sipilä is aknowledged for his expertise and craftsmanship in the field of Oxygen-15 and ^{15}O-H_2O production. My work would not have been possible without you providing us with the unique oportunty to work with maybe the best perfusion PET tracer available. My deepest gratitude goes also to the radiochemists, Olof Solin, Olli Eskola and Sarita Forsbäck, who have been able to produce the Flourine-18 labelled EF5 for its first clinical use in humans in the world. Turku PET Centre can rightfully be proud of its radiochemistry department; one of the world's

best. In PET research, the clinicians usually get most of the attention, but the true genious lies in the radiochemistry, a field far to complex for me to comprehend.

In a similarly humble fashion I would like to acknowledge Vesa Oikonen, Kaisa Liukko and Nobuyuki Kudomi for their extensive work on tracer modelling and for providing us with the tools for converting pretty images into quantitative science, the one thing we PET researchers most often pride ourselves on when speaking about the advantages of PET versus other imaging modalities.

The same goes also for the preclinical lab-bench work needed before the tracer can be used in humans and here I would like to mention Tove Grönroos, Jonna Sinkkonen and Antti Silvoniemi who have done most of the preclinical oncology-related [^{18}F]EF5-based work. Kaisa Lehtiö is acknowledged for her work of geathering patient follow-up information for the last study and for sharing her practical research experiences. I would also like to thank Paula Lindholm for her work in studies I and V.

I would like to acknowledge Sydney Evans and Cameron Koch for their pioneering work in tumour hypoxia research and in the development of EF5 at the Univeristy of Pennsylvania.

Irina Lisinen is acknowledeged for her help with the complex statistical analysis and Tony Shepherd, for his help with the preparation of one of the manuscripts.

Jacqeuline Välimäki is acknowledged for her official language review of this work.

I would like to thank my friends and colleagues at Turku PET Centre with whom I have shared many fun moments and who made the sometimes frustrating research work a pleasure: Marco, Sergey, Jarkko, Tommi, Henri, Anu, Iina, Pauliina, Ronald, Ilkka, Kari, Chunlei, Harri, Tiina, Heli and many more. Through the many formal and informal shared moments with you I have not only learned a lot about other fields of PET research but also gained new friends.

I thank the personnel of the Turku PET Centre: The small but efficient IT team of Marko Tättälainen and Rami Mikkola. Radiographers Minna Aitsinki, Heidi Betlehem, Sari Hermonen, Anne-Mari Jokinen, Tarja Keskitalo, Hannele Lehtinen, Kalevi Mölsä, Outi Numminen and Marjo Tähti are acknowledged for their skilled work, flexibility, and patience during scanning. Laboratory technologist Sanna Suominen, Heidi Lappalainen, Emilia Puhakka, Leena Tokoi and Kirsi Tammi are appreciated for their expertise in tracer and blood sample analysis. Mirja Jyrkinen is acknowledeged for her secretarial work at the Turku PET Centre. I am sure I forgot many, but that does not mean that your work is not valued.

I wish to thank all the patients who participated in our studies. Even though they have not gained any direct benefits from these studies, we were hopefuly able to learn

something about the nature of their disease and will be able to help similar patients in the future.

This work has been conducted with the financial support of the Turku Unversity Foundation, the Finnish Cancer Foundation, the Finnish Society for Nuclear Medicine, the EU BioCare project, the Turku Graduate Scholl of Clinical Sciences, several Turku University Hospital EVO grants, and the Turku Centre of Excellence on Molecular Imaging in Cardiovascular and Metabolic Research.

I wish to thank my parents Maja and Silvo, as well as my brother Gregor, for their help and support and for keeping up with my sometimes difficult ideas.

During the years I've spent in Finland I've also learned to know a lot of good people who have have become my extended family and made me feel at home when I was away from home. Irmeli, Esko, Auli, Teemu, Silja, Christian and Anton, thank you all.

Last but not least, my love and my deepest gratitude go to Henna, to whom I would like to dedicate this work. You are not only the true reason and inspiration for this work, but without you this would simply not have been possible. Not only have you endured all my endless complaints but you have also helped me with your knowledge of the pathological basis of the tumours I was imaging.

REFERENCES

Adams S, Baum R, Rink T, Schumm-Drager PM, Usadel KH & Hor G. (1998). Limited value of fluorine-18 fluorodeoxyglucose positron emission tomography for the imaging of neuroendocrine tumours. *Eur J Nucl Med* **25,** 79-83.

Aebersold DM, Burri P, Beer KT, Laissue J, Djonov V, Greiner RH & Semenza GL. (2001). Expression of hypoxia-inducible factor-1alpha: a novel predictive and prognostic parameter in the radiotherapy of oropharyngeal cancer. *Cancer Res* **61,** 2911-2916.

Ahn YJ, Kim H, Lim H, Lee M, Kang Y, Moon S, Kim HS & Kim HH. (2012). AMP-activated protein kinase: implications on ischemic diseases. *BMB Rep* **45,** 489-495.

Anderson H & Price P. (2002). Clinical measurement of blood flow in tumours using positron emission tomography: a review. *Nucl Med Commun* **23,** 131-138.

Ang KK, Harris J, Wheeler R, Weber R, Rosenthal DI, Nguyen-Tan PF, Westra WH, Chung CH, Jordan RC, Lu C, Kim H, Axelrod R, Silverman CC, Redmond KP & Gillison ML. (2010). Human papillomavirus and survival of patients with oropharyngeal cancer. *N Engl J Med* **363,** 24-35.

Arteel GE, Thurman RG & Raleigh JA. (1998). Reductive metabolism of the hypoxia marker pimonidazole is regulated by oxygen tension independent of the pyridine nucleotide redox state. *Eur J Biochem* **253,** 743-750.

Arteel GE, Thurman RG, Yates JM & Raleigh JA. (1995). Evidence that hypoxia markers detect oxygen gradients in liver: pimonidazole and retrograde perfusion of rat liver. *Br J Cancer* **72,** 889-895.

Asagi A, Ohta K, Nasu J, Tanada M, Nadano S, Nishimura R, Teramoto N, Yamamoto K, Inoue T & Iguchi H. (2012). Utility of Contrast-Enhanced FDG-PET/CT in the Clinical Management of Pancreatic Cancer: Impact on Diagnosis, Staging, Evaluation of Treatment Response, and Detection of Recurrence. *Pancreas*.

Astner ST, Shi K, Vaupel P & Molls M. (2010). Imaging of tumor physiology: impacts on clinical radiation oncology. *Exp Oncol* **32,** 149-152.

Bachur NR, Gordon SL & Gee MV. (1978). A general mechanism for microsomal activation of quinone anticancer agents to free radicals. *Cancer Res* **38,** 1745-1750.

Bali MA, Metens T, Denolin V, De Maertelaer V, Deviere J & Matos C. (2008). Pancreatic perfusion: noninvasive quantitative assessment with dynamic contrast-enhanced MR imaging without and with secretin stimulation in healthy volunteers--initial results. *Radiology* **247,** 115-121.

Bares R, Klever P, Hauptmann S, Hellwig D, Fass J, Cremerius U, Schumpelick V, Mittermayer C & Bull U. (1994). F-18 fluorodeoxyglucose PET in vivo evaluation of pancreatic glucose metabolism for detection of pancreatic cancer. *Radiology* **192,** 79-86.

Bares R, Klever P, Hellwig D, Hauptmann S, Fass J, Hambuechen U, Zopp L, Mueller B, Buell U & Schumpelick V. (1993). Pancreatic cancer detected by positron emission tomography with 18F-labelled deoxyglucose: method and first results. *Nucl Med Commun* **14,** 596-601.

Barthel H, Wilson H, Collingridge DR, Brown G, Osman S, Luthra SK, Brady F, Workman P, Price PM & Aboagye EO. (2004). In vivo evaluation of [18F]fluoroetanidazole as a new marker for imaging tumour hypoxia with positron emission tomography. *Br J Cancer* **90,** 2232-2242.

Bayer C, Shi K, Astner ST, Maftei CA & Vaupel P. (2011). Acute versus chronic hypoxia: why a simplified classification is simply not enough. *Int J Radiat Oncol Biol Phys* **80,** 965-968.

Bentzen SM. (2005). Theragnostic imaging for radiation oncology: dose-painting by numbers. *Lancet Oncol* **6,** 112-117.

Bergers G & Benjamin LE. (2003). Tumorigenesis and the angiogenic switch. *Nat Rev Cancer* **3,** 401-410.

Bergman J & Solin O. (1997). Fluorine-18-labeled fluorine gas for synthesis of tracer molecules. *Nucl Med Biol* **24,** 677-683.

Beyer T, Antoch G, Blodgett T, Freudenberg LF, Akhurst T & Mueller S. (2003). Dual-modality PET/CT imaging: the effect of respiratory motion on combined image quality in clinical oncology. *Eur J Nucl Med Mol Imaging* **30,** 588-596.

Bipat S, Phoa SS, van Delden OM, Bossuyt PM, Gouma DJ, Lameris JS & Stoker J. (2005). Ultrasonography, computed tomography and magnetic resonance imaging for diagnosis and determining resectability of pancreatic adenocarcinoma: a meta-analysis. *J Comput Assist Tomogr* **29,** 438-445.

Bize PE, Platon A, Becker CD & Poletti PA. (2006). Perfusion measurement in acute pancreatitis using dynamic perfusion MDCT. *AJR Am J Roentgenol* **186,** 114-118.

Blais JD, Filipenko V, Bi M, Harding HP, Ron D, Koumenis C, Wouters BG & Bell JC. (2004). Activating transcription factor 4 is translationally regulated by hypoxic stress. *Mol Cell Biol* **24,** 7469-7482.

Bland JM & Altman DG. (2003). Applying the right statistics: analyses of measurement studies. *Ultrasound Obstet Gynecol* **22,** 85-93.

Blomqvist G. (1984). On the construction of functional maps in positron emission tomography. *J Cereb Blood Flow Metab* **4,** 629-632.

Boellaard R. (2009). Standards for PET image acquisition and quantitative data analysis. *J Nucl Med* **50 Suppl 1,** 11S-20S.

Borbath I, Van Beers BE, Lonneux M, Schoonbroodt D, Geubel A, Gigot JF & Deprez PH. (2005). Preoperative assessment of pancreatic tumors using magnetic resonance imaging, endoscopic ultrasonography, positron emission tomography and laparoscopy. *Pancreatology* **5,** 553-561.

Brix G, Bellemann ME, Hauser H & Doll J. (2002). [Recovery coefficients for the quantification of the arterial input functions from dynamic PET measurements: experimental and theoretical determination]. *Nuklearmedizin* **41,** 184-190.

Brizel DM, Sibley GS, Prosnitz LR, Scher RL & Dewhirst MW. (1997). Tumor hypoxia adversely affects the prognosis of carcinoma of the head and neck. *Int J Radiat Oncol Biol Phys* **38,** 285-289.

Brown JM. (1993). SR 4233 (tirapazamine): a new anticancer drug exploiting hypoxia in solid tumours. *Br J Cancer* **67,** 1163-1170.

Brown JM, Diehn M & Loo BW, Jr. (2010). Stereotactic ablative radiotherapy should be combined with a hypoxic cell radiosensitizer. *Int J Radiat Oncol Biol Phys* **78,** 323-327.

Brown JM & Siim BG. (1996). Hypoxia-Specific Cytotoxins in Cancer Therapy. *Semin Radiat Oncol* **6,** 22-36.

Brown JM & Wilson WR. (2004). Exploiting tumour hypoxia in cancer treatment. *Nat Rev Cancer* **4,** 437-447.

Bruehlmeier M, Roelcke U, Schubiger PA & Ametamey SM. (2004). Assessment of hypoxia and perfusion in human brain tumors using PET with 18F-fluoromisonidazole and 15O-H2O. *J Nucl Med* **45,** 1851-1859.

Burke D, Davies MM, Zweit J, Flower MA, Ott RJ, Dworkin MJ, Glover C, McCready VR, Carnochan P & Allen-Mersh TG. (2001). Continuous angiotensin II infusion increases tumour: normal blood flow ratio in colo-rectal liver metastases. *Br J Cancer* **85,** 1640-1645.

Burkhardt JK, Riina H, Shin BJ, Christos P, Kesavabhotla K, Hofstetter CP, Tsiouris AJ & Boockvar JA. (2012). Intra-arterial delivery of bevacizumab after blood-brain barrier disruption for the treatment of recurrent glioblastoma: progression-free survival and overall survival. *World Neurosurg* **77,** 130-134.

Busch TM, Hahn SM, Evans SM & Koch CJ. (2000). Depletion of tumor oxygenation during photodynamic therapy: detection by the hypoxia marker EF3 [2-(2-nitroimidazol-1[H]-yl)-N-(3,3,3-trifluoropropyl)acetamide]. *Cancer Res* **60,** 2636-2642.

Busk M, Horsman MR, Jakobsen S, Keiding S, van der Kogel AJ, Bussink J & Overgaard J. (2008). Imaging hypoxia in xenografted and murine tumors with 18F-fluoroazomycin arabinoside: a comparative study involving microPET, autoradiography, PO2-polarography, and fluorescence microscopy. *Int J Radiat Oncol Biol Phys* **70,** 1202-1212.

Bussink J, Kaanders JH, Rijken PF, Peters JP, Hodgkiss RJ, Marres HA & van der Kogel AJ. (1999). Vascular architecture and microenvironmental parameters in human squamous cell carcinoma xenografts: effects of carbogen and nicotinamide. *Radiother Oncol* **50,** 173-184.

Carmeliet P & Jain RK. (2000). Angiogenesis in cancer and other diseases. *Nature* **407,** 249-257.

Chaplin DJ, Horsman MR & Trotter MJ. (1990). Effect of nicotinamide on the microregional heterogeneity of oxygen delivery within a murine tumor. *J Natl Cancer Inst* **82,** 672-676.

Chapman JD. (1979). Hypoxic sensitizers--implications for radiation therapy. *N Engl J Med* **301,** 1429-1432.

Chen L, Zhang Z & Guan Y. (2012). 18F-HX4 hypoxia imaging with PET/CT in head and neck cancer: a comparison with 18F-FMISO. *Nucl Med Commun*.

Chen Y & Hu L. (2009). Design of anticancer prodrugs for reductive activation. *Med Res Rev* **29,** 29-64.

Chiche J, Brahimi-Horn MC & Pouyssegur J. (2010a). Tumour hypoxia induces a metabolic shift causing acidosis: a common feature in cancer. *J Cell Mol Med* **14,** 771-794.

Chiche J, Ilc K, Brahimi-Horn MC & Pouyssegur J. (2010b). Membrane-bound carbonic anhydrases are key pH regulators controlling tumor growth and cell migration. *Adv Enzyme Regul* **50,** 20-33.

Christofk HR, Vander Heiden MG, Harris MH, Ramanathan A, Gerszten RE, Wei R, Fleming MD, Schreiber SL & Cantley LC. (2008). The M2 splice isoform of pyruvate kinase is important for cancer metabolism and tumour growth. *Nature* **452,** 230-233.

Cline JM, Rosner GL, Raleigh JA & Thrall DE. (1997). Quantification of CCI-103F labeling heterogeneity in canine solid tumors. *Int J Radiat Oncol Biol Phys* **37,** 655-662.

Cline JM, Thrall DE, Rosner GL & Raleigh JA. (1994). Distribution of the hypoxia marker CCI-103F in canine tumors. *Int J Radiat Oncol Biol Phys* **28,** 921-933.

Coenegrachts K, Van Steenbergen W, De Keyzer F, Vanbeckevoort D, Bielen D, Chen F, Dockx S, Maes F & Bosmans H. (2004). Dynamic contrast-enhanced MRI of the pancreas: initial results in healthy volunteers and patients with chronic pancreatitis. *J Magn Reson Imaging* **20,** 990-997.

Conway DI, Hashibe M, Boffetta P, Wunsch-Filho V, Muscat J, La Vecchia C & Winn DM. (2009). Enhancing epidemiologic research on head and neck cancer: INHANCE - The international head and neck cancer epidemiology consortium. *Oral Oncol* **45,** 743-746.

Cummins EP, Comerford KM, Scholz C, Bruning U & Taylor CT. (2007). Hypoxic regulation of NF-kappaB signaling. *Methods Enzymol* **435,** 479-492.

Daisne JF, Duprez T, Weynand B, Lonneux M, Hamoir M, Reychler H & Gregoire V. (2004). Tumor volume in pharyngolaryngeal squamous cell carcinoma: comparison at CT, MR imaging, and FDG PET and validation with surgical specimen. *Radiology* **233,** 93-100.

Daisne JF, Sibomana M, Bol A, Doumont T, Lonneux M & Gregoire V. (2003). Tri-dimensional automatic segmentation of PET volumes based on measured source-to-background ratios: influence of reconstruction algorithms. *Radiother Oncol* **69,** 247-250.

De Gaetano AM, Rufini V, Castaldi P, Gatto AM, Filograna L, Giordano A & Bonomo L. (2012).

Clinical applications of (18)F-FDG PET in the management of hepatobiliary and pancreatic tumors. *Abdom Imaging*.

de Langen AJ, Lubberink M, Boellaard R, Spreeuwenberg MD, Smit EF, Hoekstra OS & Lammertsma AA. (2008). Reproducibility of Tumor Perfusion Measurements Using 15O-Labeled Water and PET. *J Nucl Med*.

Dearling JL, Lewis JS, Mullen GE, Rae MT, Zweit J & Blower PJ. (1998). Design of hypoxia-targeting radiopharmaceuticals: selective uptake of copper-64 complexes in hypoxic cells in vitro. *Eur J Nucl Med* **25,** 788-792.

Dehdashti F, Grigsby PW, Mintun MA, Lewis JS, Siegel BA & Welch MJ. (2003a). Assessing tumor hypoxia in cervical cancer by positron emission tomography with 60Cu-ATSM: relationship to therapeutic response-a preliminary report. *Int J Radiat Oncol Biol Phys* **55,** 1233-1238.

Dehdashti F, Mintun MA, Lewis JS, Bradley J, Govindan R, Laforest R, Welch MJ & Siegel BA. (2003b). In vivo assessment of tumor hypoxia in lung cancer with 60Cu-ATSM. *Eur J Nucl Med Mol Imaging* **30,** 844-850.

Delbeke D, Rose DM, Chapman WC, Pinson CW, Wright JK, Beauchamp RD, Shyr Y & Leach SD. (1999). Optimal interpretation of FDG PET in the diagnosis, staging and management of pancreatic carcinoma. *J Nucl Med* **40,** 1784-1791.

Dhup S, Dadhich RK, Porporato PE & Sonveaux P. (2012). Multiple biological activities of lactic acid in cancer: influences on tumor growth, angiogenesis and metastasis. *Curr Pharm Des* **18,** 1319-1330.

Diederichs CG, Staib L, Vogel J, Glasbrenner B, Glatting G, Brambs HJ, Beger HG & Reske SN. (2000). Values and limitations of 18F-fluorodeoxyglucose-positron-emission tomography with preoperative evaluation of patients with pancreatic masses. *Pancreas* **20,** 109-116.

Dische S, Saunders MI, Anderson P, Stratford MR & Minchinton A. (1982). Clinical experience with nitroimidazoles as radiosensitizers. *Int J Radiat Oncol Biol Phys* **8,** 335-338.

Dolbier WR, Jr., Li AR, Koch CJ, Shiue CY & Kachur AV. (2001). [18F]-EF5, a marker for PET detection of hypoxia: synthesis of precursor and a new fluorination procedure. *Appl Radiat Isot* **54,** 73-80.

Doss M, Zhang JJ, Belanger MJ, Stubbs JB, Hostetler ED, Alpaugh K, Kolb HC & Yu JQ. Biodistribution and radiation dosimetry of the hypoxia marker 18F-HX4 in monkeys and humans determined by using whole-body PET/CT. *Nucl Med Commun* **31,** 1016-1024.

Dubois L, Landuyt W, Cloetens L, Bol A, Bormans G, Haustermans K, Labar D, Nuyts J, Gregoire V & Mortelmans L. (2008). [18F]EF3 is not superior to [18F]FMISO for PET-based hypoxia evaluation as measured in a rat rhabdomyosarcoma tumour model. *Eur J Nucl Med Mol Imaging* **36,** 209-218.

Dubois LJ, Lieuwes NG, Janssen MH, Peeters WJ, Windhorst AD, Walsh JC, Kolb HC, Ollers MC, Bussink J, van Dongen GA, van der Kogel A & Lambin P. Preclinical evaluation and validation of [18F]HX4, a promising hypoxia marker for PET imaging. *Proc Natl Acad Sci U S A* **108,** 14620-14625.

Dunnwald LK, Gralow JR, Ellis GK, Livingston RB, Linden HM, Specht JM, Doot RK, Lawton TJ, Barlow WE, Kurland BF, Schubert EK & Mankoff DA. (2008). Tumor metabolism and blood flow changes by positron emission tomography: relation to survival in patients treated with neoadjuvant chemotherapy for locally advanced breast cancer. *J Clin Oncol* **26,** 4449-4457.

Durand RE & Raleigh JA. (1998). Identification of nonproliferating but viable hypoxic tumor cells in vivo. *Cancer Res* **58,** 3547-3550.

Eary JF & Mankoff DA. (1998). Tumor metabolic rates in sarcoma using FDG PET. *J Nucl Med* **39,** 250-254.

Ebos JM, Lee CR, Cruz-Munoz W, Bjarnason GA, Christensen JG & Kerbel RS. (2009). Accelerated metastasis after short-term treatment with a potent inhibitor of tumor angiogenesis. *Cancer Cell* **15,** 232-239.

Edwards DI. (1993). Nitroimidazole drugs--action and resistance mechanisms. I. Mechanisms of action. *J Antimicrob Chemother* **31,** 9-20.

El Fakhri G, Kardan A, Sitek A, Dorbala S, Abi-Hatem N, Lahoud Y, Fischman A, Coughlan M, Yasuda T & Di Carli MF. (2009). Reproducibility and accuracy of quantitative myocardial blood flow assessment with (82)Rb PET: comparison with (13)N-ammonia PET. *J Nucl Med* **50,** 1062-1071.

Erdi YE, Mawlawi O, Larson SM, Imbriaco M, Yeung H, Finn R & Humm JL. (1997). Segmentation of lung lesion volume by adaptive positron emission tomography image thresholding. *Cancer* **80,** 2505-2509.

Eskola O, Gronroos TJ, Forsback S, Tuomela J, Komar G, Bergman J, Harkonen P, Haaparanta M, Minn H & Solin O. (2011). Tracer Level Electrophilic Synthesis and Pharmacokinetics of the Hypoxia Tracer [(18)F]EF5. *Mol Imaging Biol*.

Evans SM, Du KL, Chalian AA, Mick R, Zhang PJ, Hahn SM, Quon H, Lustig R, Weinstein GS & Koch CJ. (2007). Patterns and levels of hypoxia in head and neck squamous cell carcinomas and their relationship to patient outcome. *Int J Radiat Oncol Biol Phys* **69,** 1024-1031.

Evans SM, Fraker D, Hahn SM, Gleason K, Jenkins WT, Jenkins K, Hwang WT, Zhang P, Mick R & Koch CJ. (2006). EF5 binding and clinical outcome in human soft tissue sarcomas. *Int J Radiat Oncol Biol Phys* **64,** 922-927.

Evans SM, Kachur AV, Shiue CY, Hustinx R, Jenkins WT, Shive GG, Karp JS, Alavi A, Lord EM, Dolbier WR, Jr. & Koch CJ. (2000). Noninvasive detection of tumor hypoxia using the 2-nitroimidazole [18F]EF1. *J Nucl Med* **41,** 327-336.

Evans SM & Koch CJ. (2003). Prognostic significance of tumor oxygenation in humans. *Cancer Lett* **195,** 1-16.

Farma JM, Santillan AA, Melis M, Walters J, Belinc D, Chen DT, Eikman EA & Malafa M. (2008). PET/CT fusion scan enhances CT staging in patients with pancreatic neoplasms. *Ann Surg Oncol* **15,** 2465-2471.

Fletcher JW, Djulbegovic B, Soares HP, Siegel BA, Lowe VJ, Lyman GH, Coleman RE, Wahl R, Paschold JC, Avril N, Einhorn LH, Suh WW, Samson D, Delbeke D, Gorman M & Shields AF. (2008). Recommendations on the use of 18F-FDG PET in oncology. *J Nucl Med* **49,** 480-508.

Folkman J. (1971). Tumor angiogenesis: therapeutic implications. *N Engl J Med* **285,** 1182-1186.

Folkman J. (2002). Role of angiogenesis in tumor growth and metastasis. *Semin Oncol* **29,** 15-18.

Ford EC, Kinahan PE, Hanlon L, Alessio A, Rajendran J, Schwartz DL & Phillips M. (2006). Tumor delineation using PET in head and neck cancers: threshold contouring and lesion volumes. *Med Phys* **33,** 4280-4288.

Fritscher-Ravens A, Knoefel WT, Krause C, Swain CP, Brandt L & Patel K. (2005). Three-dimensional linear endoscopic ultrasound-feasibility of a novel technique applied for the detection of vessel involvement of pancreatic masses. *Am J Gastroenterol* **100,** 1296-1302.

Gandara DR, Lara PN, Jr., Goldberg Z, Le QT, Mack PC, Lau DH & Gumerlock PH. (2002). Tirapazamine: prototype for a novel class of therapeutic agents targeting tumor hypoxia. *Semin Oncol* **29,** 102-109.

Garcia-Parra R, Wood D, Shah RB, Siddiqui J, Hussain H, Park H, Desmond T, Meyer C & Piert M. Investigation on tumor hypoxia in resectable primary prostate cancer as demonstrated by 18F-FAZA PET/CT utilizing multimodality fusion techniques. *Eur J Nucl Med Mol Imaging* **38,** 1816-1823.

Gatenby RA & Gillies RJ. (2004). Why do cancers have high aerobic glycolysis? *Nat Rev Cancer* **4,** 891-899.

Gattani AM, Mandeli J & Bruckner HW. (1996). Tumor markers in patients with pancreatic carcinoma. *Cancer* **78,** 57-62.

Giatromanolaki A, Koukourakis MI, Sivridis E, Turley H, Talks K, Pezzella F, Gatter KC & Harris AL. (2001). Relation of hypoxia inducible factor 1 alpha and 2 alpha in operable non-small cell lung cancer to angiogenic/molecular profile of tumours and survival. *Br J Cancer* **85,** 881-890.

Gimbrone MA, Jr. & Gullino PM. (1976). Angiogenic capacity of preneoplastic lesions of the murine mammary gland as a marker of neoplastic transformation. *Cancer Res* **36,** 2611-2620.

Goldman E. (1907). The growth of malignant disease in man and in lower animals with special reference to the vascular system. *Lancet* **2,** 1236-1239.

Gosalvez M & Weinhouse S. (1976). Control mechanisms of oxygen and glucose utilization in tumours. *Adv Exp Med Biol* **75,** 587-596.

Graeber TG, Osmanian C, Jacks T, Housman DE, Koch CJ, Lowe SW & Giaccia AJ. (1996). Hypoxia-mediated selection of cells with diminished apoptotic potential in solid tumours. *Nature* **379,** 88-91.

Graeber TG, Peterson JF, Tsai M, Monica K, Fornace AJ, Jr. & Giaccia AJ. (1994). Hypoxia induces accumulation of p53 protein, but activation of a G1-phase checkpoint by low-oxygen conditions is independent of p53 status. *Mol Cell Biol* **14,** 6264-6277.

Graham MM, Peterson LM & Hayward RM. (2000). Comparison of simplified quantitative analyses of FDG uptake. *Nucl Med Biol* **27,** 647-655.

Gray LH. (1961). Radiobiologic basis of oxygen as a modifying factor in radiation therapy. *Am J Roentgenol Radium Ther Nucl Med* **85,** 803-815.

Gray LH, Conger AD, Ebert M, Hornsey S & Scott OC. (1953). The concentration of oxygen dissolved in tissues at the time of irradiation as a factor in radiotherapy. *Br J Radiol* **26,** 638-648.

Gronroos T. (2006). [18F]Fluoroerythronitroimidazole, Tumor Hypoxia and Positron Emission Tomography. In *Annales Universitatis Turkuensis Series D 740*, pp. 72. University of Turku, Turku.

Gronroos T, Bentzen L, Marjamaki P, Murata R, Horsman MR, Keiding S, Eskola O, Haaparanta M, Minn H & Solin O. (2004a). Comparison of the biodistribution of two hypoxia markers [18F]FETNIM and [18F]FMISO in an experimental mammary carcinoma. *Eur J Nucl Med Mol Imaging* **31,** 513-520.

Gronroos T, Tuomela J, Eskola O, Forsback S, Haapanranta M & Evans SM. (2004b). Bioditribution of the hypoxia marker 18F-EF5 in mice bearing a prostate cancer tumour model. *Eur J Nucl Med Mol Imaging* **31**.

Groshar D, McEwan AJ, Parliament MB, Urtasun RC, Golberg LE, Hoskinson M, Mercer JR, Mannan RH, Wiebe LI & Chapman JD. (1993). Imaging tumor hypoxia and tumor perfusion. *J Nucl Med* **34,** 885-888.

Grosu AL, Nestle U & Weber WA. (2009). How to use functional imaging information for radiotherapy planning. *Eur J Cancer* **45 Suppl 1,** 461-463.

Groves AM, Wishart GC, Shastry M, Moyle P, Iddles S, Britton P, Gaskarth M, Warren RM, Ell PJ & Miles KA. (2008). Metabolic-flow relationships in primary breast cancer: feasibility of combined PET/dynamic contrast-enhanced CT. *Eur J Nucl Med Mol Imaging*.

Groves AM, Wishart GC, Shastry M, Moyle P, Iddles S, Britton P, Gaskarth M, Warren RM, Ell PJ & Miles KA. (2009). Metabolic-flow relationships in primary breast cancer: feasibility of combined PET/dynamic contrast-enhanced CT. *Eur J Nucl Med Mol Imaging* **36,** 416-421.

Guise CP, Wang AT, Theil A, Bridewell DJ, Wilson WR & Patterson AV. (2007). Identification of human reductases that activate the dinitrobenzamide mustard prodrug PR-104A: a role for NADPH:cytochrome P450 oxidoreductase under hypoxia. *Biochem Pharmacol* **74,** 810-820.

Haerle SK, Huber GF, Hany TF, Ahmad N & Schmid DT. Is there a correlation between 18F-FDG-PET standardized uptake value, T-classification, histological grading and the anatomic subsites in newly diagnosed squamous cell carcinoma of the head and neck? *Eur Arch Otorhinolaryngol* **267,** 1635-1640.

Hanahan D & Weinberg RA. (2000). The hallmarks of cancer. *Cell* **100,** 57-70.

Hanahan D & Weinberg RA. (2011). Hallmarks of cancer: the next generation. *Cell* **144,** 646-674.

Heinrich S, Goerres GW, Schafer M, Sagmeister M, Bauerfeind P, Pestalozzi BC, Hany TF, von

Schulthess GK & Clavien PA. (2005). Positron emission tomography/computed tomography influences on the management of resectable pancreatic cancer and its cost-effectiveness. *Ann Surg* **242,** 235-243.

Hellwig D, Graeter TP, Ukena D, Groeschel A, Sybrecht GW, Schaefers HJ & Kirsch CM. (2007). 18F-FDG PET for mediastinal staging of lung cancer: which SUV threshold makes sense? *J Nucl Med* **48,** 1761-1766.

Herholz K, Ziffling P, Staffen W, Pawlik G, Wagner R, Wienhard K & Heiss WD. (1988). Uncoupling of hexose transport and phosphorylation in human gliomas demonstrated by PET. *Eur J Cancer Clin Oncol* **24,** 1139-1150.

Hermans R, Meijerink M, Van den Bogaert W, Rijnders A, Weltens C & Lambin P. (2003). Tumor perfusion rate determined noninvasively by dynamic computed tomography predicts outcome in head-and-neck cancer after radiotherapy. *Int J Radiat Oncol Biol Phys* **57,** 1351-1356.

Herzog BA, Husmann L, Valenta I, Gaemperli O, Siegrist PT, Tay FM, Burkhard N, Wyss CA & Kaufmann PA. (2009). Long-term prognostic value of 13N-ammonia myocardial perfusion positron emission tomography added value of coronary flow reserve. *J Am Coll Cardiol* **54,** 150-156.

Hirasawa S, Tsushima Y, Takei H, Hirasawa H, Taketomi-Takahashi A, Takano A, Oriuchi N & Endo K. (2007). Inverse correlation between tumor perfusion and glucose uptake in human head and neck tumors. *Acad Radiol* **14,** 312-318.

Hockel M, Schlenger K, Knoop C & Vaupel P. (1991). Oxygenation of carcinomas of the uterine cervix: evaluation by computerized O2 tension measurements. *Cancer Res* **51,** 6098-6102.

Hockel M & Vaupel P. (2001). Tumor hypoxia: definitions and current clinical, biologic, and molecular aspects. *J Natl Cancer Inst* **93,** 266-276.

Hoeben BA, Kaanders JH, Franssen GM, Troost EG, Rijken PF, Oosterwijk E, van Dongen GA, Oyen WJ, Boerman OC & Bussink J. (2010). PET of hypoxia with 89Zr-labeled cG250-F(ab')2 in head and neck tumors. *J Nucl Med* **51,** 1076-1083.

Hoekstra CJ, Stroobants SG, Hoekstra OS, Smit EF, Vansteenkiste JF & Lammertsma AA. (2002). Measurement of perfusion in stage IIIA-N2 non-small cell lung cancer using H(2)(15)O and positron emission tomography. *Clin Cancer Res* **8,** 2109-2115.

Hoogsteen IJ, Lok J, Marres HA, Takes RP, Rijken PF, van der Kogel AJ & Kaanders JH. (2009). Hypoxia in larynx carcinomas assessed by pimonidazole binding and the value of CA-IX and vascularity as surrogate markers of hypoxia. *Eur J Cancer* **45,** 2906-2914.

Horsman MR. (1998). Measurement of tumor oxygenation. *Int J Radiat Oncol Biol Phys* **42,** 701-704.

Horsman MR & Overgaard J. (2002). Overcoming tumour radioresistance resulting from hypoxia. In *Basic clinical radiobiology*, 3rd ed. edn, ed. Steel GG. Arnold, London.

Hosoki T. (1983). Dynamic CT of pancreatic tumors. *AJR Am J Roentgenol* **140,** 959-965.

Hosten N, Lemke AJ, Wiedenmann B, Bohmig M & Rosewicz S. (2000). Combined imaging techniques for pancreatic cancer. *Lancet* **356,** 909-910.

Houghton PJ, Lock R, Carol H, Morton CL, Phelps D, Gorlick R, Kolb EA, Keir ST, Reynolds CP, Kang MH, Maris JM, Wozniak AW, Gu Y, Wilson WR & Smith MA. (2011). Initial testing of the hypoxia-activated prodrug PR-104 by the pediatric preclinical testing program. *Pediatr Blood Cancer* **57,** 443-453.

Hui EP, Chan AT, Pezzella F, Turley H, To KF, Poon TC, Zee B, Mo F, Teo PM, Huang DP, Gatter KC, Johnson PJ & Harris AL. (2002). Coexpression of hypoxia-inducible factors 1alpha and 2alpha, carbonic anhydrase IX, and vascular endothelial growth factor in nasopharyngeal carcinoma and relationship to survival. *Clin Cancer Res* **8,** 2595-2604.

Hunter FW, Wang J, Patel R, Hsu HL, Hickey AJ, Hay MP & Wilson WR. (2012). Homologous recombination repair-dependent cytotoxicity of the benzotriazine di-N-oxide CEN-209: comparison with other hypoxia-activated prodrugs. *Biochem Pharmacol* **83,** 574-585.

Hunter GJ, Hamberg LM, Alpert NM, Choi NC & Fischman AJ. (1996). Simplified measurement of deoxyglucose utilization rate. *J Nucl Med* **37,** 950-955.

Iida H, Kanno I, Miura S, Murakami M, Takahashi K & Uemura K. (1986). Error analysis of a quantitative cerebral blood flow measurement using H2(15)O autoradiography and positron emission tomography, with respect to the dispersion of the input function. *J Cereb Blood Flow Metab* **6,** 536-545.

Isozaki M, Kiyono Y, Arai Y, Kudo T, Mori T, Maruyama R, Kikuta K & Okazawa H. (2011). Feasibility of 62Cu-ATSM PET for evaluation of brain ischaemia and misery perfusion in patients with cerebrovascular disease. *Eur J Nucl Med Mol Imaging* **38,** 1075-1082.

Jadvar H & Fischman AJ. (2001). Evaluation of pancreatic carcinoma with FDG PET. *Abdom Imaging* **26,** 254-259.

Jain RK. (2005). Normalization of tumor vasculature: an emerging concept in antiangiogenic therapy. *Science* **307,** 58-62.

Jameson MB, Rischin D, Pegram M, Gutheil J, Patterson AV, Denny WA & Wilson WR. (2010). A phase I trial of PR-104, a nitrogen mustard prodrug activated by both hypoxia and aldo-keto reductase 1C3, in patients with solid tumors. *Cancer Chemother Pharmacol* **65,** 791-801.

Janssen MH, Aerts HJ, Ollers MC, Bosmans G, Lee JA, Buijsen J, De Ruysscher D, Lambin P, Lammering G & Dekker AL. (2009). Tumor delineation based on time-activity curve differences assessed with dynamic fluorodeoxyglucose positron emission tomography-computed tomography in rectal cancer patients. *Int J Radiat Oncol Biol Phys* **73,** 456-465.

Jiang BH, Rue E, Wang GL, Roe R & Semenza GL. (1996a). Dimerization, DNA binding, and transactivation properties of hypoxia-inducible factor 1. *J Biol Chem* **271,** 17771-17778.

Jiang BH, Semenza GL, Bauer C & Marti HH. (1996b). Hypoxia-inducible factor 1 levels vary exponentially over a physiologically relevant range of O2 tension. *Am J Physiol* **271,** C1172-1180.

Jin GY, Li SJ, Moulder JE & Raleigh JA. (1990). Dynamic measurements of hexafluoromisonidazole (CCI-103F) retention in mouse tumours by 1H/19F magnetic resonance spectroscopy. *Int J Radiat Biol* **58,** 1025-1034.

Joost HG & Thorens B. (2001). The extended GLUT-family of sugar/polyol transport facilitators: nomenclature, sequence characteristics, and potential function of its novel members (review). *Mol Membr Biol* **18,** 247-256.

Kaanders JH, Wijffels KI, Marres HA, Ljungkvist AS, Pop LA, van den Hoogen FJ, de Wilde PC, Bussink J, Raleigh JA & van der Kogel AJ. (2002). Pimonidazole binding and tumor vascularity predict for treatment outcome in head and neck cancer. *Cancer Res* **62,** 7066-7074.

Kallinowski F, Zander R, Hoeckel M & Vaupel P. (1990). Tumor tissue oxygenation as evaluated by computerized-pO2-histography. *Int J Radiat Oncol Biol Phys* **19,** 953-961.

Kasperk RK, Riesener KP, Wilms K & Schumpelick V. (2001). Limited value of positron emission tomography in treatment of pancreatic cancer: surgeon's view. *World J Surg* **25,** 1134-1139.

Keogan MT, Tyler D, Clark L, Branch MS, McDermott VG, DeLong DM & Coleman RE. (1998). Diagnosis of pancreatic carcinoma: role of FDG PET. *AJR Am J Roentgenol* **171,** 1565-1570.

Knuuti J, Kajander S, Maki M & Ukkonen H. (2009). Quantification of myocardial blood flow will reform the detection of CAD. *J Nucl Cardiol* **16,** 497-506.

Koch CJ, Hahn SM, Rockwell K, Jr., Covey JM, McKenna WG & Evans SM. (2001). Pharmacokinetics of EF5 [2-(2-nitro-1-H-imidazol-1-yl)-N-(2,2,3,3,3-pentafluoropropyl) acetamide] in human patients: implications for hypoxia measurements in vivo by 2-nitroimidazoles. *Cancer Chemother Pharmacol* **48,** 177-187.

Koch CJ, Scheuermann JS, Divgi C, Judy KD, Kachur AV, Freifelder R, Reddin JS, Karp J, Stubbs JB, Hahn SM, Driesbaugh J, Smith D, Prendergast S & Evans SM. (2010). Biodistribution and dosimetry of (18)F-EF5 in cancer patients with preliminary comparison of (18)F-EF5 uptake versus EF5 binding

in human glioblastoma. *Eur J Nucl Med Mol Imaging* **37,** 2048-2059.

Koivuviita N, Tertti R, Jarvisalo M, Pietila M, Hannukainen J, Sundell J, Nuutila P, Knuuti J & Metsarinne K. (2009). Increased basal myocardial perfusion in patients with chronic kidney disease without symptomatic coronary artery disease. *Nephrol Dial Transplant* **24,** 2773-2779.

Komar G, Kauhanen S, Liukko K, Seppanen M, Kajander S, Ovaska J, Nuutila P & Minn H. (2009). Decreased blood flow with increased metabolic activity: a novel sign of pancreatic tumor aggressiveness. *Clin Cancer Res* **15,** 5511-5517.

Koshy M, Paulino AC, Howell R, Schuster D, Halkar R & Davis LW. (2005). F-18 FDG PET-CT fusion in radiotherapy treatment planning for head and neck cancer. *Head Neck* **27,** 494-502.

Koukourakis MI, Giatromanolaki A, Sivridis E, Simopoulos C, Turley H, Talks K, Gatter KC & Harris AL. (2002). Hypoxia-inducible factor (HIF1A and HIF2A), angiogenesis, and chemoradiotherapy outcome of squamous cell head-and-neck cancer. *Int J Radiat Oncol Biol Phys* **53,** 1192-1202.

Krak NC, Hoekstra OS & Lammertsma AA. (2004). Measuring response to chemotherapy in locally advanced breast cancer: methodological considerations. *Eur J Nucl Med Mol Imaging* **31 Suppl 1,** S103-111.

Kroep JR, Van Groeningen CJ, Cuesta MA, Craanen ME, Hoekstra OS, Comans EF, Bloemena E, Hoekstra CJ, Golding RP, Twisk JW, Peters GJ, Pinedo HM & Lammertsma AA. (2003). Positron emission tomography using 2-deoxy-2-[18F]-fluoro-D-glucose for response monitoring in locally advanced gastroesophageal cancer; a comparison of different analytical methods. *Mol Imaging Biol* **5,** 337-346.

Krohn KA, Link JM & Mason RP. (2008). Molecular imaging of hypoxia. *J Nucl Med* **49 Suppl 2,** 129S-148S.

Kubo S, Yamamoto K, Magata Y, Iwasaki Y, Tamaki N, Yonekura Y & Konishi J. (1991). Assessment of pancreatic blood flow with positron emission tomography and oxygen-15 water. *Ann Nucl Med* **5,** 133-138.

Kudomi N, Koivuviita N, Liukko KE, Oikonen VJ, Tolvanen T, Iida H, Tertti R, Metsarinne K, Iozzo P & Nuutila P. (2009). Parametric renal blood flow imaging using [15O]H2O and PET. *Eur J Nucl Med Mol Imaging* **36,** 683-691.

Kuppersmith RB, Greco SC, Teh BS, Donovan DT, Grant W, Chiu JK, Cain RB & Butler EB. (1999). Intensity-modulated radiotherapy: first results with this new technology on neoplasms of the head and neck. *Ear Nose Throat J* **78,** 238, 241-236, 248 passim.

Kurdziel KA, Figg WD, Carrasquillo JA, Huebsch S, Whatley M, Sellers D, Libutti SK, Pluda JM, Dahut W, Reed E & Bacharach SL. (2003). Using positron emission tomography 2-deoxy-2-[18F]fluoro-D-glucose, 11CO, and 15O-water for monitoring androgen independent prostate cancer. *Mol Imaging Biol* **5,** 86-93.

Lapela M, Eigtved A, Jyrkkio S, Grenman R, Kurki T, Lindholm P, Nuutinen J, Sutinen E, Solin O, Bjornskov I, Bretlau P, Friberg L, Holm S, Jensen M, Sand Hansen H & Minn H. (2000). Experience in qualitative and quantitative FDG PET in follow-up of patients with suspected recurrence from head and neck cancer. *Eur J Cancer* **36,** 858-867.

Laughlin KM, Evans SM, Jenkins WT, Tracy M, Chan CY, Lord EM & Koch CJ. (1996). Biodistribution of the nitroimidazole EF5 (2-[2-nitro-1H-imidazol-1-yl]-N-(2,2,3,3,3-pentafluoropropyl) acetamide) in mice bearing subcutaneous EMT6 tumors. *J Pharmacol Exp Ther* **277,** 1049-1057.

Lawrentschuk N, Lee FT, Jones G, Rigopoulos A, Mountain A, O'Keefe G, Papenfuss AT, Bolton DM, Davis ID & Scott AM. (2011). Investigation of hypoxia and carbonic anhydrase IX expression in a renal cell carcinoma xenograft model with oxygen tension measurements and (1)(2)I-cG250 PET/CT. *Urol Oncol* **29,** 411-420.

Lawson CL & Hanson RJ. (1987). *Solving least squares problems*. Society for Industrial Mathematics.

Lee DJ, Cosmatos D, Marcial VA, Fu KK, Rotman M, Cooper JS, Ortiz HG, Beitler JJ, Abrams RA, Curran WJ & et al. (1995). Results of an RTOG phase III trial (RTOG 85-27) comparing radiotherapy plus etanidazole with radiotherapy alone for locally advanced head and neck carcinomas. *Int J Radiat Oncol Biol Phys* **32,** 567-576.

Lee SS, Byun JH, Park BJ, Park SH, Kim N, Park B, Kim JK & Lee MG. (2008). Quantitative analysis of diffusion-weighted magnetic resonance imaging of the pancreas: usefulness in characterizing solid pancreatic masses. *J Magn Reson Imaging* **28,** 928-936.

Lee ST & Scott AM. (2007). Hypoxia positron emission tomography imaging with 18f-fluoromisonidazole. *Semin Nucl Med* **37,** 451-461.

Leenders KL. (1994). PET: blood flow and oxygen consumption in brain tumors. *J Neurooncol* **22,** 269-273.

Lehtio K, Eskola O, Viljanen T, Oikonen V, Gronroos T, Sillanmaki L, Grenman R & Minn H. (2004). Imaging perfusion and hypoxia with PET to predict radiotherapy response in head-and-neck cancer. *Int J Radiat Oncol Biol Phys* **59,** 971-982.

Lehtio K, Oikonen V, Gronroos T, Eskola O, Kalliokoski K, Bergman J, Solin O, Grenman R, Nuutila P & Minn H. (2001). Imaging of blood flow and hypoxia in head and neck cancer: initial evaluation with [(15)O]H(2)O and [(18)F]fluoroerythronitroimidazole PET. *J Nucl Med* **42,** 1643-1652.

Lemke AJ, Niehues SM, Hosten N, Amthauer H, Boehmig M, Stroszczynski C, Rohlfing T, Rosewicz S & Felix R. (2004). Retrospective digital image fusion of multidetector CT and 18F-FDG PET: clinical value in pancreatic lesions--a prospective study with 104 patients. *J Nucl Med* **45,** 1279-1286.

Lewis JS, McCarthy DW, McCarthy TJ, Fujibayashi Y & Welch MJ. (1999). Evaluation of 64Cu-ATSM in vitro and in vivo in a hypoxic tumor model. *J Nucl Med* **40,** 177-183.

Lewis JS, Sharp TL, Laforest R, Fujibayashi Y & Welch MJ. (2001). Tumor uptake of copper-diacetyl-bis(N(4)-methylthiosemicarbazone): effect of changes in tissue oxygenation. *J Nucl Med* **42,** 655-661.

Li D, Xie K, Wolff R & Abbruzzese JL. (2004). Pancreatic cancer. *Lancet* **363,** 1049-1057.

Li SJ, Jin GY & Moulder JE. (1991). Prediction of tumor radiosensitivity by hexafluoromisonidazole retention monitored by [1H]/[19F] magnetic resonance spectroscopy. *Cancer Commun* **3,** 133-139.

Lievre A, Bachet JB, Le Corre D, Boige V, Landi B, Emile JF, Cote JF, Tomasic G, Penna C, Ducreux M, Rougier P, Penault-Llorca F & Laurent-Puig P. (2006). KRAS mutation status is predictive of response to cetuximab therapy in colorectal cancer. *Cancer Res* **66,** 3992-3995.

Linder KE, Chan YW, Cyr JE, Malley MF, Nowotnik DP & Nunn AD. (1994). TcO(PnA.O-1-(2-nitroimidazole)) [BMS-181321], a new technetium-containing nitroimidazole complex for imaging hypoxia: synthesis, characterization, and xanthine oxidase-catalyzed reduction. *J Med Chem* **37,** 9-17.

Liu Q, Sun JD, Wang J, Ahluwalia D, Baker AF, Cranmer LD, Ferraro D, Wang Y, Duan JX, Ammons WS, Curd JG, Matteucci MD & Hart CP. (2012). TH-302, a hypoxia-activated prodrug with broad in vivo preclinical combination therapy efficacy: optimization of dosing regimens and schedules. *Cancer Chemother Pharmacol* **69,** 1487-1498.

Liukko KE, Oikonen VJ, Tolvanen TK, Virtanen KA, Viljanen AP, Sipilä HT, Nuutila P & Iozzo P. (2007). Non-Invasive Estimation of Subcutaneous and Visceral Adipose Tissue Blood Flow by Using [15O]H2O PET with Image Derived Input Functions. *The Open Medical Imaging Journal* **1,** 2007.

Ljungkvist AS, Bussink J, Kaanders JH & van der Kogel AJ. (2007). Dynamics of tumor hypoxia measured with bioreductive hypoxic cell markers. *Radiat Res* **167,** 127-145.

Ljungkvist AS, Bussink J, Rijken PF, Kaanders JH, van der Kogel AJ & Denekamp J. (2002). Vascular architecture, hypoxia, and proliferation in first-generation xenografts of human head-and-neck

squamous cell carcinomas. *Int J Radiat Oncol Biol Phys* **54,** 215-228.

Lodge MA, Jacene HA, Pili R & Wahl RL. (2008). Reproducibility of tumor blood flow quantification with 15O-water PET. *J Nucl Med* **49,** 1620-1627.

Loening AM & Gambhir SS. (2003). AMIDE: a free software tool for multimodality medical image analysis. *Mol Imaging* **2,** 131-137.

Logan TF, Jadali F, Egorin MJ, Mintun M, Sashin D, Gooding WE, Choi Y, Bishop H, Trump DL, Gardner D, Kirkwood J, Vlock D & Johnson C. (2002). Decreased tumor blood flow as measured by positron emission tomography in cancer patients treated with interleukin-1 and carboplatin on a phase I trial. *Cancer Chemother Pharmacol* **50,** 433-444.

Loges S, Mazzone M, Hohensinner P & Carmeliet P. (2009). Silencing or fueling metastasis with VEGF inhibitors: antiangiogenesis revisited. *Cancer Cell* **15,** 167-170.

Longo R, Cacciamani F, Naso G & Gasparini G. (2008). Pancreatic cancer: From molecular signature to target therapy. *Crit Rev Oncol Hematol*.

Lyshchik A, Higashi T, Nakamoto Y, Fujimoto K, Doi R, Imamura M & Saga T. (2005). Dual-phase 18F-fluoro-2-deoxy-D-glucose positron emission tomography as a prognostic parameter in patients with pancreatic cancer. *Eur J Nucl Med Mol Imaging* **32,** 389-397.

Lytras D, Connor S, Bosonnet L, Jayan R, Evans J, Hughes M, Garvey CJ, Ghaneh P, Sutton R, Vinjamuri S & Neoptolemos JP. (2005). Positron emission tomography does not add to computed tomography for the diagnosis and staging of pancreatic cancer. *Dig Surg* **22,** 55-61; discussion 62.

MacManus M, Nestle U, Rosenzweig KE, Carrio I, Messa C, Belohlavek O, Danna M, Inoue T, Deniaud-Alexandre E, Schipani S, Watanabe N, Dondi M & Jeremic B. (2009). Use of PET and PET/CT for radiation therapy planning: IAEA expert report 2006-2007. *Radiother Oncol* **91,** 85-94.

Mahy P, De Bast M, Leveque PH, Gillart J, Labar D, Marchand J & Gregoire V. (2004). Preclinical validation of the hypoxia tracer 2-(2-nitroimidazol-1-yl)- N-(3,3,3-[(18)F]trifluoropropyl)acetamide, [(18)F]EF3. *Eur J Nucl Med Mol Imaging* **31,** 1263-1272.

Maier FC, Kneilling M, Reischl G, Cay F, Bukala D, Schmid A, Judenhofer MS, Rocken M, Machulla HJ & Pichler BJ. (2011). Significant impact of different oxygen breathing conditions on noninvasive in vivo tumor-hypoxia imaging using [18F]-fluoro-azomycinarabino-furanoside ([18F]FAZA). *Radiat Oncol* **6,** 165.

Mankoff DA, Dunnwald LK, Gralow JR, Ellis GK, Charlop A, Lawton TJ, Schubert EK, Tseng J & Livingston RB. (2002). Blood flow and metabolism in locally advanced breast cancer: relationship to response to therapy. *J Nucl Med* **43,** 500-509.

Mannan RH, Somayaji VV, Lee J, Mercer JR, Chapman JD & Wiebe LI. (1991). Radioiodinated 1-(5-iodo-5-deoxy-beta-D-arabinofuranosyl)-2-nitroimidazole (iodoazomycin arabinoside: IAZA): a novel marker of tissue hypoxia. *J Nucl Med* **32,** 1764-1770.

Martin L, Lartigau E, Weeger P, Lambin P, Le Ridant AM, Lusinchi A, Wibault P, Eschwege F, Luboinski B & Guichard M. (1993). Changes in the oxygenation of head and neck tumors during carbogen breathing. *Radiother Oncol* **27,** 123-130.

Mayer A, Hockel M & Vaupel P. (2008). Endogenous hypoxia markers: case not proven! *Adv Exp Med Biol* **614,** 127-136.

McKeage MJ, Gu Y, Wilson WR, Hill A, Amies K, Melink TJ & Jameson MB. (2011). A phase I trial of PR-104, a pre-prodrug of the bioreductive prodrug PR-104A, given weekly to solid tumour patients. *BMC Cancer* **11,** 432.

McKeage MJ, Jameson MB, Ramanathan RK, Rajendran J, Gu Y, Wilson WR, Melink TJ & Tchekmedyian NS. (2012). PR-104 a bioreductive pre-prodrug combined with gemcitabine or docetaxel in a phase Ib study of patients with advanced solid tumours. *BMC Cancer* **12,** 496.

Mehanna H, Jones TM, Gregoire V & Ang KK. (2010). Oropharyngeal carcinoma related to human papillomavirus. *BMJ* **340,** c1439.

Meyer E. (1989). Simultaneous correction for tracer arrival delay and dispersion in CBF measurements by the H215O autoradiographic method and dynamic PET. *J Nucl Med* **30,** 1069-1078.

Miles KA, Hayball MP & Dixon AK. (1995). Measurement of human pancreatic perfusion using dynamic computed tomography with perfusion imaging. *Br J Radiol* **68,** 471-475.

Miles KA & Williams RE. (2008). Warburg revisited: imaging tumour blood flow and metabolism. *Cancer Imaging* **8,** 81-86.

Mineura K, Shioya H, Kowada M, Ogawa T, Hatazawa J & Uemura K. (1999). Blood flow and metabolism of oligodendrogliomas: a positron emission tomography study with kinetic analysis of 18F-fluorodeoxyglucose. *J Neurooncol* **43,** 49-57.

Minn H, Gronroos TJ, Komar G, Eskola O, Lehtio K, Tuomela J, Seppanen M & Solin O. (2008). Imaging of tumor hypoxia to predict treatment sensitivity. *Curr Pharm Des* **14,** 2932-2942.

Minn H, Leskinen-Kallio S, Lindholm P, Bergman J, Ruotsalainen U, Teras M & Haaparanta M. (1993). [18F]fluorodeoxyglucose uptake in tumors: kinetic vs. steady-state methods with reference to plasma insulin. *J Comput Assist Tomogr* **17,** 115-123.

Minn H, Suilamo S & Seppala J. (2010). Impact of PET/CT on planning of radiotherapy in head and neck cancer. *Q J Nucl Med Mol Imaging* **54,** 521-532.

Minn H, Zasadny KR, Quint LE & Wahl RL. (1995). Lung cancer: reproducibility of quantitative measurements for evaluating 2-[F-18]-fluoro-2-deoxy-D-glucose uptake at PET. *Radiology* **196,** 167-173.

Molls M, Vaupel P & Brown JM. (1998). *Blood perfusion and microenvironment of human tumors : implications for clinical radiooncology*. Springer, Berlin ; London.

Mosteller RD. (1987). Simplified calculation of body-surface area. *N Engl J Med* **317,** 1098.

Mueller-Klieser W & Walenta S. (1993). Geographical mapping of metabolites in biological tissue with quantitative bioluminescence and single photon imaging. *Histochem J* **25,** 407-420.

Muramoto S, Uematsu H, Sadato N, Tsuchida T, Matsuda T, Hatabu H, Yonekura Y & Itoh H. (2002). H(2) (15)0 positron emission tomography validation of semiquantitative prostate blood flow determined by double-echo dynamic MRI: a preliminary study. *J Comput Assist Tomogr* **26,** 510-514.

Nakamoto Y, Higashi T, Sakahara H, Tamaki N, Kogire M, Doi R, Hosotani R, Imamura M & Konishi J. (2000). Delayed (18)F-fluoro-2-deoxy-D-glucose positron emission tomography scan for differentiation between malignant and benign lesions in the pancreas. *Cancer* **89,** 2547-2554.

Nakata B, Nishimura S, Ishikawa T, Ohira M, Nishino H, Kawabe J, Ochi H & Hirakawa K. (2001). Prognostic predictive value of 18F-fluorodeoxyglucose positron emission tomography for patients with pancreatic cancer. *Int J Oncol* **19,** 53-58.

Nalluri SR, Chu D, Keresztes R, Zhu X & Wu S. (2008). Risk of Venous Thromboembolism With the Angiogenesis Inhibitor Bevacizumab in Cancer Patients: A Meta-analysis. *JAMA* **300,** 2277-2285.

Nekolla SG & Saraste A. (2011). Novel F-18-Labeled PET Myocardial Perfusion Tracers: Bench to Bedside. *Curr Cardiol Rep* **13,** 145-150.

Ni XG, Bai XF, Mao YL, Shao YF, Wu JX, Shan Y, Wang CF, Wang J, Tian YT, Liu Q, Xu DK & Zhao P. (2005). The clinical value of serum CEA, CA19-9, and CA242 in the diagnosis and prognosis of pancreatic cancer. *Eur J Surg Oncol* **31,** 164-169.

Nishiyama Y, Yamamoto Y, Yokoe K, Monden T, Sasakawa Y, Tsutsui K, Satoh K & Ohkawa M. (2005). Contribution of whole body FDG-PET to the detection of distant metastasis in pancreatic cancer. *Ann Nucl Med* **19,** 491-497.

Nordsmark M, Bentzen SM, Rudat V, Brizel D, Lartigau E, Stadler P, Becker A, Adam M, Molls M, Dunst J, Terris DJ & Overgaard J. (2005). Prognostic value of tumor oxygenation in 397 head and neck tumors after primary radiation therapy. An

international multi-center study. *Radiother Oncol* **77,** 18-24.

Obata A, Yoshimi E, Waki A, Lewis JS, Oyama N, Welch MJ, Saji H, Yonekura Y & Fujibayashi Y. (2001). Retention mechanism of hypoxia selective nuclear imaging/radiotherapeutic agent cu-diacetyl-bis(N4-methylthiosemicarbazone) (Cu-ATSM) in tumor cells. *Ann Nucl Med* **15,** 499-504.

Okazawa H, Kosiwatanarek A, Kimura Y, Kiyono Y, Mori T & Fujieda S. (2011). Predictive value of tracer accumulation to evaluate effects of cancer therapy studied using Cu-62 ATSM and F-18 FDG PET in head-and-neck cancers. *Eur J Nucl Med Mol Imaging* **38, Supplement 2**.

Olive PL, Aquino-Parsons C, MacPhail SH, Liao SY, Raleigh JA, Lerman MI & Stanbridge EJ. (2001). Carbonic anhydrase 9 as an endogenous marker for hypoxic cells in cervical cancer. *Cancer Res* **61,** 8924-8929.

Olive PL, Durand RE, Raleigh JA, Luo C & Aquino-Parsons C. (2000). Comparison between the comet assay and pimonidazole binding for measuring tumour hypoxia. *Br J Cancer* **83,** 1525-1531.

Oosterwijk E, Ruiter DJ, Hoedemaeker PJ, Pauwels EK, Jonas U, Zwartendijk J & Warnaar SO. (1986). Monoclonal antibody G 250 recognizes a determinant present in renal-cell carcinoma and absent from normal kidney. *Int J Cancer* **38,** 489-494.

Osinsky S, Zavelevich M & Vaupel P. (2009). Tumor hypoxia and malignant progression. *Exp Oncol* **31,** 80-86.

Overgaard J. (1994). Clinical evaluation of nitroimidazoles as modifiers of hypoxia in solid tumors. *Oncol Res* **6,** 509-518.

Overgaard J, Hansen HS, Overgaard M, Bastholt L, Berthelsen A, Specht L, Lindelov B & Jorgensen K. (1998). A randomized double-blind phase III study of nimorazole as a hypoxic radiosensitizer of primary radiotherapy in supraglottic larynx and pharynx carcinoma. Results of the Danish Head and Neck Cancer Study (DAHANCA) Protocol 5-85. *Radiother Oncol* **46,** 135-146.

Papadopoulou MV, Ji M & Bloomer WD. (2011). Hypoxia-Dependent Retinal Toxicity of NLCQ-1 (NSC 709257) in BALB/c Mice. Comparison with Tirapazamine. *Basic Clin Pharmacol Toxicol*.

Patlak CS & Blasberg RG. (1985). Graphical evaluation of blood-to-brain transfer constants from multiple-time uptake data. Generalizations. *J Cereb Blood Flow Metab* **5,** 584-590.

Patterson AV, Ferry DM, Edmunds SJ, Gu Y, Singleton RS, Patel K, Pullen SM, Hicks KO, Syddall SP, Atwell GJ, Yang S, Denny WA & Wilson WR. (2007). Mechanism of action and preclinical antitumor activity of the novel hypoxia-activated DNA cross-linking agent PR-104. *Clin Cancer Res* **13,** 3922-3932.

Paulino AC, Koshy M, Howell R, Schuster D & Davis LW. (2005). Comparison of CT- and FDG-PET-defined gross tumor volume in intensity-modulated radiotherapy for head-and-neck cancer. *Int J Radiat Oncol Biol Phys* **61,** 1385-1392.

Peltoniemi P, Lonnroth P, Laine H, Oikonen V, Tolvanen T, Gronroos T, Strindberg L, Knuuti J & Nuutila P. (2000). Lumped constant for [(18)F]fluorodeoxyglucose in skeletal muscles of obese and nonobese humans. *Am J Physiol Endocrinol Metab* **279,** E1122-1130.

Picchio M, Beck R, Haubner R, Seidl S, Machulla HJ, Johnson TD, Wester HJ, Reischl G, Schwaiger M & Piert M. (2008). Intratumoral spatial distribution of hypoxia and angiogenesis assessed by 18F-FAZA and 125I-Gluco-RGD autoradiography. *J Nucl Med* **49,** 597-605.

Piert M, Machulla HJ, Picchio M, Reischl G, Ziegler S, Kumar P, Wester HJ, Beck R, McEwan AJ, Wiebe LI & Schwaiger M. (2005). Hypoxia-specific tumor imaging with 18F-fluoroazomycin arabinoside. *J Nucl Med* **46,** 106-113.

Pike VW. (2009). PET radiotracers: crossing the blood-brain barrier and surviving metabolism. *Trends Pharmacol Sci* **30,** 431-440.

Plossl K, Chandra R, Qu W, Lieberman BP, Kung MP, Zhou R, Huang B & Kung HF. (2008). A novel gallium bisaminothiolate complex as a myocardial perfusion imaging agent. *Nucl Med Biol* **35,** 83-90.

Prokesch RW, Chow LC, Beaulieu CF, Bammer R & Jeffrey RB, Jr. (2002). Isoattenuating pancreatic adenocarcinoma at multi-detector row CT: secondary signs. *Radiology* **224,** 764-768.

Pryma DA, O'Donoghue JA, Humm JL, Jungbluth AA, Old LJ, Larson SM & Divgi CR. (2011). Correlation of in vivo and in vitro measures of carbonic anhydrase IX antigen expression in renal masses using antibody 124I-cG250. *J Nucl Med* **52,** 535-540.

Raab-Traub N. (2002). Epstein-Barr virus in the pathogenesis of NPC. *Semin Cancer Biol* **12,** 431-441.

Rajendran JG & Mankoff DA. (2007). Positron Emission Tomography Imaging of Blood Flow and Hypoxia in Tumors. In *In Vivo Imaging of Cancer Therapy*, ed. Shields AF & Price P, pp. 47-71. Humana Press.

Raleigh JA, Dewhirst MW & Thrall DE. (1996). Measuring Tumor Hypoxia. *Semin Radiat Oncol* **6,** 37-45.

Rasey JS, Hofstrand PD, Chin LK & Tewson TJ. (1999). Characterization of [18F]fluoroetanidazole, a new radiopharmaceutical for detecting tumor hypoxia. *J Nucl Med* **40,** 1072-1079.

Reischl G, Dorow DS, Cullinane C, Katsifis A, Roselt P, Binns D & Hicks RJ. (2007). Imaging of tumor hypoxia with [124I]IAZA in comparison with [18F]FMISO and [18F]FAZA--first small animal PET results. *J Pharm Pharm Sci* **10,** 203-211.

Reivich M, Kuhl D, Wolf A, Greenberg J, Phelps M, Ido T, Casella V, Fowler J, Hoffman E, Alavi A, Som P & Sokoloff L. (1979). The [18F]fluorodeoxyglucose method for the measurement of local cerebral glucose utilization in man. *Circ Res* **44,** 127-137.

Renehan AG, Tyson M, Egger M, Heller RF & Zwahlen M. (2008). Body-mass index and incidence of cancer: a systematic review and meta-analysis of prospective observational studies. *Lancet* **371,** 569-578.

Reske SN, Grillenberger KG, Glatting G, Port M, Hildebrandt M, Gansauge F & Beger HG. (1997). Overexpression of glucose transporter 1 and increased FDG uptake in pancreatic carcinoma. *J Nucl Med* **38,** 1344-1348.

Rischin D, Hicks RJ, Fisher R, Binns D, Corry J, Porceddu S & Peters LJ. (2006). Prognostic significance of [18F]-misonidazole positron emission tomography-detected tumor hypoxia in patients with advanced head and neck cancer randomly assigned to chemoradiation with or without tirapazamine: a substudy of Trans-Tasman Radiation Oncology Group Study 98.02. *J Clin Oncol* **24,** 2098-2104.

Rischin D, Peters LJ, O'Sullivan B, Giralt J, Fisher R, Yuen K, Trotti A, Bernier J, Bourhis J, Ringash J, Henke M & Kenny L. (2010). Tirapazamine, cisplatin, and radiation versus cisplatin and radiation for advanced squamous cell carcinoma of the head and neck (TROG 02.02, HeadSTART): a phase III trial of the Trans-Tasman Radiation Oncology Group. *J Clin Oncol* **28,** 2989-2995.

Rockwell S & Moulder JE. (1990). Hypoxic fractions of human tumors xenografted into mice: a review. *Int J Radiat Oncol Biol Phys* **19,** 197-202.

Rofstad EK & Danielsen T. (1999). Hypoxia-induced metastasis of human melanoma cells: involvement of vascular endothelial growth factor-mediated angiogenesis. *Br J Cancer* **80,** 1697-1707.

Rufini V, Baum RP, Castaldi P, Treglia G, De Gaetano AM, Carreras C, Kaemmerer D, Hommann M, Horsch D, Bonomo L & Giordano A. (2012). Role of PET/CT in the functional imaging of endocrine pancreatic tumors. *Abdom Imaging*.

Sahani DV, Shah ZK, Catalano OA, Boland GW & Brugge WR. (2008). Radiology of pancreatic adenocarcinoma: current status of imaging. *J Gastroenterol Hepatol* **23,** 23-33.

Schick V, Franzius C, Beyna T, Oei ML, Schnekenburger J, Weckesser M, Domschke W, Schober O, Heindel W, Pohle T & Juergens KU. (2008). Diagnostic impact of 18F-FDG PET-CT evaluating solid pancreatic lesions versus endosonography, endoscopic retrograde cholangio-pancreatography with intraductal ultrasonography and abdominal ultrasound. *Eur J Nucl Med Mol Imaging* **35,** 1775-1785.

Schima W, Ba-Ssalamah A, Kolblinger C, Kulinna-Cosentini C, Puespoek A & Gotzinger P. (2007). Pancreatic adenocarcinoma. *Eur Radiol* **17,** 638-649.

Semenza GL. (2010). Defining the role of hypoxia-inducible factor 1 in cancer biology and therapeutics. *Oncogene* **29,** 625-634.

Sendler A, Avril N, Helmberger H, Stollfuss J, Weber W, Bengel F, Schwaiger M, Roder JD & Siewert JR. (2000). Preoperative evaluation of pancreatic masses with positron emission tomography using 18F-fluorodeoxyglucose: diagnostic limitations. *World J Surg* **24,** 1121-1129.

Seo S, Doi R, Machimoto T, Kami K, Masui T, Hatano E, Ogawa K, Higashi T & Uemoto S. (2008). Contribution of 18F-fluorodeoxyglucose positron emission tomography to the diagnosis of early pancreatic carcinoma. *J Hepatobiliary Pancreat Surg* **15,** 634-639.

Shiozaki T, Sadato N, Senda M, Ishii K, Tsuchida T, Yonekura Y, Fukuda H & Konishi J. (2000). Noninvasive estimation of FDG input function for quantification of cerebral metabolic rate of glucose: optimization and multicenter evaluation. *J Nucl Med* **41,** 1612-1618.

Siegel R, Naishadham D & Jemal A. (2012). Cancer statistics, 2012. *CA Cancer J Clin* **62,** 10-29.

Smalley KS, Brafford PA & Herlyn M. (2005). Selective evolutionary pressure from the tissue microenvironment drives tumor progression. *Semin Cancer Biol* **15,** 451-459.

Sobin LH. (2002). TNM: Classification of malignant tumours. In *International Union Against Cancer (UICC)*, 6th edn, ed. Wittenkind C, pp. 93 - 96. Wiley, New York, NY.

Sofuni A, Iijima H, Moriyasu F, Nakayama D, Shimizu M, Nakamura K, Itokawa F & Itoi T. (2005). Differential diagnosis of pancreatic tumors using ultrasound contrast imaging. *J Gastroenterol* **40,** 518-525.

Sokoloff L. (1977). Relation between physiological function and energy metabolism in the central nervous system. *J Neurochem* **29,** 13-26.

Sperti C, Bissoli S, Pasquali C, Frison L, Liessi G, Chierichetti F & Pedrazzoli S. (2007). 18-fluorodeoxyglucose positron emission tomography enhances computed tomography diagnosis of malignant intraductal papillary mucinous neoplasms of the pancreas. *Ann Surg* **246,** 932-937; discussion 937-939.

Sperti C, Pasquali C, Chierichetti F, Ferronato A, Decet G & Pedrazzoli S. (2003). 18-Fluorodeoxyglucose positron emission tomography in predicting survival of patients with pancreatic carcinoma. *J Gastrointest Surg* **7,** 953-959; discussion 959-960.

Steel GG. (2002). *Basic clinical radiobiology*. Arnold, London.

Stockmann C, Doedens A, Weidemann A, Zhang N, Takeda N, Greenberg JI, Cheresh DA & Johnson RS. (2008). Deletion of vascular endothelial growth factor in myeloid cells accelerates tumorigenesis. *Nature*.

Strobel K, Heinrich S, Bhure U, Soyka J, Veit-Haibach P, Pestalozzi BC, Clavien PA & Hany TF. (2008). Contrast-enhanced 18F-FDG PET/CT: 1-stop-shop imaging for assessing the resectability of pancreatic cancer. *J Nucl Med* **49,** 1408-1413.

Sun JD, Liu Q, Wang J, Ahluwalia D, Ferraro D, Wang Y, Duan JX, Ammons WS, Curd JG, Matteucci MD & Hart CP. Selective tumor hypoxia targeting by hypoxia-activated prodrug TH-302 inhibits tumor growth in preclinical models of cancer. *Clin Cancer Res* **18,** 758-770.

Sun JD, Liu Q, Wang J, Ahluwalia D, Ferraro D, Wang Y, Duan JX, Ammons WS, Curd JG, Matteucci MD & Hart CP. (2012). Selective tumor hypoxia targeting by hypoxia-activated prodrug TH-302 inhibits tumor growth in preclinical models of cancer. *Clin Cancer Res* **18,** 758-770.

Sundin A, Garske U & Orlefors H. (2007). Nuclear imaging of neuroendocrine tumours. *Best Pract Res Clin Endocrinol Metab* **21,** 69-85.

Tajima Y, Matsuzaki S, Furui J, Isomoto I, Hayashi K & Kanematsu T. (2004). Use of the time-signal intensity curve from dynamic magnetic resonance imaging to evaluate remnant pancreatic fibrosis after

pancreaticojejunostomy in patients undergoing pancreaticoduodenectomy. *Br J Surg* **91,** 595-600.

Tappenden P, Jones R, Paisley S & Carroll C. (2007). Systematic review and economic evaluation of bevacizumab and cetuximab for the treatment of metastatic colorectal cancer. *Health Technol Assess* **11,** 1-128, iii-iv.

Teh BS, Woo SY & Butler EB. (1999). Intensity modulated radiation therapy (IMRT): a new promising technology in radiation oncology. *Oncologist* **4,** 433-442.

Teras M, Tolvanen T, Johansson JJ, Williams JJ & Knuuti J. (2007). Performance of the new generation of whole-body PET/CT scanners: Discovery STE and Discovery VCT. *Eur J Nucl Med Mol Imaging* **34,** 1683-1692.

Tewson TJ. (1997). Synthesis of [18F]fluoroetanidazole: a potential new tracer for imaging hypoxia. *Nucl Med Biol* **24,** 755-760.

Thomlinson RH & Gray LH. (1955). The histological structure of some human lung cancers and the possible implications for radiotherapy. *Br J Cancer* **9,** 539-549.

Thorwarth D & Alber M. (2010). Implementation of hypoxia imaging into treatment planning and delivery. *Radiother Oncol* **97,** 172-175.

Thorwarth D, Eschmann SM, Paulsen F & Alber M. (2007). Hypoxia dose painting by numbers: a planning study. *Int J Radiat Oncol Biol Phys* **68,** 291-300.

Thorwarth D, Eschmann SM, Scheiderbauer J, Paulsen F & Alber M. (2005). Kinetic analysis of dynamic 18F-fluoromisonidazole PET correlates with radiation treatment outcome in head-and-neck cancer. *BMC Cancer* **5,** 152.

Thorwarth D & Schaefer A. (2010). Functional target volume delineation for radiation therapy on the basis of positron emission tomography and the correlation with histopathology. *Q J Nucl Med Mol Imaging* **54,** 490-499.

Toustrup K, Sorensen BS, Lassen P, Wiuf C, Alsner J & Overgaard J. (2012). Gene expression classifier predicts for hypoxic modification of radiotherapy with nimorazole in squamous cell carcinomas of the head and neck. *Radiother Oncol* **102,** 122-129.

Troost EG, Bussink J, Kaanders JH, van Eerd J, Peters JP, Rijken PF, Boerman OC & van der Kogel AJ. (2005). Comparison of different methods of CAIX quantification in relation to hypoxia in three human head and neck tumor lines. *Radiother Oncol* **76,** 194-199.

Troost EG, Schinagl DA, Bussink J, Oyen WJ & Kaanders JH. (2010). Clinical evidence on PET-CT for radiation therapy planning in head and neck tumours. *Radiother Oncol* **96,** 328-334.

Tsuchida T, Sadato N, Yonekura Y, Nakamura S, Takahashi N, Sugimoto K, Waki A, Yamamoto K, Hayashi N & Ishii Y. (1999). Noninvasive measurement of cerebral metabolic rate of glucose using standardized input function. *J Nucl Med* **40,** 1441-1445.

Tsuzuki Y, Fukumura D, Oosthuyse B, Koike C, Carmeliet P & Jain RK. (2000). Vascular endothelial growth factor (VEGF) modulation by targeting hypoxia-inducible factor-1alpha--> hypoxia response element--> VEGF cascade differentially regulates vascular response and growth rate in tumors. *Cancer Res* **60,** 6248-6252.

Urtasun RC, Parliament MB, McEwan AJ, Mercer JR, Mannan RH, Wiebe LI, Morin C & Chapman JD. (1996). Measurement of hypoxia in human tumours by non-invasive spect imaging of iodoazomycin arabinoside. *Br J Cancer Suppl* **27,** S209-212.

Wahl RL. (2004). Why nearly all PET of abdominal and pelvic cancers will be performed as PET/CT. *J Nucl Med* **45 Suppl 1,** 82S-95S.

Wakabayashi H, Nishiyama Y, Otani T, Sano T, Yachida S, Okano K, Izuishi K & Suzuki Y. (2008). Role of 18F-fluorodeoxyglucose positron emission tomography imaging in surgery for pancreatic cancer. *World J Gastroenterol* **14,** 64-69.

Valk PE. (2003). *Positron emission tomography : basic science and clinical practice*. Springer, London ; New York.

van Dalen JA, Hoffmann AL, Dicken V, Vogel WV, Wiering B, Ruers TJ, Karssemeijer N & Oyen WJ. (2007). A novel iterative method for lesion

delineation and volumetric quantification with FDG PET. *Nucl Med Commun* **28,** 485-493.

van den Hoff J, Burchert W, Muller-Schauenburg W, Meyer GJ & Hundeshagen H. (1993). Accurate local blood flow measurements with dynamic PET: fast determination of input function delay and dispersion by multilinear minimization. *J Nucl Med* **34,** 1770-1777.

van Kouwen MC, Jansen JB, van Goor H, de Castro S, Oyen WJ & Drenth JP. (2005). FDG-PET is able to detect pancreatic carcinoma in chronic pancreatitis. *Eur J Nucl Med Mol Imaging* **32,** 399-404.

Vanderkooi JM, Erecinska M & Silver IA. (1991). Oxygen in mammalian tissue: methods of measurement and affinities of various reactions. *Am J Physiol* **260,** C1131-1150.

Wang D, Schultz CJ, Jursinic PA, Bialkowski M, Zhu XR, Brown WD, Rand SD, Michel MA, Campbell BH, Wong S, Li XA & Wilson JF. (2006). Initial experience of FDG-PET/CT guided IMRT of head-and-neck carcinoma. *Int J Radiat Oncol Biol Phys* **65,** 143-151.

Wang J, Foehrenbacher A, Su J, Patel R, Hay MP, Hicks KO & Wilson WR. (2012). The 2-nitroimidazole EF5 is a biomarker for oxidoreductases that activate the bioreductive prodrug CEN-209 under hypoxia. *Clin Cancer Res* **18,** 1684-1695.

Warburg O. (1956a). On respiratory impairment in cancer cells. *Science* **124,** 269-270.

Warburg O. (1956b). On the origin of cancer cells. *Science* **123,** 309-314.

Warburg O, Wind F & Negelein E. (1927). The Metabolism of Tumors in the Body. *J Gen Physiol* **8,** 519-530.

Varghese AJ, Gulyas S & Mohindra JK. (1976). Hypoxia-dependent reduction of 1-(2-nitro-1-imidazolyl)-3-methoxy-2-propanol by Chinese hamster ovary cells and KHT tumor cells in vitro and in vivo. *Cancer Res* **36,** 3761-3765.

Varia MA, Calkins-Adams DP, Rinker LH, Kennedy AS, Novotny DB, Fowler WC, Jr. & Raleigh JA. (1998). Pimonidazole: a novel hypoxia marker for complementary study of tumor hypoxia and cell proliferation in cervical carcinoma. *Gynecol Oncol* **71,** 270-277.

Vaupel P, Hockel M & Mayer A. (2007). Detection and characterization of tumor hypoxia using pO2 histography. *Antioxid Redox Signal* **9,** 1221-1235.

Vaupel P & Mayer A. (2007). Hypoxia in cancer: significance and impact on clinical outcome. *Cancer Metastasis Rev* **26,** 225-239.

Vaupel P, Schlenger K, Knoop C & Hockel M. (1991). Oxygenation of human tumors: evaluation of tissue oxygen distribution in breast cancers by computerized O2 tension measurements. *Cancer Res* **51,** 3316-3322.

Weinhouse S. (1976). The Warburg hypothesis fifty years later. *Z Krebsforsch Klin Onkol Cancer Res Clin Oncol* **87,** 115-126.

Weiss GJ, Infante JR, Chiorean EG, Borad MJ, Bendell JC, Molina JR, Tibes R, Ramanathan RK, Lewandowski K, Jones SF, Lacouture ME, Langmuir VK, Lee H, Kroll S & Burris HA, 3rd. (2011). Phase 1 study of the safety, tolerability, and pharmacokinetics of TH-302, a hypoxia-activated prodrug, in patients with advanced solid malignancies. *Clin Cancer Res* **17,** 2997-3004.

Wells P, Jones T & Price P. (2003). Assessment of inter- and intrapatient variability in C15O2 positron emission tomography measurements of blood flow in patients with intra-abdominal cancers. *Clin Cancer Res* **9,** 6350-6356.

Westerterp M, Pruim J, Oyen W, Hoekstra O, Paans A, Visser E, van Lanschot J, Sloof G & Boellaard R. (2007). Quantification of FDG PET studies using standardised uptake values in multi-centre trials: effects of image reconstruction, resolution and ROI definition parameters. *Eur J Nucl Med Mol Imaging* **34,** 392-404.

Wijffels KI, Kaanders JH, Rijken PF, Bussink J, van den Hoogen FJ, Marres HA, de Wilde PC, Raleigh JA & van der Kogel AJ. (2000). Vascular architecture and hypoxic profiles in human head and neck squamous cell carcinomas. *Br J Cancer* **83,** 674-683.

Viljanen AP, Lautamaki R, Jarvisalo M, Parkkola R, Huupponen R, Lehtimaki T, Ronnemaa T, Raitakari OT, Iozzo P & Nuutila P. (2009). Effects of weight loss on visceral and abdominal subcutaneous adipose tissue blood-flow and insulin-mediated glucose uptake in healthy obese subjects. *Ann Med* **41,** 152-160.

Wilson CB, Lammertsma AA, McKenzie CG, Sikora K & Jones T. (1992). Measurements of blood flow and exchanging water space in breast tumors using positron emission tomography: a rapid and noninvasive dynamic method. *Cancer Res* **52,** 1592-1597.

Wilson WR & Hay MP. (2011). Targeting hypoxia in cancer therapy. *Nat Rev Cancer* **11,** 393-410.

Wong DF & Pomper MG. (2003). Predicting the success of a radiopharmaceutical for in vivo imaging of central nervous system neuroreceptor systems. *Mol Imaging Biol* **5,** 350-362.

Wong TZ, Lacy JL, Petry NA, Hawk TC, Sporn TA, Dewhirst MW & Vlahovic G. (2008). PET of hypoxia and perfusion with 62Cu-ATSM and 62Cu-PTSM using a 62Zn/62Cu generator. *AJR Am J Roentgenol* **190,** 427-432.

Workman P. (1992). Bioreductive mechanisms. *Int J Radiat Oncol Biol Phys* **22,** 631-637.

Wu HM, Bergsneider M, Glenn TC, Yeh E, Hovda DA, Phelps ME & Huang SC. (2003). Measurement of the global lumped constant for 2-deoxy-2-[18F]fluoro-D-glucose in normal human brain using [15O]water and 2-deoxy-2-[18F]fluoro-D-glucose positron emission tomography imaging. A method with validation based on multiple methodologies. *Mol Imaging Biol* **5,** 32-41.

Wykoff CC, Beasley NJ, Watson PH, Turner KJ, Pastorek J, Sibtain A, Wilson GD, Turley H, Talks KL, Maxwell PH, Pugh CW, Ratcliffe PJ & Harris AL. (2000). Hypoxia-inducible expression of tumor-associated carbonic anhydrases. *Cancer Res* **60,** 7075-7083.

Yamaguchi A, Taniguchi H, Kunishima S, Koh T & Yamagishi H. (2000). Correlation between angiographically assessed vascularity and blood flow in hepatic metastases in patients with colorectal carcinoma. *Cancer* **89,** 1236-1244.

Yuan H, Schroeder T, Bowsher JE, Hedlund LW, Wong T & Dewhirst MW. (2006). Intertumoral differences in hypoxia selectivity of the PET imaging agent 64Cu(II)-diacetyl-bis(N4-methylthiosemicarbazone). *J Nucl Med* **47,** 989-998.

Zasadny KR, Tatsumi M & Wahl RL. (2003). FDG metabolism and uptake versus blood flow in women with untreated primary breast cancers. *Eur J Nucl Med Mol Imaging* **30,** 274-280.

Zhu D, Lou J, Wu H, Luo P & Li L. (2010). Correlation of pharmacokinetic features and tissue distribution with toxicity of Q39, a hypoxic cell cytotoxic agent. *Pharmazie* **65,** 683-689.

Ziemer LS, Evans SM, Kachur AV, Shuman AL, Cardi CA, Jenkins WT, Karp JS, Alavi A, Dolbier WR, Jr. & Koch CJ. (2003). Noninvasive imaging of tumor hypoxia in rats using the 2-nitroimidazole 18F-EF5. *Eur J Nucl Med Mol Imaging* **30,** 259-266.

Zimny M, Buell U, Diederichs CG & Reske SN. (1998). False-positive FDG PET in patients with pancreatic masses: an issue of proper patient selection? *Eur J Nucl Med* **25,** 1352.